universität wien

MASTERARBEIT / MASTER'S THESIS

Titel der Masterarbeit / Title of the Master's Thesis

Analysis of Sediments from Caves in the Northern Rim of the Dachstein Massif

verfasst von / submitted by

Franziska Margarete Holzer

angestrebter akademischer Grad / in partial fulfilment of the requirements for the degree of

Master of Science (MSc)

Wien, 2022 / Vienna, 2022

Studienkennzahl lt. Studienblatt / degree programme code as it appears on the student record sheet:	A 066 815
Studienrichtung lt. Studienblatt / degree programme as it appears on the student record sheet:	Erdwissenschaften
Betreut von / Supervisor:	Ao. Univ. Prof. Mag. Dr. Susanne Gier
Mitbetreut von / Co-Supervisor:	Mag. Dr. Lukas Plan

Abstract

The interest for caves from a geological point of view was only established in Austria at the beginning of the 20th century. Since then, however, the study of clastic cave sediments has rarely been the focus of research. Only recently have master's theses taken up this topic. and an idealised profile was developed of the sedimentary deposits of Dachstein-Mammuthöhle and surrounding caves of the same altitude.

This work intends to supplement the initial results by analysing samples from four different caves at different altitudes of the northern rim of the Dachstein Massif: Hirlatzhöhle, Mammuthöhle, Dachstein-Rieseneishöhle, Günter-Stummer-Höhle. Besides the study of sedimentary structures, the sedimentological methods used were X-ray diffraction (XRD) for the bulk mineralogy as well as clay mineralogy, grain size analysis, measurements of the total organic carbon (TOC), and microscopy of thin sections. To compare the results with other caves, reference samples were taken from Eisriesenwelt and Schönberg-Höhlensystem.

In the caves of the Giant Cave Level (Mammuthöhle, Rieseneishöhle; 1,200 - 1,800 m a.s.l.) the idealised sediment profile can be found. The base is a greenish Augenstein sediment that is poorly sorted and is rich in quartz and mica. Overlying is a dark cave loam with a high percentage of clay. Due to the presence of illite and goethite, it is likely to be remains of palaeosols, which were washed into the caves. Carbonate conglomerates follow, but they were deposited only locally. At the top of the profile is a carbonate-rich bright cave loam with a thickness up to 2 m.

The underlying Berger Cave Level (Hirlatzhöhle; 900 - 1,000 m a.s.l.) is characterised by laminated bright cave loam, which is up to 6 m thick. The thicker brighter laminae are coarser and enriched in quartz and calcite, whereas the darker laminae are more abundant in clay minerals. The sediment is assumed being glaciolacustrine varves: The light-coloured deposits originate from more energetic meltwater during summer; in winter the remaining fine-grained clay minerals sediment. At higher altitudes also occurs dark cave loam below the bright cave loam.

In the Ruin Cave Level (Günter-Stummer-Höhle; 2,200 $\pm$ 300 m a.s.l.), the highest level, only dark cave loam can be found. However, the composition of the samples consists also of boehmite and anatase. These minerals indicate a high degree of weathering and are known to comprise laterites. Due to the required conditions, the lateritization is proposed to be before Middle Miocene times.

The distribution and possible altitude-dependency of the lateritic sediments remain uncertain. Also, dating the laterites is of interest because it could be an indication of the age of the caves of the Ruin Cave Level.

Kurzfassung

Höhlen haben das geologische Interesse in Österreich erst Anfang des 20. Jahrhunderts geweckt. Seither stand die Untersuchung der klastischen Höhlensedimente aber nur selten im Vordergrund der Forschung, bis sich Masterarbeiten dieser Thematik zuwandten. Dabei wurde ein idealisiertes Profil der Sedimente der Dachstein-Mammuthöhle und umliegender Höhlen der gleichen Höhenlage erstellt.

In dieser Arbeit sollen bereits existierende Ergebnisse erweitert werden. Dafür wurden Proben aus vier Höhlen – Hirlatzhöhle, Mammuthöhle, Dachstein-Rieseneishöhle, Günter-Stummer-Höhle – aus unterschiedlichen Höhenlagen vom nördlichen Rand des Dachsteinmassivs analysiert. Neben sedimentologischen Untersuchungen vor Ort wurden Röntgendiffraktionsuntersuchungen (XRD) der Gesamt- sowie der Tonmineralogie, die Sieb- und Sedimentationsanalyse, die Analyse des gesamten organischen Kohlenstoffs (TOC) und Dünnschliffuntersuchungen durchgeführt. Für den Vergleich der Ergebnisse wurden Proben aus der Eisriesenwelt und dem Schönberg-Höhlensystem untersucht.

In den Höhlen des Riesenhöhlenniveaus (Mammuthöhle, Rieseneishöhle; 1,200 - 1,800 m a.s.l.) ist das Sedimentprofil zu finden. Ein unsortiertes, quarz- und glimmerreiches, grünliches Augensteingemisch bildet die Basis. Es folgt feinkörniger dunkler Höhlenton. Aufgrund von Illit und Goethit in der Zusammensetzung dürfte es sich um eingespülte Reste von Paläoböden handeln. Lokal gibt es darüber karbonatische Konglomerate. Zuletzt kommt 2 m heller Höhlenton.

Das darunterliegende Bergerhöhlenniveau (Hirlatzhöhle; 900 - 1,000 m a.s.l.) ist gekennzeichnet durch den karbonatreichen, laminierten hellen Höhlenton, der bis zu 6 m mächtig ist. Die mächtigeren hellen Lagen sind grobkörniger und reicher an Quarz sowie Kalzit, die dunklen Lagen hingegen haben einen höheren Tonmineralgehalt. Bei dem hellen Höhlenton könnte es sich um glazio-lakustrine Warven handeln: die hellen Sommerablagerungen stammen aus energiereicherem Schmelzwasser; im Winter sedimentieren die feinkörnigen Tonminerale. In höheren Lagen tritt auch dunkler Höhlenton unterhalb des hellen Höhlentons auf.

Im Ruinenhöhlenniveau (Günter-Stummer-Höhle; 2,200 $\pm$ 300 m a.s.l.), dem höchsten Niveau, ist nur dunkler Höhlenton vorzufinden. Dieser zeigt jedoch ein Auftreten von Böhmit und Anatas, die als typische Lateritminerale gelten und somit starke Verwitterung andeuten. Aufgrund der erforderlichen Bildungsbedingungen wird angenommen, dass der Laterit sich vor dem Mittelmiozän gebildet hat.

Die Verbreitung und die Höhenabhängigkeit der Laterite bleiben ungeklärt. Ebenso wäre ihre Datierung von Interesse, da sie Hinweise auf das Alter der Höhlen des Ruinenhöhlenniveaus liefern könnte.

Contents

1 Introduction

Since the existence of humankind, caves exert a significant interest. They provide shelter, are a storage space, or serve for ritual uses (Agnolin, 2021, and references therein). More recently, caves are seen as pristine and unknown subterraneous landscapes to be discovered. Caves are also an important habitat for animals (Assmann et al, 2010, and references therein) and due to their preserving function, they are often sites for remains of already extinct species (e.g., Ehrenberg, 1964; Rosendahl et al, 2005, and references therein; Warburton & Prideaux, 2021, and references therein).

Hence, caves serve as one of the most frequent locations for archaeological excavations (Agnolin, 2021, and references therein) and typically, anthropological as well as palaeontological finds are discovered in cave sediments (Jelínek, 1983; Ward et al, 2016, and references therein). Cave sediments, like sediments on the surface, are subject to the simple depositional principle that younger sediments superimpose older ones. This allows conclusions regarding the relative chronological sequences and in addition, the sediments provide information about the depositional and climatic conditions as well as the provenance of the material. However, the sedimentary sequence can be disturbed due to external circumstances. Nevertheless, the depositional circumstances can still be reconstructed, but other sedimentological tools and additionally also dating methods have to be used (Häuselmann, 2004).

The importance of taking the stratigraphy on excavation sites into account was known since the beginning of the 19th century. However, the significance was still neglected until the middle of the 20th century and arbitrary excavation strategies were continued (Ward et al, 2016, and references therein). Only a few archaeologists like Joseph Szombathy were an exception (Svoboda, 2006, and references therein). Szombathy began a thorough exploration of a part of the Mladeč caves in 1881 and 1882 including a stratigraphic profile and the stratigraphic position of the finds (Svoboda, 2006, and references therein). The Mladeč cave system is situated in a karstic limestone formation in central Moravia, Czech Republic (Svoboda, 2006). The caves are partly filled with interglacial and interstadial sediments of the last glacial maximum (Jelínek, 1983). The finds of Szombathy included human skulls and other human remains in a sediment layer together with Upper Pleistocene fauna (Jelínek, 1983, and references therein). The skulls are representatives of the early sapiens group *Homo sapiens sapiens* from Upper

Palaeolithic times (Jelínek, 1983; Svoboda, 2006).

The processes behind the formation of a cave and the sediments formed and deposited in it over time can be used as clues for interpreting the geological history and the climatic conditions of the Earth (Häuselmann, 2004). However, the interest of cave sediments as a distinct geological research field and not being related to archaeological excavation was established only at the beginning of the 20th century. A pioneering role of speleology especially in Austria was played by Dachstein-Mammuthöhle, a cave in the northern rim of the Dachstein Massif and its discoverer Hermann Bock in 1910 (Bock & Lahner, 1913a). He already put forward theories about its formation, partly based on contained cave sediments (Bock, 1913).

Since then a lot of – also controversial – research papers were published about the genesis of the caves in the Dachstein Massif (e.g. Bock, 1926/27; Lahner, 1937; Lahner 1948; Arnberger, 1953; Plan & Xaver, 2010) although some of the studies are limited to the mere description of newly discovered cave areas (e.g., Lehmann, 1922; Arnberger, 1954; Schauberger, 1957). Rarely, the focus was on the depositional processes of cave sediments and their mineralogical composition as well as grain size distribution (e.g., Spöcker, 1925; Franke & Illming, 1963; Seemann, 1973; Schauberger, 1983).

Recently, the attention shifted again to the sediments in the caves of the Dachstein Massif. The reason for this were master's theses with a research focus on some of these caves (Salomon, 2015; Bethke, 2020). However, there were still many open questions, especially regarding the clay mineralogy of the sediments. Therefore, this master's thesis has the aim to analyse in particular the clay mineralogy of samples coming from four caves at different altitudes of the northern rim of the Dachstein Massif: Dachstein-Mammuthöhle, Dachstein-Rieseneishöhle, Günter-Stummer-Höhle, and Hirlatzhöhle. Not only the clay minerals were of interest, but also further sedimentological parameters were determined. These are the bulk mineralogical composition, the grain size distribution, as well as the content of the organic carbon of the different sediment layers. Also, thin sections of rock samples were made. In addition, the results should be compared to reference samples examined with the same criteria. The samples were taken of sediments from two caves outside the Dachstein Massif: Eisriesenwelt (Tennengebirge), and Schönberg-Höhlensystem (Totes Gebirge).

The work aimed at a better and more comprehensive understanding of the sediments and their origin, respectively deposition conditions. Moreover, a specific focus lied on a sediment that represents the top of a widespread profile and shows a bright beige and darker brown varve-like lamination. The question whether and how these laminae differ sedimentologically was investigated. Also, to what extent evidences can be found that the laminae are really varves was pursued.

2 Geography and Geology

In the following, the geographical locations of the caves of interest (Fig. 1) are described in more detail and a look is taken at the geological situation of the study area.

2.1 Location of caves

The main focus of this work is on four different caves – Dachstein-Mammuthöhle, Dachstein-Rieseneishöhle, Günter-Stummer-Höhle, Hirlatzhöhle – that are located in the northern rim of the Dachstein Massif, a part of the Dachsteingebirge in Upper Austria. The Dachstein Massif extends over the federal states of Upper Austria, Salzburg as well as Styria (Fig. 2).

With regard to comparison, samples of two other caves that are situated in the adjacent mountain ranges were also included in the analyses. Tennengebirge is in the W and Totes Gebirge NE of the Dachstein Massif. The reference samples were derived from Eisriesenwelt in Tennengebirge (Fig. 3) in Salzburg and from Schönberg-Höhlensystem in Totes Gebirge (Fig. 4). The mountain range of Totes Gebirge extends in Upper Austria and Styria. Totes Gebirge is known as the largest karst area in Austria (702 km^2; Geyer et al, 2016; Spötl & Plan, 2016), followed by Dachstein Massif (576 km^2; Spötl & Plan, 2016). Tennengebirge with an extent of 259 km^2 (Spötl & Plan, 2016)and a height up to 2,430 m a.s.l. is also considered being rich in number as well as size of caves (Pointner & Klappacher, 2016). The key data of the different caves were taken from the spelix database, an Austria-wide cave index (spelix.at).

Dachstein-Mammuthöhle

The Dachstein-Mammuthöhle (Fig. 2; Austrian Cave Register #1547/9; UTM coordinates of the main entrance 33T 402,829 / 5,265,422), later on only called Mammuthöhle, is located S of Obertraun at 1,321 m a.s.l. Up to today, 67.7 km were measured of the cave system, and it has an altitude difference of 1,207 m. The cave extends beneath Angeralm, Schönbergalm, Mittagskogel, and at the edges it also reaches below the Krippenstein (Seemann, 1973). It was discovered in 1910 (Bock & Lahner, 1913a) as the first large cave system in the NCA (Plan & Xaver, 2010) and nowadays, a small part of Mammuthöhle is a show cave.

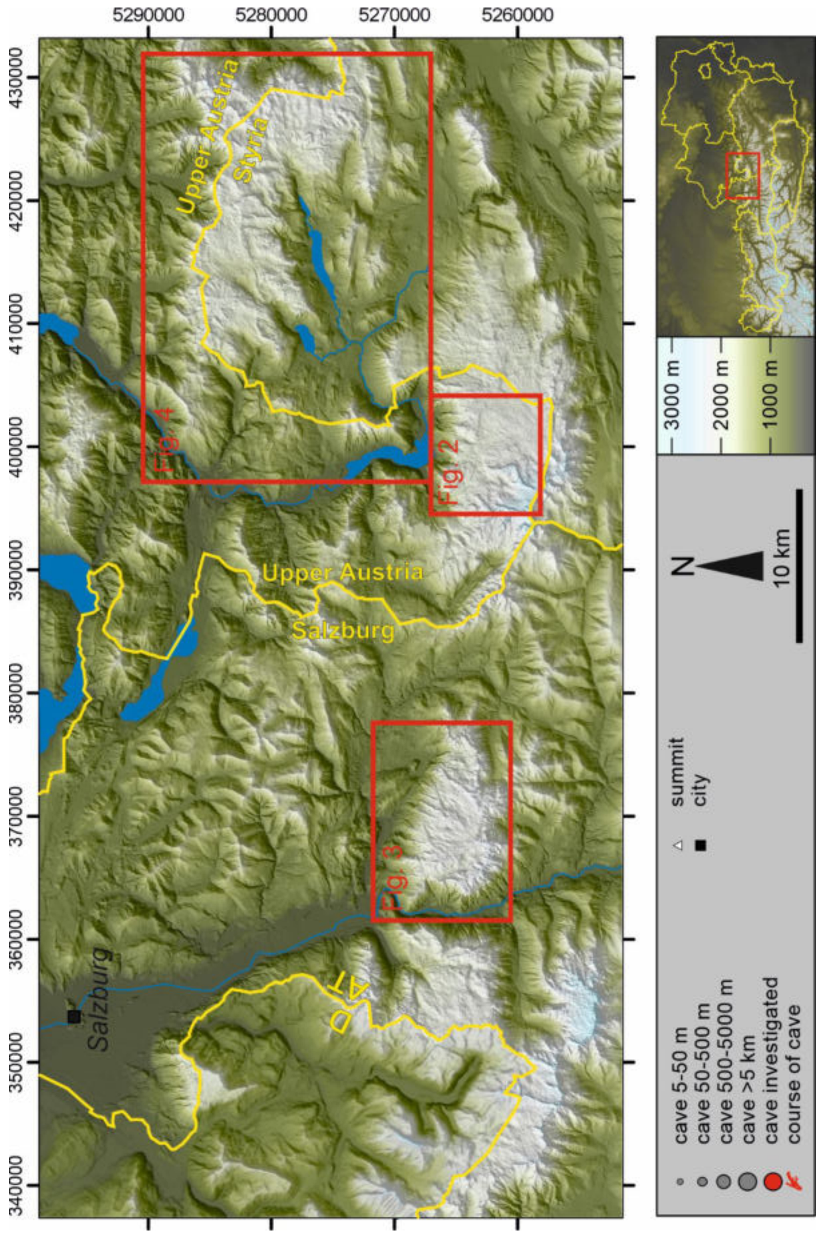

Figure 1: Location of the study areas Dachstein Massif (Fig. 2), Tennengebirge (Fig. 3), and Totes Gebirge (Fig. 4). Coordinates: UTM 33T. The map legend is also valid for the following more detailed geographic maps (modified from Plan and Bauer, 2016).

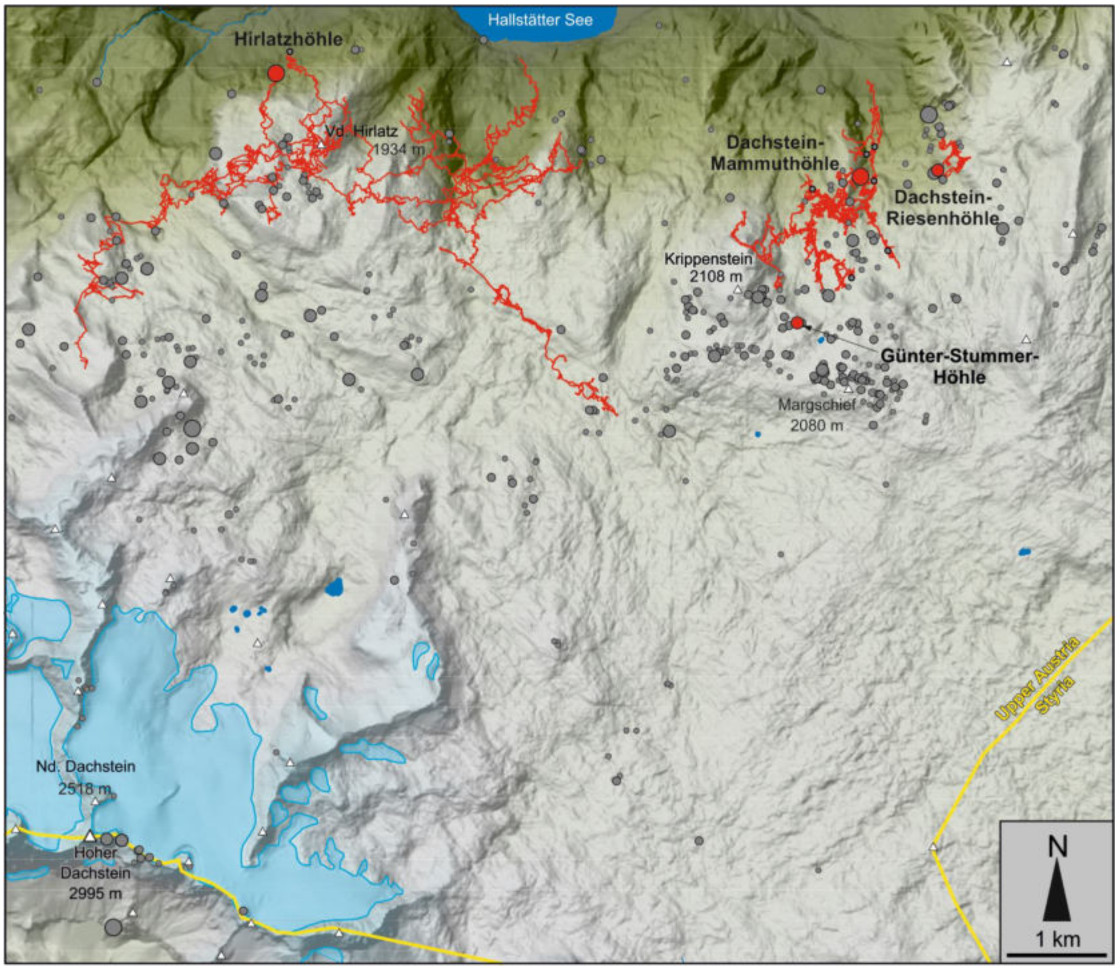

Figure 2: Dachstein Massif with all known (grey) and the studied (red) caves (modified from Plan and Bauer, 2016). Explanation, see Fig 1.

Dachstein-Rieseneishöhle
Dachstein-Rieseneishöhle (Fig. 2; #1547/17; 33T 403,564 / 5,265,391) - from now on only called Rieseneishöhle – opens at 1,421 m a.s.l. and is S of Obertraun. The explored length of the cave, which is located in Schönbergwand, is 2.7 km and the altitude difference 90 m. Like Mammuthöhle it is accessible from the middle station Schönbergalm of the cable car to Krippenstein. However, it is to the E of the middle station and not to the W like Mammuthöhle. It was also discovered in 1910 and was the largest ice cave in Europe at this time (Bock & Lahner, 1913b). It is used for commercial purpose as well.

Günter-Stummer-Höhle
Günter-Stummer-Höhle (Fig. 2; #1547/260; 33T 402,829 / 5,265,422) is the highest of the sampled caves at an elevation of 1,968 m a.s.l. Like Mammuthöhle and Rieseneishöhle it is located S of Obertraun. The cave has a known length of 993 m and a depth of 90 m.

Hirlatzhöhle
Hirlatzhöhle (Fig. 2; #1546/7; 33T 396,966 / 5,266,505), the third-longest cave of Austria with a known length of 113.6 km and a elevation difference of 1.6 km, is situated NE of Hallstatt. The main entrance is at 870 m a.s.l. on the foot of the N face of Mt. Hirlatz and was first entered in 1949 after two failed attempts (Leutner, 1998). Starting from there, the cave extends to the E to the karstic great spring named Kessel, to the S to Wiesberghaus, and in W direction beyond Mt. Grünkogel (Bossert & Buchegger, 1998).

Eisriesenwelt
Eisriesenwelt (#1511/24; 33T 363,955 / 5,263,545) is located in the SW part of Tennengebirge, NE of Tenneck at 1,641 m a.s.l. (Fig. 3). The cave, which is also a show cave and famous for its permanent ice, has a measured length of 42 km and an altitude difference of 442 m. Therefore, it is the largest cave system of Tennengebirge (Pointner & Klappacher, 2016).

Schönberg-Höhlensystem
Schönberg-Höhlensystem (#1626/55; 33T 409,055 / 5,285,655) in Totes Gebirge (Fig. 4) is by far the longest cave system of Austria, after a connection between Feuertal-Höhlensystem and Raucherkarhöhle could be found in 2007 (Zeitlhofer & Knobloch, 2008). It has a length of 153.1 km and a difference in altitude of 1.1 km. The location of Schönberg-Höhlensystem is S of Ebensee and N of Altaussee. The entrance Separatistenschacht is at an elevation of 1,718 m a.s.l.

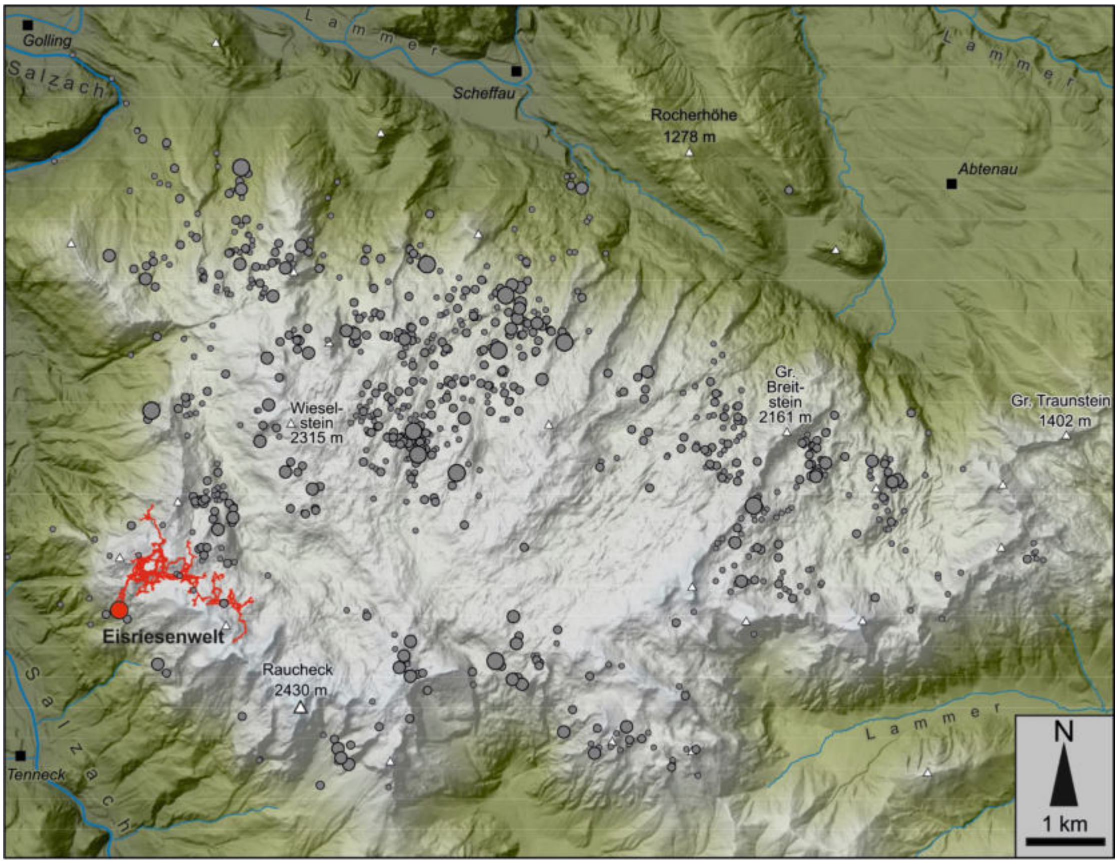

Figure 3: Tennengebirge with all known caves (grey) and the reference cave Eisriesenwelt (red; modified from Plan and Bauer, 2016). Explanation, see Fig 1.

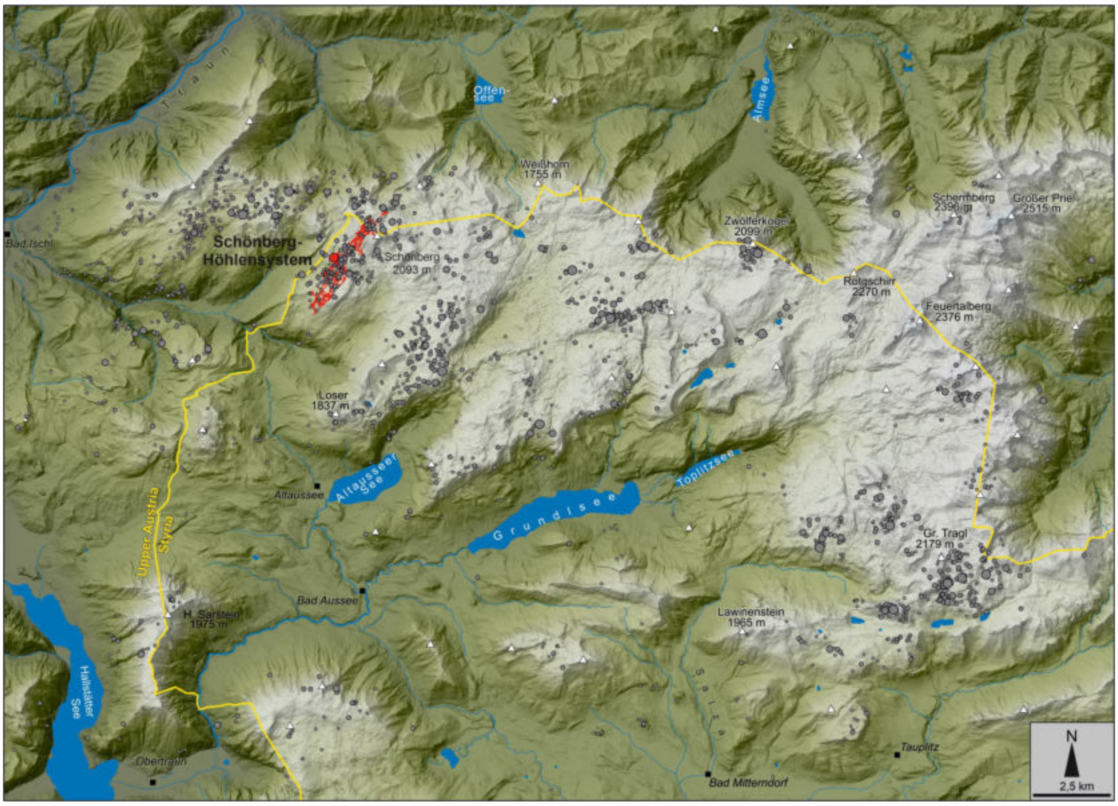

Figure 4: Totes Gebirge with all known caves (grey) and the reference cave Schönberg-Höhlensystem (red; modified from Plan and Bauer, 2016). Explanation, see Fig 1.

2.2 Geology

The study areas are located in the central part of the Northern Calcareous Alps (NCA), a part of the Eastern Alps (Fig. 5). The NCA are a nappe stack within the Austroalpine nappe complex that is the topmost tectonic unit of the Eastern Alps. The NCA have an extent of 500 km length and 20 to 50 km width. They compose several nappe systems (Mandl, 2000). The Dachstein Massif belongs to the Dachstein nappes of the Juvavic nappe complex whereas Tennengebirge is a part of the Staufen-Höllengebirge nappe that was thrusted from SE onto the Totengebirge nappe where Totes Gebirge is located. Both of these nappes are included in the Tirolic nappe system (Tollmann, 1985).

Part of the plateaus of Dachstein Massif, Tennengebirge, and Totes Gebirge are mostly at altitudes between 1,800 and 2,500 m a.s.l. (Frisch et al, 2001). They consist of a sedimentary succession that was only locally metamorphically overprinted and therefore, the original features are often preserved. At the base there are Lower Triassic Werfener Schichten, which are siliciclastic sand- and mudstones, followed by Wettersteinkalk and Wettersteindolomit of Middle and Upper Triassic times (Mandl, 2000). Next, there is the most predominant sedimentary succession of Triassic Hauptdolomit, overlain after a transitional zone by Dachsteinkalk Formation with a possible thickness up to 2 km (Kuffner, 1998; Mandl, 2000). The carbonates are shallow platform as well as basinal carbonates of a passive continental margin (Mandl, 2000). On top of the succession there are remains of Hierlatzkalk and of the Augenstein Formation (Behm et al, 2016). Hierlatzkalk is a reddish Jurassic limestone that developed in basinal conditions (Mandl, 2000). It only occurs as crevasse fillings of the plateau (Behm et al, 2016).

The sedimentation of the Augenstein Formation began after an uplift pulse in the Central Alps around Early to Late Oligocene. The central and eastern NCA were the lowlands next to the marine molasse to the N and therefore functioned as the deposition site for the Augenstein Formation (Frisch et al, 1998). The catchment area of the material consists of Variscan Paleozoic terrains from the E part of the Eastern Alps as well as the post-Variscan Austroalpine crystalline basement of the NCA (Frisch et al, 2001). Therefore, the Augenstein Formation is composed of pebbles as well as sandstone, which are rich in polycrystalline quartz, but also black carbonates, greenstones, or rhyolites are detectable (Winkler-Hermaden, 1957; Frisch et al, 2001). The lithologies are weakly metamorphosed with a grade up to greenschist or partially even amphibolite facies (Frisch et al, 2001). The Augenstein Formation had an estimated thickness of several 100 m (Winkler-Hermaden, 1957) or even 1.3 km to more than 2 km (Frisch et al, 2001).

The Augenstein Formation deposited onto the Dachstein paleosurface. The paleosurface developed prior from latest Eocene to Early Oligocene (Frisch et al, 1998) and was formed as a hilly karstified surface. It is best preserved on the

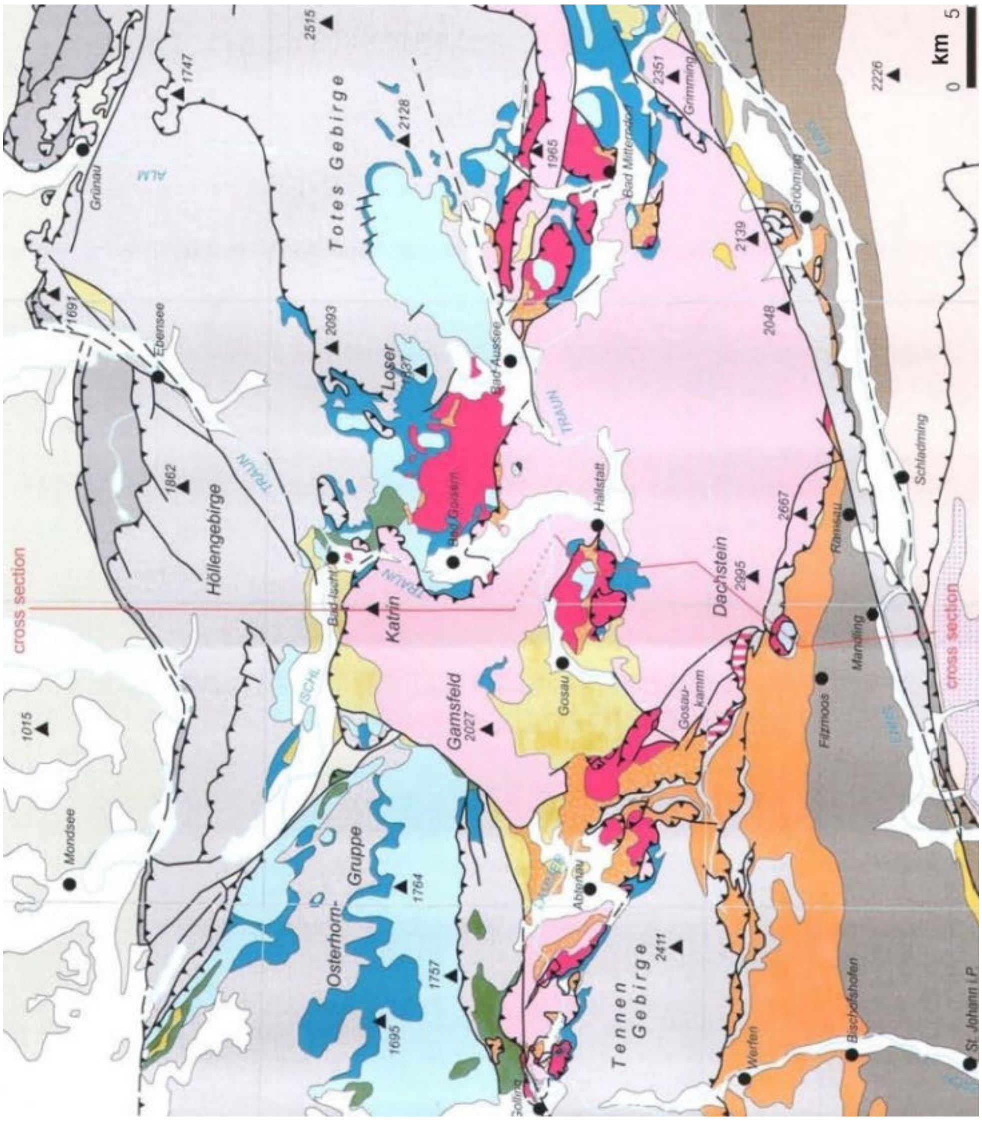

(a)

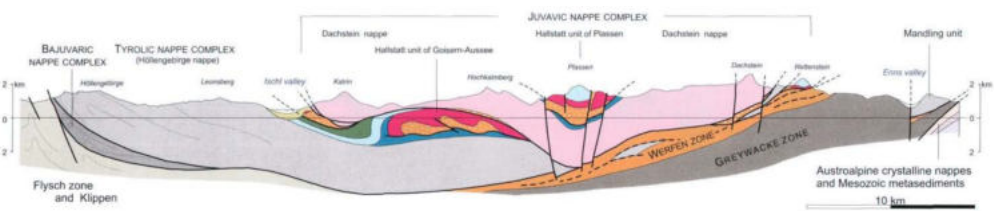

(b)

Figure 5: (a) Geological map of the NCA in the Salzkammergut Region. (b) Cross-section along the red line, showing the nappe complex (Mandl, 2000).

Dachstein massif. Also, the Tennengebirge as well as Totes Gebirge are considered having modified Dachstein paleosurfaces (Frisch et al, 2001).

Following the collision of the European and the Adriatic plates, lateral E-directed extrusion occurred mainly in Early and Middle Miocene (Fig. 6; Mandl, 2000). As a consequence of the highly active tectonically extensive phase, the N-directed drainage system of the Eastern Alps changed drastically.

Therefore, any further deposition of the large gravel fans of the Augenstein Formation terminated. Instead, the erosion of the sediment occurred (Frisch et al, 1998). The remains of the Augenstein Formation are rarely in autochthonous positions preserved in depressions of the karst plateaus, but mostly allochthonous in form of accumulated loose pebbles (Frisch et al, 2001) and as weathering products (Plan et al, 2009).

In addition, also in Miocene times the exhumation of the central part of the Eastern Alps took place (Fig. 6; Frisch et al, 2000). However, the process of uplifting was occurring in several pulses rather than being continuous. The erosion was happening mainly subterraneous and therefore several mostly horizontal cave levels were developed during stages of tectonic quiescence, only controlled by the general main drainage system (Haseke-Knapczyk, 1989; Frisch et al, 2001). The cave levels are intersected by vertical shafts whose formation occurred during as well as after stages of uplift (Frisch et al, 2001).

The NCA are characterised to have cave systems that developed in two stages: first, the development was under phreatic as well as epiphreatic conditions, followed by younger cave passages that are of vadose origin (Audra et al, 2002; Plan et al, 2009; Plan & Xaver, 2010). The older stages are developed as galleries, mazes, or rarely also pits, whereas canyons and shafts are characteristic of vadose formation (Plan & Xaver, 2010).

The different cave levels are from top to base the Ruin, the Giant, the Berger, and the Spring or Source Cave Level (Haseke-Knapczyk, 1989; Frisch et al, 2001). The cave levels contain a span of elevation of several 100 m, however, the absolute altitude differs depending on the massif (Fischer, 1990).

The Ruin Cave Level often has small- or medium-sized caves (Kuffner, 1998) that are already partially destroyed due to ongoing surface erosion. Usually, this level is located near the Dachstein paleosurface (Frisch et al, 2001; 2002) between 2,200 $\pm$ 300 m a.s.l. and was developed in middle Eocene to Early Oligocene (Frisch et al, 2002). Günter-Stummer-Höhle is associated with the Ruin Cave Level.

In contrast, the Giant Cave Level is characterised by large systems of cave passages that can have lengths of several tens of kilometres (Fischer, 1990; Kuffner, 1998). This cave level was probably formed in the Upper Miocene and Pliocene, and it is situated several 100 m below the Dachstein paleosurface (Frisch et al,

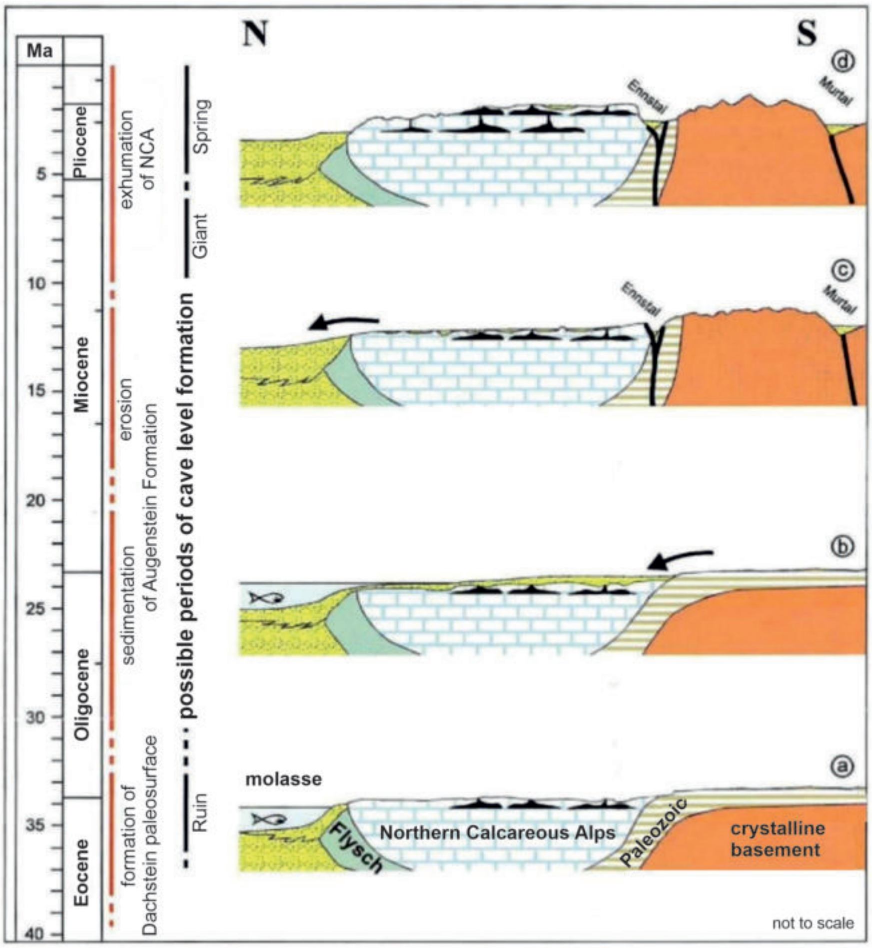

Figure 6: Geomorphological evolution of the central part of the Eastern Alps, starting with the Late Eocene. (a) Development of Dachstein paleosurface and of the Ruin Cave Level. (b) Deposition of the Augenstein Formation onto the paleosurface. (c) Erosion and redeposition of the Augenstein Formation after a tectonically extensive phase terminated the sedimentation. (d) Exhumation of the NCA and therefore development of the Giant and Spring Cave Level (modified from Frisch et al, 2002).

2001; Häuselmann et al, 2020). This means for the NCA an altitude between 1,200 and 1,800 m a.s.l. (Fischer, 1990) and therefore, the cave systems of Mammuthöhle and Rieseneishöhle, Eisriesenwelt, as well as Schönberg-Höhlensystem belong to the Giant Cave Level (Pointner & Klappacher, 2016; Häuselmann et al, 2020).

The next lower level is the Berger Cave Level that is located between 900 and 1,000 m a.s.l. (Haseke-Knapczyk, 1989). However, this cave level is not always seen as an independent level (Frisch et al, 2002).

At the base, there is the Spring Cave Level, whose formation began in Pliocene. The mouths of the (epi)phreatic, hydrologically active systems are near the valley floors (800 m a.s.l.; Frisch et al, 2001; 2002). Hirlatzhöhle is approximately at this altitude level, but still can not be assigned to a cave level (Häuselmann et al, 2020).

In Pleistocene times, the NCA were glacially overprinted by Alpine ice stream networks during glacial periods (Plan & Xaver, 2010). This phase was most characteristic for today's landscape appearance (Behm et al, 2016). Due to the extent of the ice streams, the input as well as the output areas were blocked by the glacier (Ford & Williams, 2007; Plan et al, 2009) and their glacial sediments. As a consequence of the obstructing pre-existing springs, the karstic water level started to rise several 100 m. This caused a drastical decrease in flow velocity to the point of stagnant water conditions and a deposition within the caves of fine-grained sediments enriched in carbonates is possible (Schauberger, 1957; Audra et al, 2006; Plan & Xaver, 2010).

3 State of Research

Cave sediments are important characteristics of caves and can provide evidences about the history of cave development. Therefore, a lot of work was carried out on the general aspects of the sediments, but also on the caves of the study areas.

3.1 General aspects on cave sediments

In principle, cave sediments can be classified into three different types: chemical, clastic as well as biogenic. Generally, the mineralogical composition is largely depending on the source (Springer, 2012).

This work focuses on clastic cave sediments. Clastic cave sediments can have two different origins: allochthonous or autochthonous. Sediments from an autochthonous origin evolve either from insoluble residues of the bedrock (Farrant & Smart, 2011) or walls and ceilings of the caves. The latter happens due to breakdowns of pre-existing zones of weakness (bedding planes, faults, joints) or collapses induced by decreasing mechanical strength of rock mass or frost weathering (Sasowsky, 2003).

Nevertheless, the main part of the clastic sediments are allochthonous and therefore have an external origin (Gillieson, 2003). The material is derived from erosion and followed by transport (Farrant & Smart, 2011). The way of transport into caves, which are an ideal sediment trap, is gravitational and lateral by mainly fluviatile processes (Farrant, 2003). The grain sizes of the clastic sediments are a sure indication for the flow velocity in the area (Häuselmann, 2004). Also, ice, wind, or gravity in steep parts as transport media are possible, especially in entrance areas (Farrant, 2003). The incoming material may be already weathered as well as sorted before it enters a cave system. Once in this unique surrounding, the chemical weathering is reduced by the conditions of complete darkness, constant temperatures, and high humidity. Therefore, the water is often saturated with respect to calcite (Gillieson, 2003).

For the cave sediments different facies types were developed: channel, thalweg, slackwater, diamicton, and backswamp facies (Fig. 7; Bosch & White, 2004). The concept of these facies is used in order to reconstruct the geomorphic history as well as the depositional relationships of the sediments (Springer, 2012). The facies types are depending on the mechanism of transport as well as the mechanism of deposition. However, the distinction of the facies is made on size of particles and the sorting degree (Fig. 8; Bosch & White, 2004).

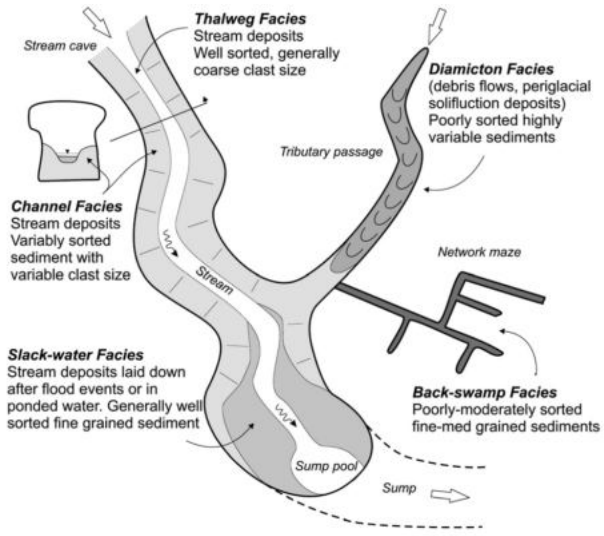

Figure 7: Clastic cave sediments classified in schematic passages of a stream cave (Farrant & Smart, 2011).

The channel facies is characterised by sediments that were transported mainly as bedload. As a result of different flow conditions, the material is roughly stratified and has particle sizes of silt, sand, or gravel. Within the beds, which have a variable thickness, the sediments are well or partially sorted. Sediments of this facies type assemble the main part of the material within the cave passages (Bosch & White, 2004).

The thalweg facies can be recognised due to a good sorting of coarse material. The coarseness is caused due to active streams that were cutting through the channel facies as secondary streams and transport this material as bedload. Meanwhile, the finer material is sorted out and as a result, the material is coarser and shows a better sorting than the sediments of the channel facies. The facies can only develop if the stream has at least a moderate flow velocity (Bosch & White, 2004).

The slackwater facies develops after muddy floodwaters become ponded in cave passages and the suspended load, which consists of clay or silt, is able to sediment. This occurs under epiphreatic or phreatic conditions (Bosch & White, 2004) and only if nearly stagnant water as well as the presence of sufficient material is provided (Seemann, 1973). Furthermore, the absence of coarser particles, the high percentage of clay fraction, and the fact that there is almost no interaction with the layers below are also indicators for a deposition within a calm environment

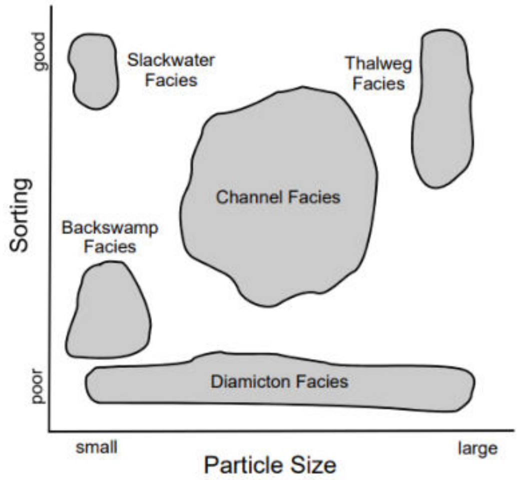

Figure 8: Sediment facies classified regarding particle size and sorting (modified from Bosch & White, 2004).

(Franke & Ilming, 1963). Due to the accumulation from the suspension, the sorting of the fine-grained material is good, and often it is well laminated. Mostly, the deposited suspended load represents the final layer of the cave sediments and at the same time is the most widespread disclosed one (Bosch & White, 2004).

The sediments of the diamicton facies deposit as suspended load of debris flows. For this reason, the material shows a wide range of particle size from clay to boulders, which implicates a lack of sorting, and it is also unbedded (Bosch & White, 2004).

The original sources of the backswamp facies are deposits of weathered bedrock or infiltrated material of overlying soil. The lateral transport is very limited, and the material consists mainly of clay and silt, but also silicified fossils, insoluble residues, or chert fragments can be found (Bosch & White, 2004).

3.2 Sedimentological work in the caves of the study areas

Looking at the cave sediments of the study areas Dachstein Massif, Tennengebirge, and Totes Gebirge in particular, some sedimentological work has already been undertaken in the last decades.

3.2.1 Mammuthöhle and Rieseneishöhle

In Mammuthöhle and Rieseneishöhle, cave sediments are abundant and due to recurrent characteristics a profile was recognisable. Therefore, an idealised profile was created by Bethke (2020) based on the cave sediments of these two caves (Fig. 9). This sediment profile is recurring in the caves of the Dachstein Massif.

At the base, on top of the bedrock, there is a greenish sediment mixture. It had variable particle sizes as well as a different good degree of sorting. Thus, it was assumed that there were several fillings in the course of time. The first fillings could have probably already happened within the first stages of the development of the caves. Observed imbrications indicated a paleoflow in W direction, at least in Mammuthöhle. The depositional facies were thalweg or channel facies, depending on the grade of sorting. Analysis of heavy minerals (Bethke, 2020) showed consistent results with studies in Hirlatzhöhle and Totes Gebirge (Kuffner, 1998). Therefore, a similar source area could be assumed. Since heavy mineral analysis of Augenstein clasts from all over the NCA were in accordance, modified Augenstein Formation as the source material for these depositions was presumed (Kuffner, 1998; Frisch et al, 2001; Bethke, 2020).

Next, there is a dark cave loam that appeared without lamination and had a low carbonate content (Bethke, 2020). It had a dark brownish colour and the presence of illite and goethite indicated soil material of interglacial periods as origin (Schachtschabel et al, 1984). The dark cave loam could be assigned to slackwater or backswamp facies (Bethke, 2020).

Above the dark cave loam may follow conglomerates and conglomeratic breccia of the diamicton facies that occurs only locally in Mammuthöhle. The sediment consisted mainly of carbonates, but also Augensteine and pseudo-pisolitic iron ore could be components (Bethke, 2020). The latter were pseudomorphs of pyrite and marcasite (Bauer, 1955). If the sediment was lithified, the cement was mainly calcite, clay, and sometimes limonite (Seemann, 1973).

The bright cave loam – first mentioned by Seemann (1973) by the German name "Heller Höhlenton" – could only be found as the top layer of the sequence up to the Giant Cave Level. There, its thickness seemed to be 1 m at most, and in general, it is increasing with a decreasing sea level (Bethke, 2020) to the extent of several meters (Schauberger, 1983). The bright cave loam was probably formed under conditions of slackwater facies (Bethke, 2020). The sedimentation in stagnant water conditions may have been induced due to Pleistocene glaciers blocking the valleys and therefore most of the cave entrances were closed by the ice. As a result, backflooding occurred and in interglacial times the cave systems were filled with subglacial meltwater (Franke & Illming, 1963; Schauberger, 1983). The water transported mainly fine fraction into the cave and it deposited in thin, varve-liked structures (Häuselmann, 2004). Analyses showed that the sediment was mostly

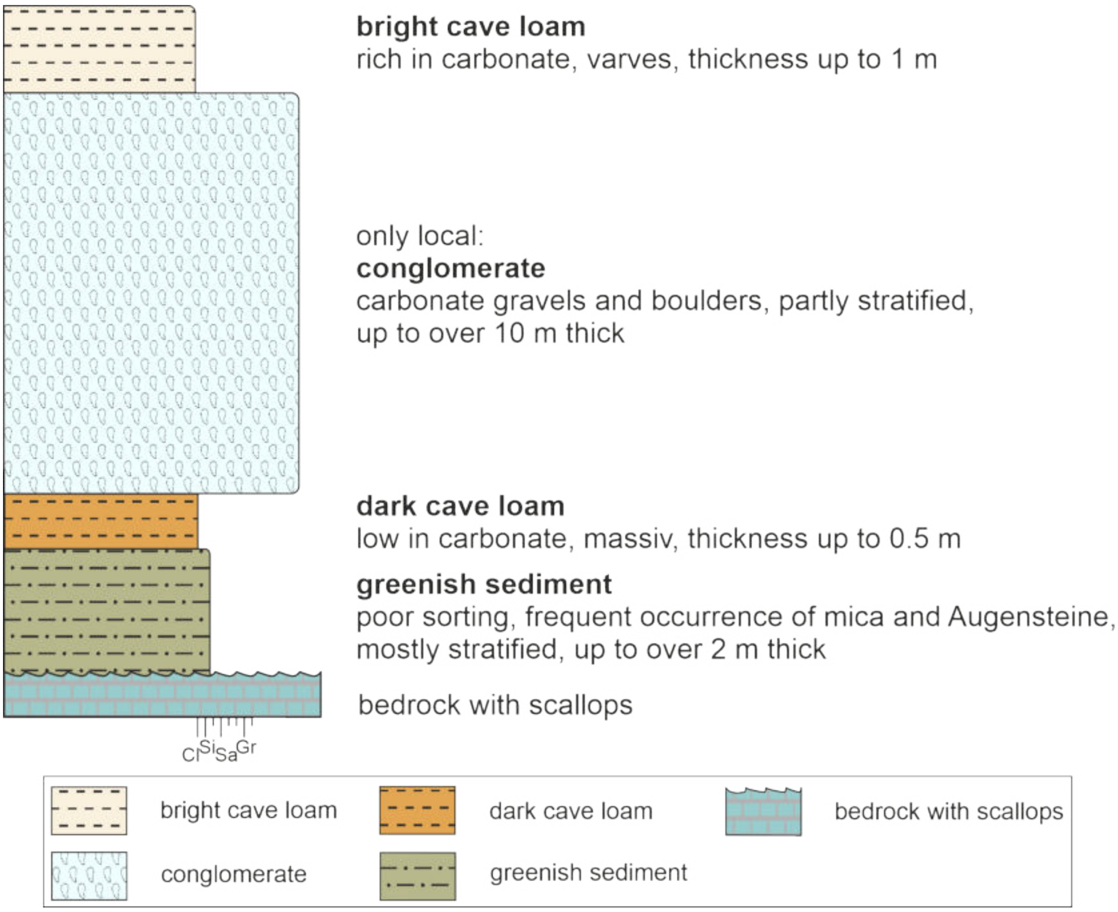

Figure 9: Idealised profile of cave sediments in Mammuthöhle and Rieseneishöhle. Subsequent faults and redepositions are not considered (modified from Bethke, 2020).

composed of clay (50.4 %) and silt (42.7 %; Franke & Illming, 1963). The layers consisted of alternating bright and dark laminae with a thickness within mm-range (Seemann, 1973). This structure was considered to be due to seasonal or longer climatic rhythms (Spöcker, 1925). After the retreat of the glacier, there was runoff of the backwater waters and thus also partial erosion of already existing deposits occurred (Schauberger, 1983).

The bright cave loam consisted in general of calcite, quartz, dolomite, ankerite, muscovite, chlorite, biotite, and K-feldspar when looking at the bulk composition (Salomon et al, 2018). Due to the surrounding geology, a high content of carbonate was expected and characteristic for the sediment (Häuselmann, 2004). Regarding the clay mineralogy it consisted of illite, smecite, chlorite, and kaolinite. The compositions were very similar for the bright and the dark laminae, nevertheless, there were differences detectable (Salomon et al, 2018). The brighter laminae were analysed as being enriched in carbonates (Bethke, 2020) and in quartz (Salomon, 2015). In contrast, the darker laminae showed a reduced amount of mica and the clay minerals are more abundant. These laminae were enriched in clastic material (Salomon et al, 2018). As already mentioned, the laminating was assumed to be annual varve-like depositions of fluvio-lacustrine sediments (Spöcker, 1925) caused due to rhythmical climatic variabilities (Seemann, 1973).

Heavy mineral analysis showed predominant presence of garnet, epidote, zoisite, hornblende, and opaque minerals in the sediments of Mammuthöhle and Rieseneishöhle. (Seemann et al, 1999; Bethke, 2020). However, zircon was enriched in the sediments of Rieseneishöhle (Seemann et al, 1999). Bright cave loam of Hirlatzhöhle had epidote, zoisite, and zircon as the main part of the heavy mineral fraction (Salomon et al, 2018). In addition, a study in the western part of Totes Gebirge was in line with these results (Kuffner, 1998). The analyses led to the conclusion that the source rock had amphibolite facies and was later overprinted with conditions of greenschist facies (Salomon, 2015). Regarding the provenance of the sediments the results were concordant with being originally of the Augenstein Formation from the Austroalpine crystalline Basement (Frisch et al, 2001) and the presumption that the main source of the clays in caves in the NCA were the weathering products of this formation (Plan et al, 2009).

In Mammuthöhle attempts of dating the bright cave loam were carried out by determining the age of flowstone that was directly above and underneath the sediment. The results of the uranium-thorium dating showed a possible depositional range between 715 and 407 ka (Bethke, 2020) respectively a minimum age of the sediment of 7 ± 2 ka (Plan & Xaver, 2010).

In comparison to the allochthonous material, the autochthonous sediments are mainly present as breakdown material in large-scale passages. Especially in Rieseneishöhle breakdown material is the topmost sediment layer in large chambers and the bright cave loam is missing in these areas. Therefore, Seemann et al (1999) assumed that the loam was older and was covered. Due to the thickness of the breakdown layer of up to 60 m and the great areal extent, the older sediments or the bedrock are hardly visible (Seemann et al, 1999). In order to obtain a sediment profile, excavations were usually necessary (Bethke, 2020).

3.2.2 Hirlatzhöhle

In Hirlatzhöhle the cave sediments consisted mainly of slightly consolidated gravel bed loads of siliceous carbonates directly on the basement rock. Schauberger (1983) proposed that these carbonates were "Doggerkieselschiefer" and from Middle Jurassic times. In the E part there were carbonate conglomerates (Schauberger, 1957). In the conglomerates and in the Hirlatzhöhle in general, the amount of Augensteine was small, especially compared to the sediments of Mammuthöhle. According to Schauberger (1983), the cover of Augensteine on top of the Dachstein paleosurface W of Gjaidalm was missing or only sparsely developed.

The youngest and most widespread sediment is the bright cave loam, described as silty floury sand with a distinctive lamination. It is the covering layer in the cave passages and the higher it gets, the finer and thicker it is. Therefore, the yellowish-brown sediment can have a thickness up to several meters (Schauberger, 1983). In Hirlatzhöhle, the lamination of dark and light laminae is particularly well pronounced (Salomon et al, 2018). Measurements of the stable isotopes ^{13}C and ^{18}C in the fine sediment showed that the carbonate content originates exclusively from the erosion of the surrounding Dachsteinkalk Formation (Pavuza, 1998).

3.2.3 Totes Gebirge and Tennengebirge

The cave sediments of Totes Gebirge mainly comprise loam and sand, but also pebbles could be present. According to Kuffner (1998), the sediments could have three different origins. First, the material originated autochthonously from the surrounding geology (Dachsteinkalk Formation, chert), this included also fossil residues like nanofossils and foraminifera. Next, the material was washed into the caves from the outside and therefore remains of the Augenstein Formation or chert and radiolarites as residues of a former overlaying lithology occurred in the sediment. Last, the most rarely found sediment was from materials formed in the caves. This included calcite crystals, flowstones, and sandstones.

The occurring sediments in Totes Gebirge are in accordance with the deposited material in the caves of Tennengebirge. Clastic sediments found in the Ruin Cave Levels of Tennengebirge are cemented sands with components of quartz and Fe-oxides and solidified clay. In the clay sometimes gravels of Augensteine and Fe-oxide nodules are present. In the caves of the Giant Cave Level there are sands and fine silts. These sediments originated from the weathering as well as reworking of the Augenstein Formation and the metamorphic zones of the central Alps in general (Audra et al, 2002).

In Eisriesenwelt, breakdown material occurs very often and allochthonous sediment is rare. However, a repeating sediment profile was discovered, but this mostly required excavation and drilling. The base of the profile is a brown-greenish sediment that was abundant in Augenstein. The grain size distribution of the material ranged from silt to pebbles and had therefore a poor sorting. The younger sediment on top is a red-brownish clay (Plan et al, 2021).

4 Materials and Methods

In the studied caves, samples were collected and analysed with different sedimentological methods, which are described in more details below. A summary of the methods used for specific samples can be seen in Tab. 1.

4.1 Outcrops

In four of the six caves of interest – Mammuthöhle, Rieseneishöhle, Hirlatzhöhle, Günter-Stummer-Höhle – the outcrops were examined after sedimentological aspects and samples were taken (Tab. 1). The sediments as well as the sedimentary rocks were evaluated according to their thickness, their – as far as recognisable – composition, the colour, their texture, and further characteristics. These recorded data, together with the results of analytical methods, later resulted in profiles in which the sampling locations were marked.

In some outcrops, a hand-operated earth drill was used. With this, a depth of up to 3.5 m could be reached under optimal conditions. Sample material could be taken with the help of the helical tip.

The samples from Eisriesenwelt and Schönberg-Höhlensystem were provided by Lukas Plan without the author having been on site, as well as sample HIH 20 from Hirlatzhöhle.

4.2 X-ray diffraction

For the X-ray diffraction (XRD) analysis for the bulk samples, first of all, a part of the sample material had to be dried at 60 °C and then finely ground using an agate mortar. After, the material was pressed into the designated sample holder. Next, the measurements were carried out with a PANanalytical PW3040/60 X'Pert PRO diffractometer using a copper $K\alpha$ radiation at 40 kV and 40 mA. The analyses were run at a range from 2° to 70° 2θ angle. All the settings were set with the program X'Pert Data Collector. Finally, the results were interpreted with the program X'Pert HighScore Plus, a database of minerals for the suitable peak patterns. The program X'Pert Data Viewer was used for labelling as well as comparing the diffraction diagrams.

Table 1: Sample list and the analyses used. DRH = Rieseneishöhle, ERW = Eisriesenwelt, GSH = Günter-Stummer-Höhle, HIH = Hirlatzhöhle, MH T = Mammuthöhle, SHS = Schönberg-Höhlensystem.

sample	outcrop	position	XRD bulk composition	XRD texture free	XRD clay mineralogy	particle size analysis	TOC	thin section
MH T01	1	Sklavengang	x		x	x	x	
MH T02	1	Sklavengang	x			x	x	
MH T03	3	Krippensteingang, shortly before Huziwand	x		x	x	x	
MH T04	3	Krippensteingang, shortly before Huziwand	x			x	x	
MH T05	3	Krippensteingang, after crossing	x			x	x	
MH T06	5	junction Solaris						x
MH T07	4	after junction Solaris, SS 100	x			x	x	
MH T08	6	Sklavengang	x		x	x	x	
MH T09	6	Sklavengang	x			x	x	
MH T10	6	Sklavengang	x			x	x	
MH T11	6	Sklavengang	x	x	x	x	x	
MH T12	14	Paläotraun	x				x	
MH T13	14	Paläotraun	x	x			x	
ERW KD	7	Kirchendach	x		x	x	x	
HIH 01	8	aufsteigender Tunnel, before ramp						x
HIH 02	9	aufsteigender Tunnel, upper part						x
HIH 03	10	Lehmklamm, orographically right	x	x	x	x	x	
HIH 04	10	Lehmklamm, orographically right	x	x	x	x	x	
HIH 05	10	Lehmklamm, orographically right	x				x	
HIH 06	11	Lehmbachschwinde						
HIH 07	12	between S-Gang and Brückenhalle	x	x			x	
HIH 08	12	between S-Gang and Brückenhalle	x	x	x	x	x	
HIH 09	12	between S-Gang and Brückenhalle	x	x	x	x	x	
HIH 10	13	between bivouac and junction Wasserklamm	x				x	
HIH 20	20	150 m after Wetterscheide						
SHS 02	15	E of Gigantendom			x	x	x	
DRH 01	16	Lehmhalle			x	x	x	
GSH 01	17	Mammutlabyrinth, SS 164	x		x	x	x	
GSH 02	17	Mammutlabyrinth, SS 164	x		x	x	x	
GSH 03	17	Mammutlabyrinth, SS 164	x		x	x	x	
GSH 04	18	Mammutlabyrinth, SS 125						x
GSH 05	19	Jausengang, SS 118						x

The principle of the XRD forms Bragg's Law, which describes the constructive interference of a diffracted X-ray beam with a certain wavelength and incidence angle at the lattice planes of the minerals. The sample is irradiated with a monochromatic X-ray beam that is produced in an X-ray tube with an anode made out of copper. The signal is only detectable in case a constructive interference occurs if the spacing of the lattice planes being integer multiples of the wavelength. The detector scans all angles and records the intensity of each reflection. The result is an individual diffraction pattern of each mineral, allowing its identification. Usually, it is presented as a XRD pattern that plots the intensity I against the diffraction angle 2θ.

Every sediment sample was analysed with XRD in order to get the mineralogical bulk sample composition, except the ones coming from Schönberg-Höhlensystem (SHS 02) and Rieseneishöhle (DRH 01). The mineralogical composition of the latter was already analysed by Bethke (2020).

In addition, some samples (MH T11, MH T13, HIH 03, HIH 04, HIH 07, HIH 08, HIH 09) were also analysed with regard to the quantification of the minerals. Therefore, the same dried and ground material as for the composition of the bulk sample was taken, however, the sample preparation is different. The sample surface had to be texture free, which was achieved with a sandpaper on the carrier surface while infilling the material. Afterwards, the same instrument and the same settings (40 kV, 40 mA, $2-70° 2\theta$) were used for measurements. The interpretation was undertaken using the method developed by Schultz (1964). The intensities of the main diffraction peaks of the nonclay minerals and of the collective peaks of the clay minerals (19.9° 2θ, 34.6° 2θ) were determined with the program X'Pert HighScore Plus and corrected with an individual intensity factor for each mineral. The percentage of the total clay minerals of the sample is given by the mean value of the first two corrected collective peaks. The exact subdivision of the total clay minerals was made on the XRD pattern of the clay mineralogical fraction of the sample, which was treated with ethylene glycol (description of methodology see 4.3). After the baseline was drawn, the peak areas of the main peaks were analysed and corrected by means of a separate intensity factor for each mineral.

4.3 Clay mineralogy

The focus of clay mineral analysis was on the bright cave loam, therefore, all these samples were analysed. In addition, a selection of samples of greenish sediment (MH T08), dark cave loam (MH T01, MH T03, GSH 01, GSH 02, GSH 03, DRH 01), and reference specimen (ERW KD, SHS 02) were measured.

In order to analyse the clay minerals of the samples, the clay fraction had to be extracted first. To begin with, the organic matter had to be removed. Therefore, about 10 g of the original sample material was mixed in a beaker with 100 to 150 ml of a 1:1 mixture of H_2O_2 and ionised H_2O. In case the reaction was very strong, ionised H_2O was added. Until the reaction was finished, the sample was in a drying oven at 40 ℃ and stirred regularly. Also, an ultrasound treatment was done for 2 minutes at 400 W. In the beaker there should be 300 to 400 ml liquid, otherwise, ionised H_2O has to be added up to this amount.

Next, the suspension was poured into an Atterberg cylinder and ionised H_2O was filled up to 30 cm (Fig. 10). In case the mixture flocculated, some of the sediment mixture was discharged back into the beaker and a spatula tip of sodium tripolyphosphate was added. After the calculation of Atterberg, it takes 24 hours and 33 minutes at room temperature to sediment everything greater than 0.0002 mm (clay accumulation) with the height of this cylinder (Köster, 1964). Last, the cylinder was emptied, and the collected clay dried at 40 ℃ in the drying oven.

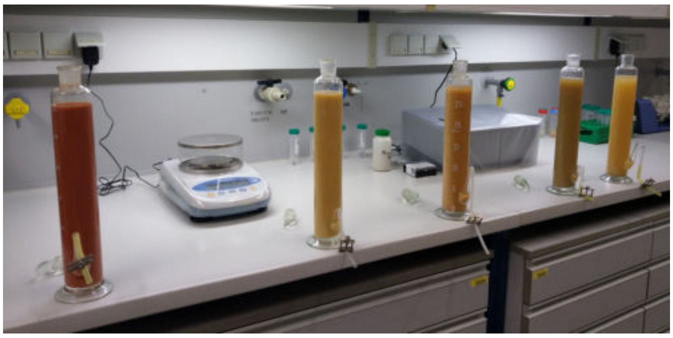

Figure 10: Sedimentation of sample material in Atterberg cylinders in order to get the clay fraction.

For the XRD measurements, the dried material was homogenised by a mortar and 50 mg was weighed twice into a test tube. One test tube was filled with 50 ml of KCl and the other centrifuge tube with 50 ml of $MgCl_2$. The test tubes were rotated permanently with a machine for approximately 24 hours and then centrifuged in order to separate the salt. The centrifugation was repeated twice with different settings (first circuit 5 min, 1,500 revolutions per minute; second circuit 10 min, 4,000 revolutions per minute) and in between the liquid of the test tube was emptied and refilled with 50 ml ionised H_2O. After the second circuit, only 5 ml was refilled and the mixture was homogenised by an ultrasonic probe (1 min, 21 % performance).

For every sample, three glass discs had to be prepared (Fig. 11). With a pipette 1 ml of sample liquid was put on each disc. Two glass slides saturated with potassium and one with magnesium saturated sediment were prepared and air dried. Furthermore, the samples saturated with potassium were either treated with ethylene glycol or tempered at 550 °C, whereas the samples saturated with magnesium were saturated with glycerol.

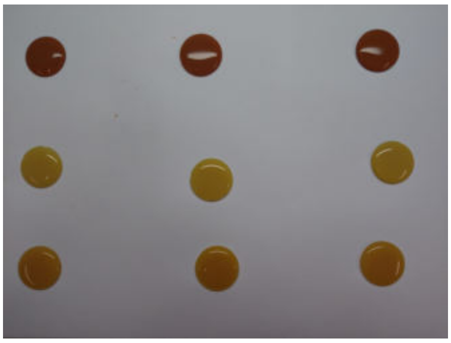

Figure 11: Preparing glass discs for XRD of the clay mineralogy. Each row represents a sample, two discs have material saturated with potassium, one with magnesium.

The X-ray diffraction measurements were undertaken with a PANanalytical PW3040/60 X'Pert PRO diffractometer. A copper Kα radiation was used at 40 kV, 40 mA, and covering a 2θ angle range from 2° to 40°. In total, each sample had to be measured five times: magnesium saturated (Mg), saturated with glycerol (Mg-Gly), potassium saturated (K), sated with ethylene glycol (KEG), and tempered (KT).

The XRD diagrams were combined with the program X'Pert Data Viewer and spacing values of lattice planes (d-values) in angstrom of the peaks were labelled. Due to the overview of the peaks in the different treated stages, the clay minerals could be identified. The identification is based on distinguishing the basal reflections of the minerals. The different treatments of the samples are necessary to identify expendable and heat sensitive minerals.

Although XRD analysis for clay minerals includes a range from 2° to 40° 2θ, most of the diagrams show only x-axis with values up to 28° 2θ. This is due to a high intensity of calcite in the bulk sample composition. This mineral has its dominant peak at 29.43° 2θ and the scaling factor would minimize the peaks of the clay minerals and they could be missed.

4.4 Grain size analysis

The procedure for the analysis of the grain size distribution is at the beginning the same as the clay mineral preparation for the XRD. This means, a mixture of ionised H_2O and H_2O_2 at the rate of 1:1 was added to 10 to 15 g of the original sample material. In case it shows a strong reaction, additional ionised H2O is needed for dilution. Until the mixture reacted off, it was in a dry oven at 40 °C. Afterwards, an ultrasound treatment was done. Each sample was stirred and had a treatment for 2 minutes with a high output.

Next, wet sieving, which means the material is washed manually with water, was undertaken. Therefore, sieves with different mesh widths (63, 125, 250, 500 µm) were used and built as a coarsening upward steeple. The smallest fraction (< 63 µm) was collected during the first run of sieving and then put into a beaker for sedimentation in the water column. The remaining material is sieved with coarsening sieve order and put directly into a dry oven at 60 °C. When the sedimentation of the fine fraction was finished – the water appears clear – the water was drained and the material was dried as well.

As soon as the different grain size fractions were dried, they were weighted. In addition, the fine fraction was analysed more specific with a micrometics Sedigraph III Particle Size Analyser. Therefore, the material was pounded carefully without generating a man-made grain size. About a spoonful was put into a beaker so that the bottom was covered and 40 ml of the liquid that was also used for calibration and rinsing of the sedigraph is added. Before the mixture was put into the sedigraph for grain size measurements, it had to be dispersed twice with an ultrasonic homogenizer for about 1 minute and an output of 20 %.

The sedigraph determines the particle size by using an X-ray beam. The beam is projected through a cell that is filled first by the reference liquid in order to get a baseline of the X-ray intensity and afterwards with the homogenised suspension. The material in suspension is sedimenting and the decrease in particle size within the measuring area of the beam is monitored due to a change in the intensity.

The results of the sedigraph have to be converted into mass percent of the total weighted sample material. In doing so, it has to be considered that the results are not 100 % of the sediment, but only of the fraction smaller than 63 µm. Finally, using the mass percent of the various grain size fractions, a cumulative grain size distribution curve can be generated.

The analysis of the grain size distribution was undertaken for the samples MH T01, MH T02, MH T03, MH T04, MH T05, MH T07, MH T08, MH T09, MH T10, MH T11, MH T13, ERW KD, HIH 03, HIH 04, HIH 08, HIH 09, DRH 01, SHS 02, GSH 01, GSH 02, GSH 03. For the samples of the bright cave loam, there was no outcome from sieving due to the fineness of their material.

4.5 Total organic carbon

In general, carbon is present as organic (OC) or inorganic carbon (IC). For the main part, the minerals calcite as well as dolomite are the provider for IC. In contrast, OC is formed by organic matter like plants, animals, microorganisms, or elemental carbon. Total organic carbon (TOC) can be defined as all carbon from organic sources and total inorganic carbon (TIC) is carbon in the form of carbonate, bicarbonate, and dissolved carbon dioxide.

For detecting the TOC percentage of the samples, the instrument Leco RC612 multiphase carbon and hydrogen/moisture determinator was used. The analysing procedure was undertaken as follows: firstly, the sample was dried in a drying chamber at 60 ℃ and afterwards finely ground. Secondly, the material was weighed into a crucible with a maximum weight of 0.100 ± 0.002 g. This was conducted twice for each sample in order to have an internal control of the results. Next, one by one, the crucibles were put by an autoloader into the combustion tube of the furnace with a dual-stage heating ramp. At 550 ℃ the organic matter decomposes to CO_2, whereas at 1,000 ℃ the inorganic carbon can be determined. The gas produced was discharged into a catalyser and detected by an infrared detector. As a result, the analysing instrument provides values of percentage of TOC, TIC, and total carbon (TC). The percentage of TC is received by summation of TOC and TIC.

For the purpose of calibration, one standard for low CO_2 detection (502 – 905 Synthetic Carbon LCRM Carbon % 4.99 ± 0.05) and one standard for high CO_2 detection (502 – 926 Calcium Oxalate LCRM % weight loss at 200 ℃ 12.3 ± 0.1, at 450 ℃ 19.5 ± 0.1, at 850 ℃ 29.6 ± 0.1) were used. The calibration took place before the actual analysis of the samples.

4.6 Thin section

In order to get information about composition and texture of the sedimentary rock samples, thin sections were made. The thin sections were analysed after general descriptive characteristics with transmitted light microscope of the type ZEISS SteREO Discovery.V20 and of the type Leica DM4500 P LED. The pictures were taken with their respective microscopy imaging software.

The analysed samples were a concretion (MH T06) from Mammuthöhle and two conglomerates (HIH 01, HIH 02) from Hirlatzhöhle, and two clay-silty sediments (GHS 04, GSH 05) from Günter-Stummer-Höhle.

5 Results

The results are now presented and they are sectioned according to the individual analytical methods.

5.1 Outcrops (O)

In this section, the outcrops where the samples were taken are described. More detailed photos and detailed plan views of the sampling sites are shown in the appendix.

5.1.1 Dachstein-Mammuthöhle

In Mammuthöhle seven outcrops were described (Fig. 12) and samples of different layers were taken. Here, the whole profile is exposed, starting from the greenish sediment at the base, followed by dark cave loam and locally also conglomerates, and the bright cave loam at the top.

O-1 Sklavengang, next to the ladder

At the outcrop of Sklavengang (Fig. 12), next to the ladder is a stream flowing and on both sides there are sedimentary sequences (Fig. 13). Both sequences were extended below the streambed with the help of a drill.

The drilling at the profile orographically right of the stream was stopped 145 cm below streambed at a hard object. As three nearby drillings ended at the same depth, it is probably the bedrock. The profile consists from base to top of 30 cm greenish sediment that has an abundance of mica. Sample MH T02 was derived from there. For the next 115 cm comes dark cave loam which has first a slightly reddish tone before it changes to a brown colour. From there sample MH T01 was taken. In the last 85 cm the sediment was water saturated and not as compact as before. Sometimes mm-thick components were found in the dark cave loam. Corresponding with the streambed level is the base of a carbonate conglomerate with a thickness of 120 cm. It is grain supported and shows fining upwards of carbonate clasts ranging from an average size of 3 cm to sand particles at the top. In the upper area are lenses of bright cave loam in between. The top of

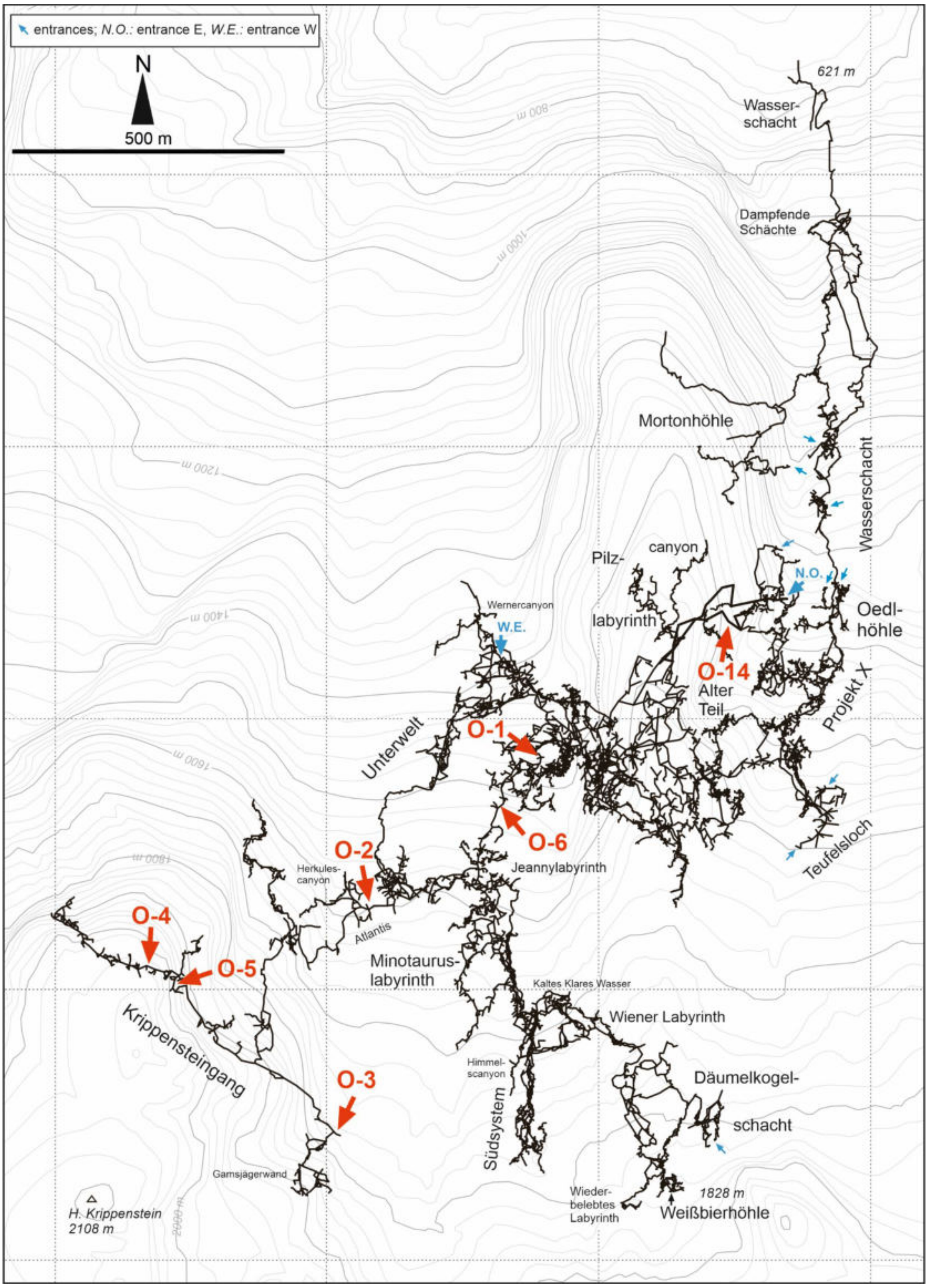

Figure 12: The generalised plan view of Mammuthöhle with the marked outcrops (modified from Behm and Plan, 2005).

the sequence is a bright brown-beige, varve-like layered bright cave loam. In the uppermost 5 cm from a total thickness of 50 cm there are deformation structures whereas in the underlaying 15 cm partially no laminae occur.

Orographically left, the drilling took reached until 90 cm below streambed and the sediment was throughout dark cave loam. Above comes 85 cm of grain-supported carbonate conglomerate with a dark brownish matrix, and the clasts have a size up to 6 cm. Also, on this side is the basis of the conglomerates consistent with the streambed. At the top there is 80 cm of bright cave loam, which is laminated. However, the uppermost 25 cm are deformed and below there are areas where layering is missing.

O-2 at the end of Atlantis, junction Herkulesschacht and Barbarengang

Bright cave loam that has desiccation cracks on the surface covers the bottom of the cave passage at the end of Atlantis (Fig. 12). The cracks have an average depth of about 50 – 60 cm and a width of 5 – 10 cm. As a result, the length of the blocks is up to 60 cm. A depth of 205 cm of bright cave loam was determined with drilling until the top of the rock was reached.

Cutting a block reveals light brown to beige clay with a varve-like texture (Fig. 14). The laminae are only in the mm range, however, the thickness is variable. There are also areas that show deformation structures and within the laminae offsets can be seen.

O-3 Krippensteingang, shortly before Huziwand

Along the path in Krippensteingang (Fig. 12), shortly before Huziwand is reached, there is dark cave loam with a thickness of 1.4 m (Fig. 15). The sediment is reworked in parts, and sporadically Augensteine are recognisable. The dark cave loam is barely covered by bright cave loam on top due to its thickness being only up to 5 mm (Fig. 16a).

It is striking that the circumstances of the sediment succession are different in a niche at the upper part of the cave passage (Fig. 16b). The dark cave loam is about 70 cm thick and the underlying bedrock is visible. At the base several thin and sandy laminae occur and, in some areas, the normally dark brown cave loam appears in a more orange tone. There, traces of bioturbation that seem like burrows with length up to 15 mm are recognisable. At the boundary surface there is a greenish, mica-rich, 1 mm lamina, followed by bright cave loam as a top lamina (Fig. 15). The latter is 10 cm thick, has a dark-light lamination, however, at the bottom it often shows deformation structures and on the surface desiccation cracks occur.

From the outcrop at the niche, two samples of dark cave loam were taken: one of

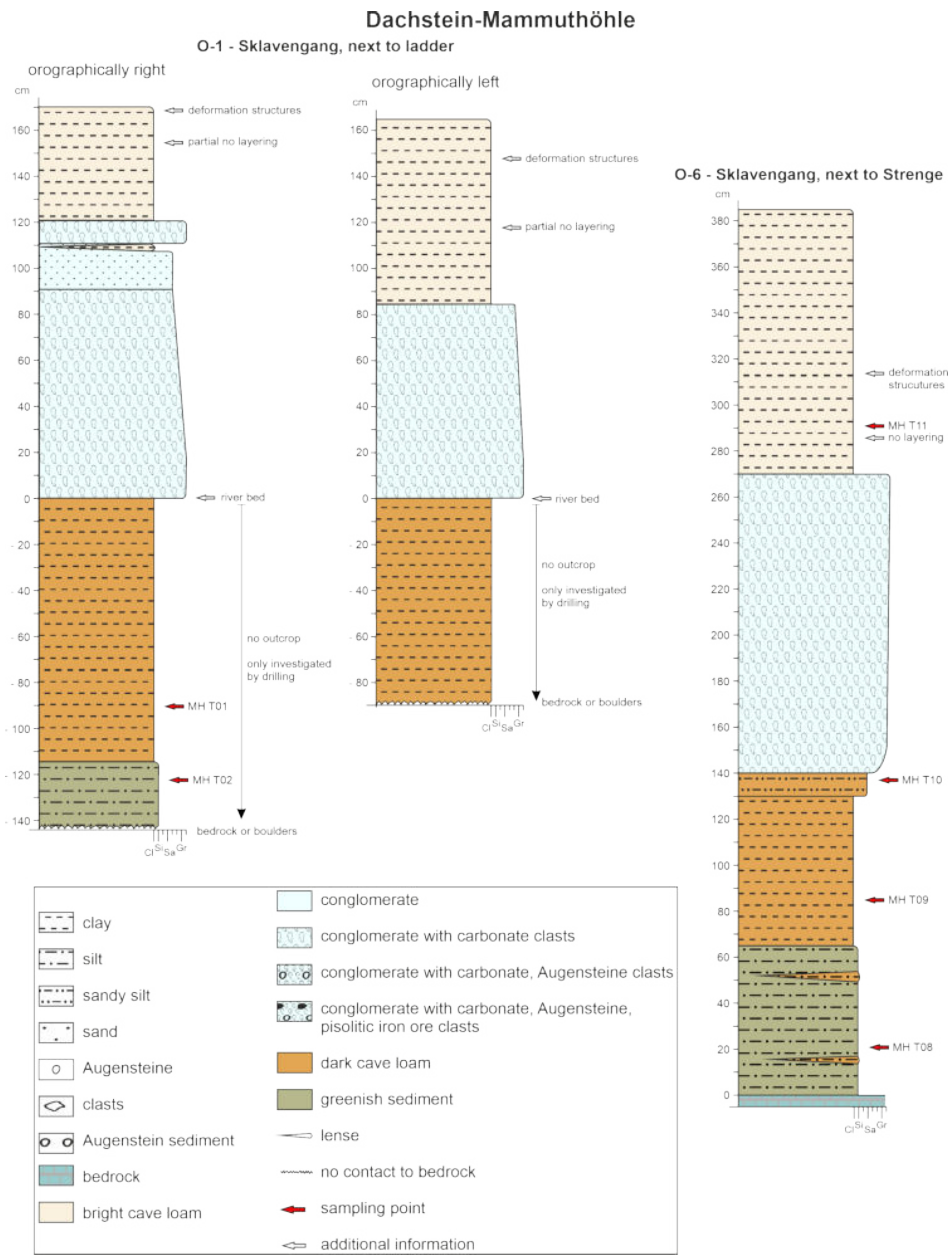

Figure 13: Profiles of outcrop 1 and 6 in Mammuthöhle and their respective sample locations. The explanation is valid for all the upcoming profiles as well.

Figure 14: Outcrop 2: Bright cave loam with the typically laminated texture (photo by E. Kaminsky).

the regular dark cave loam (MH T03) and the other of the area with bioturbation (MH T04).

At Huziwand, concretion with a wide variety of shapes and sizes protrude from the wall.

In Krippensteingang, after the crossing in direction of the Gor-Biwak, there is a sandy lamina of Augensteine at the base, followed by dark reddish clay laminae alternating with Augensteine. The outcrop thickness is about 2 m and from the clay lamina sample MH T05 was taken.

O-4 after junction Solaris, SS 100

The sedimentary succession (Fig. 15) of the outcrop at survey station 100 (Fig. 12) comprises 20 cm greenish silty sediment that is sometimes slightly reddish and it has areas of Augensteine clasts. The Augensteine are subangular, are well sorted, and have a particle size up to 5 mm. From a section without Augensteine sample MH T07 was taken. Above the greenish sediment is dark cave loam with a thickness of 85 cm. It shows fining upwards, starting with fine sandy sediment and ending with particle size of clay. In addition, at the base there are in addition very poorly sorted as well as predominantly angular clasts of dark cave loam and rarely also Augensteine. This layer is followed by bright cave loam, which has a variable thickness ranging from 80 to 180 cm. There are parts of varve-like structured

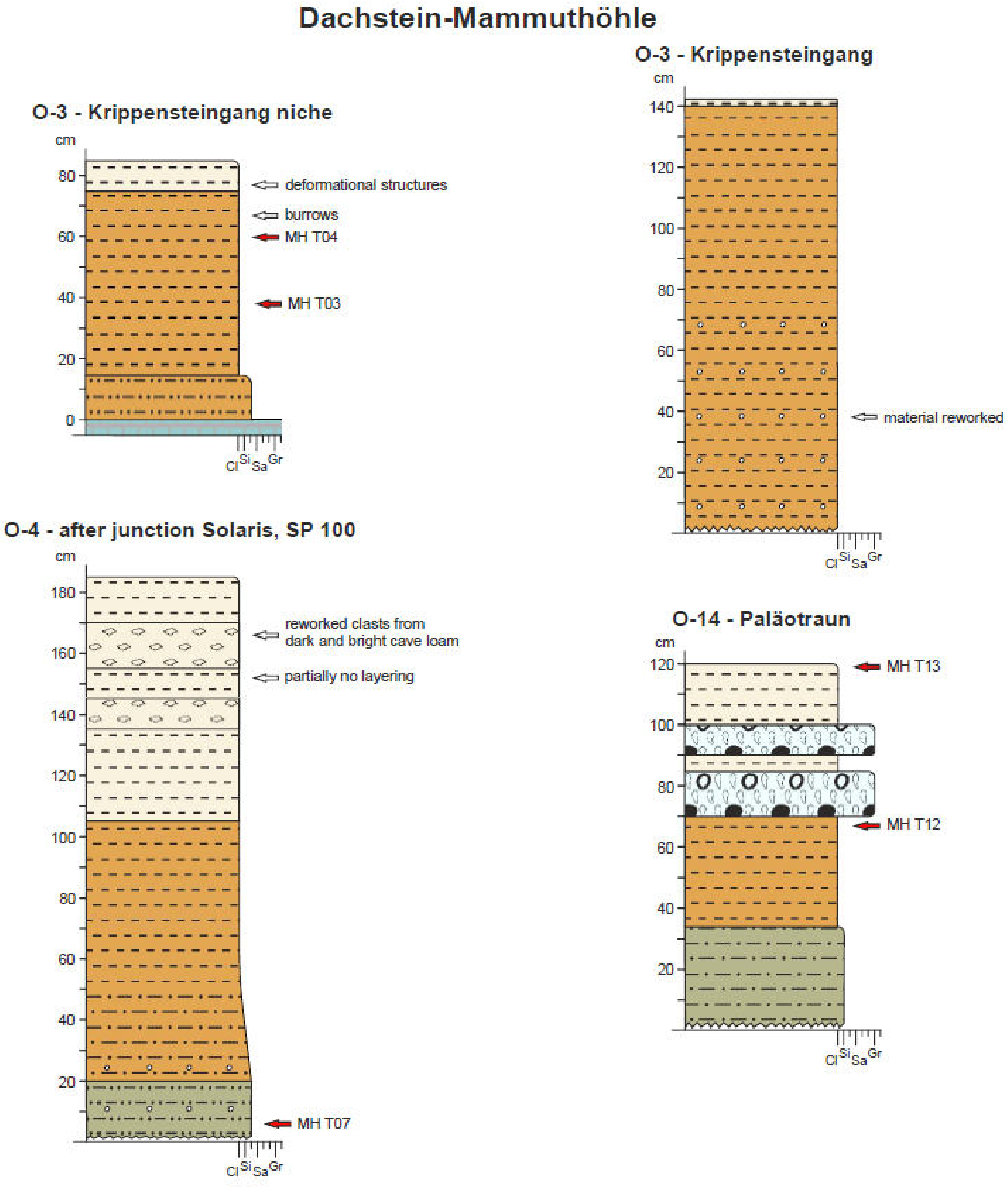

Figure 15: Profiles of outcrop 3, 4, and 14 in Mammuthöhle and their respective sample locations. Explanation, see Fig.13.

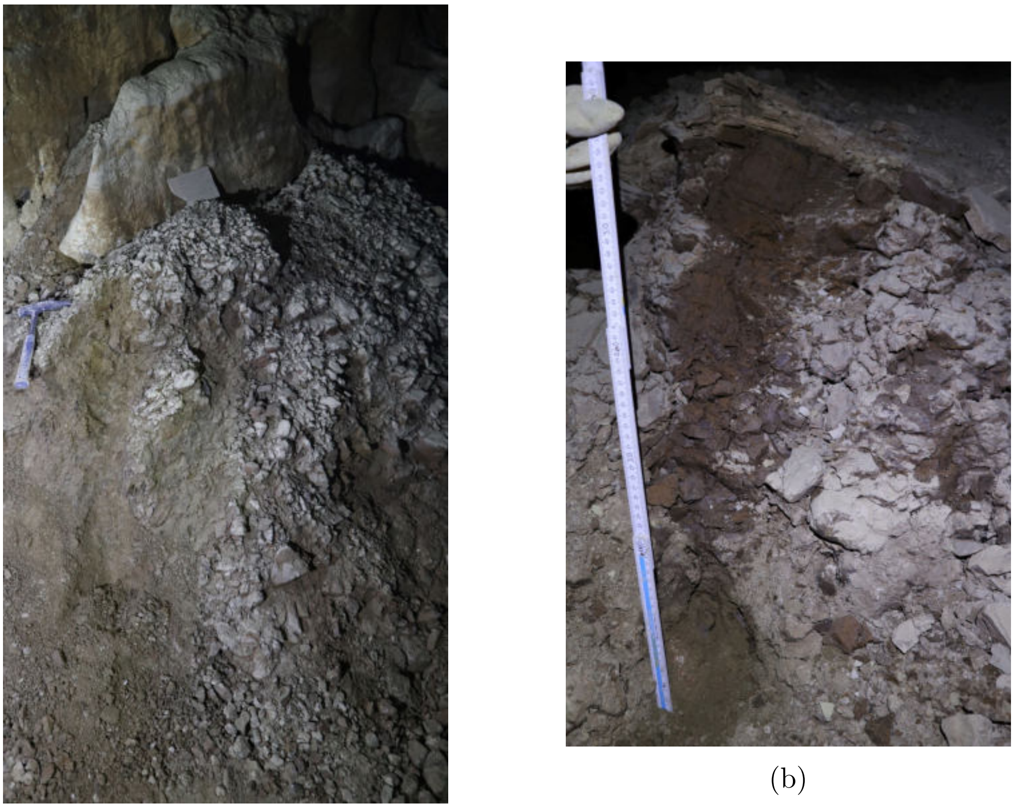

(a) (b)

Figure 16: Outcrop 3: Sediment sequences of dark cave loam at the base and bright cave loam at the top at Krippensteingang. (a) Dark cave loam with a mm-thin cover of bright cave loam. Hammer is for scale (photo by E. Kaminsky). (b) In the niche, the dark cave loam has a thickness of 70 cm, followed by 10 cm bright cave loam.

laminae and also layers with reworked angular to subangular clasts of bright and dark cave loam that are up to 10 cm.

O-5 junction Solaris

At the streambed in the area of junction Solaris (Fig. 12) are numerous loose sandstones with different shapes and sizes. Most of them are spherical like loesskindels with a diameter up to 30 cm. One concretion (MH T06) was taken in order to get an insight of its inside through a thin section.

O-6 Sklavengang, next to Strenge

The outcrop at Sklavengang next to Strenge (Fig. 12) is a sedimentary succession of 385 cm (Fig. 13). At the base, directly deposited onto the bedrock as it seems is greenish sediment, which is 65 cm thick. Within the sediment are thin laminae of sandy, mica-rich, and silver-greyish material and lenses of dark clay. They have variable thickness in the cm-range and occur more frequently in the transition area to the dark cave loam. Above, there is an 85 cm thick layer of dark cave loam. The shades of brown are variable, and sometimes the colour is even slightly reddish. The sediment appears partially crumbly (Fig. 17a) and the last 10 cm are coarser grained, in the sandy grain size range. Above is a grain-supported carbonate conglomerate. At the base, there is coarsening upwards, starting with fine gravel. Altogether, the sorting is very poor, with subangular to rounded clasts up to 25 cm. The conglomerate has a thickness of 140 cm, followed by bright cave loam of a maximum of 115 cm as the topmost section. The light brown-beige, partially crumbly clay has varve-like structures at its base as well as top, whereas in the middle part it is not laminated and partially shows deformation structures (Fig. 17b).

From this succession at least one sample of every layer was taken, except of the conglomerates. Sample MH T08 is of greenish sediment, samples MH T09 and MH T10 of dark cave loam, where the latter comes from the sandy top layer, and sample MH T11 is of bright cave loam material.

O-14 Paläotraun

Along the guide path in the show cave section of Mammuthöhle (Fig. 12) is a sedimentary succession (Fig. 18) of greenish sediment at the base (minimum thickness 30 cm), above is brown-orange dark cave loam (maximum thickness 40 cm) that is slightly fining upwards. It is followed by an approximately 30 cm thick conglomerate that consists of rounded components of carbonates, Augensteine, and pseudo-pisolitic ore and is poorly sorted with clasts up to 10 cm. Within the conglomerate is a lamina of bright cave loam. The top of the sequence is formed by

(a)

(b)

Figure 17: Outcrop 6: Detailed pictures of the sedimentary succession showing a (a) crumbly area of dark cave loam and (b) bright cave loam with laminae at the base, followed by a massive area, laminae, and deformation structures at the top.

20 cm thick bright cave loam. The thickness of each lamina is very variable and differ greatly within a few cm.

Sample MH T12 was taken of dark cave loam, whereas sample MH T13 is from a lighter lamina of the bright cave loam (Fig. 15). However, this lamina is not pure, but shows internal thin lamination in the mm range.

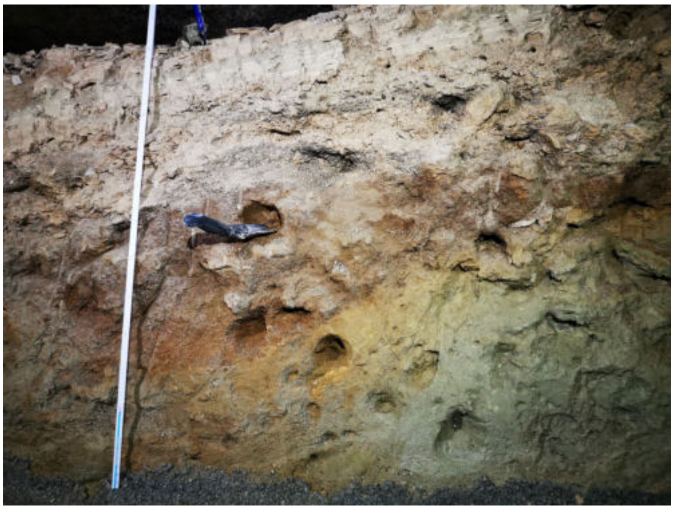

Figure 18: Outcrop 14: Sedimentary succession along guide path. The tools indicate the sampling locations of MH T12 (bottom) and MH T13 (top; photo by L. Plan).

5.1.2 Dachstein-Rieseneishöhle

In Rieseneishöhle only one outcrop was studied near the entrance of the show cave.

O-16 Lehmhalle

The outcrop at Lehmhalle, which is a pit from an excavation carried out by the University of Vienna in 1995 (Pacher, 1996), is already described and analysed by Bethke (2020). However, the clay mineralogy as well as TOC were not part of the analyses. Therefore, a sample (DRH 01) was taken from 60 cm below the ground level in a layer of dark brown-olive fine fraction and coarser material. The latter consists of mostly subangular clasts of Augensteine, carbonates, mica schist, and solidified clay plates.

The visible profile with a depth of about 2 m (Fig. 19) has as the lowest layer a grain-supported sediment mainly made of Augensteine. The grain size varies from coarse sand to rubble (Bethke, 2020). Drilling experiments could go only until 70 cm below the surface due to reaching hard objects. The drilling showed that the same sediment also occurred in depth. As a result, the layer has at least a thickness of 110 cm. Following the lowest layer comes a 90 cm thick, layered, olive-greyish clay section with enclosed sandy and silty laminae. Next, there are a thin sandstone layer (2.5 cm) and a 25 cm thick layer of fine sand in a light grey-olive colour (Bethke, 2020). From the drilling base to the last described layer, the sediment is considered to be greenish sediment.

On top is the layer of dark-brown sediment with a thickness of 30 cm where the sample comes from. It is divisible into an upper, more clastic part and a lower part, which has a higher content of clay. Above is a 13.5 cm thick layer of massive light cave clay, partially with desiccation cracks. On top there is a layer of grain-supported Augensteine of about 20 cm thickness, separated only by a 5 cm thick sandy layer. The sequence is completed by a thin layer (2 cm) of bright cave loam (Bethke, 2020).

5.1.3 Hirlatzhöhle

In Hirlatzhöhle mainly thick bright cave loam is present. This is especially the case for the passages in Alter Teil. In higher areas, a sample of darker clay could be taken as well.

O-8 Aufsteigender Tunnel, before ramp

At the lower part of Aufsteigender Tunnel outcrop 8 (Fig. 20) is located. There are several boulders of conglomerates that lie loosely on breakdown material and are also covered by it. The boulders have different diameters, the largest has approximately 2.5 m.

The conglomerate is matrix supported with a red-brownish matrix. The clasts are poorly sorted with grain sizes of up to 5 cm and are mainly subangular as well as rounded. They consist mainly of carbonates and quartz components are hardly recognisable. From outcrop 8 sample HIH 01 was taken.

O-9 Aufsteigender Tunnel, upper part

In the upper part of the cave passage (Fig. 20) there is conglomerate in situ at the bottom as well as the wall. This results in a thickness of approximately 2 m. At the base of the conglomerate, the contact with the carbonate bedrock is visible.

The matrix-supported conglomerate has a brownish matrix and is very poorly sorted. The subangular to rounded components have an average particle size of 2 cm, however, they can also be 10 cm. The conglomerate comprises quartz and carbonate components. The conglomeratic sample HIH 02 is from this outcrop.

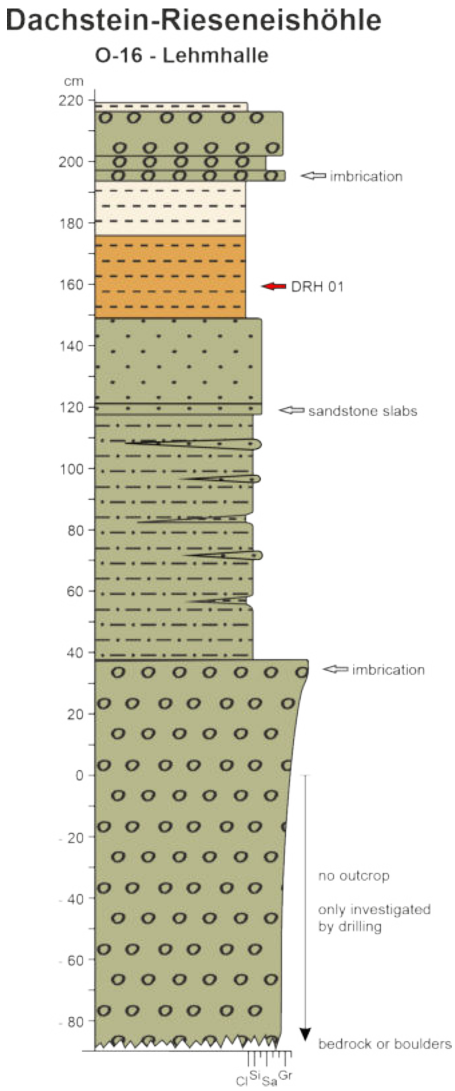

Figure 19: Profile of outcrop 16 in Rieseneishöhle and its respective sample location (modified from Bethke, 2020). Explanation, see Fig. 13.

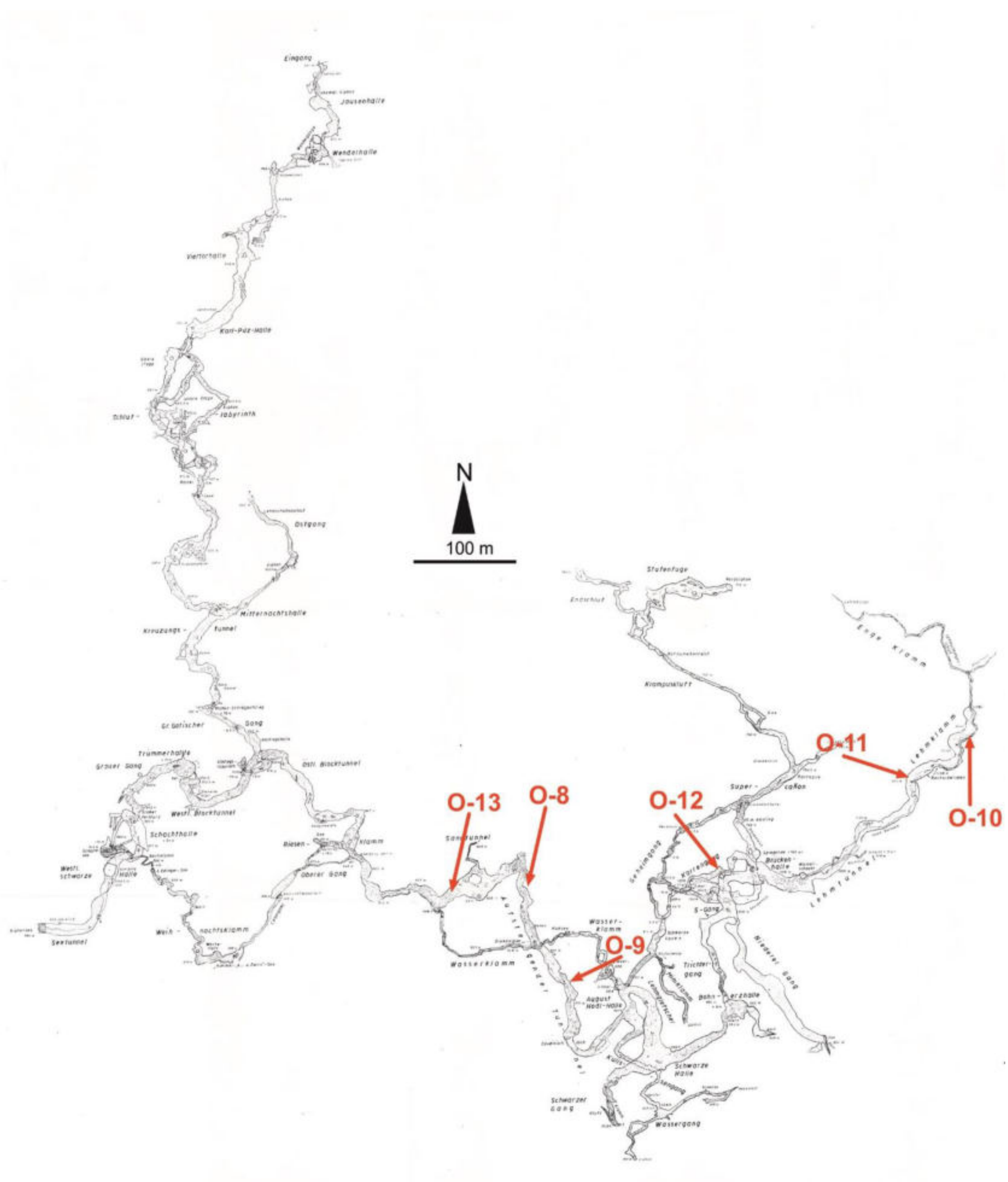

Figure 20: The plan view of Alter Teil of Hirlatzhöhle with the marked outcrops (modified from Fritsch, 1969). O-20 is in a higher area at Ostzubringer. For an exact location within Hirlatzhöhle, see appendix.

O-10 Lehmklamm, orographically right

At Lehmklamm there is an outcrop wall of bright cave loam on the orographically right side of a stream that flows towards SW (Fig. 20). The wall is 3 m high. In the most SW part, however, it loses height in the NE direction where it is only 1.8 m high (Salomon et al, 2018).

The bright cave loam consists of varve-like dark and light laminae that are to a large extent parallel and undisturbed, but they also show areas of deformation structures in between (Fig. 21). The laminae have various thicknesses, ranging from a few mm to several tens of mm. It is striking that the bright laminae occur less often and are thicker. Measurements of an area where the samples were taken as well resulted in a mean value of 5.5 mm for the light, beige-whitish laminae compared to an average of 2.5 mm for the darker, beige-brown laminae.

Around the NE corner, there is on top of the bright cave loam a 20 cm thick sandy layer with recognisable climbing ripples. These ripples indicate a direction of flow of a paleo stream towards NE which is opposite to todays.

From this outcrop a sample of a dark lamina (HIH 03) and of a light lamina (HIH 04) of the bright cave loam were extracted as well as a sample of the sandy layer (HIH 05; Fig. 22).

Figure 21: Outcrop 10: Bright cave loam with its dark and bright laminae (photo by L. Plan).

O-11 Lehmbachschwinde

An unconsolidated, grain-supported conglomerate is deposited on the bedrock with a thickness of 3 - 5 cm at outcrop 11 (Fig. 20). The sorting is poorly due to

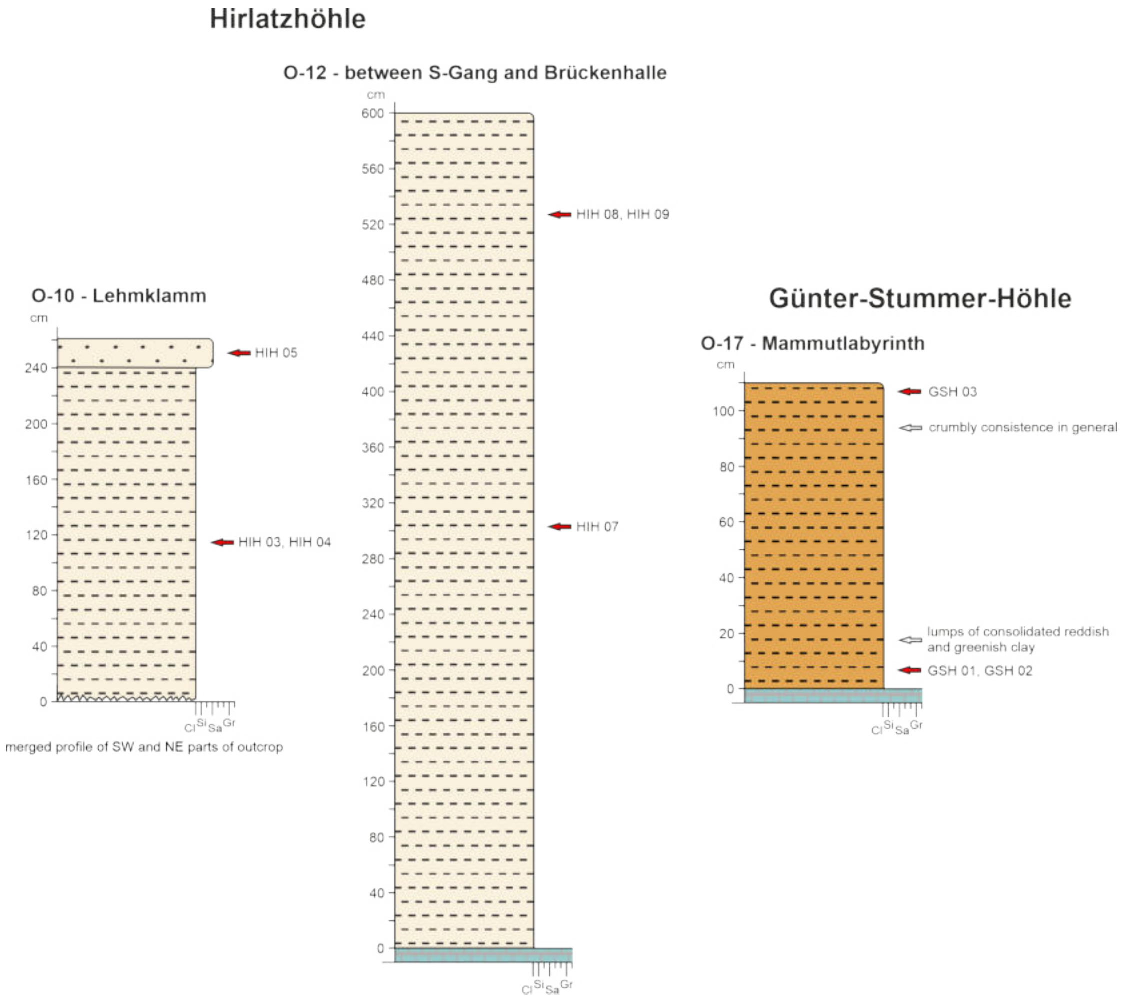

Figure 22: Profiles of outcrop 10 and 12 in Hirlatzhöhle as well as of outcrop 17 in Günter-Stummer-Höhle and their respective sample locations. Explanation, see Fig.13.

sporadic clasts that have a size of 5 cm. However, the average particle size of the well-rounded components is approximately 2 cm. The components consist of carbonate and clasts which are black-violet laminated, scratch the hammer, and react with HCl.

O-12 between S-Gang and Brückenhalle

Between S-Gang and Brückenhalle (Fig. 20) there is an outcrop of bright cave loam with a thickness of 6 m (Fig. 22). A small waterfall entering the gallery from the side has created this pit into the sediment and therefore the outcrop. It has the typical alternating dark-light, varve-like lamination (Fig. 23). The laminae have variable thicknesses, ranging from a few mm to several tens of mm. In one area of the outcrop the laminae were measured, showing an average value of 6.5 mm for the dark laminae, whereas the lighter ones are on average 15 mm thick. In addition, the analysis shows that the latter are not only thicker, but occur significantly less often.

The dark laminae are brown-beige and the bright laminae have a whitish-beige colour. They do not appear pure white because they are themselves interspersed with thinner darker laminae.

Three samples were taken from this outcrop: HIH 07 and HIH 09 were extracted from darker laminae, whereas HIH 08 from a light lamina.

Figure 23: Outcrop 12: Upper part of the thick outcrop of bright cave loam (photo by L. Plan).

O-13 between bivouac and junction Wasserklamm

A whitish, unconsolidated sediment repeatedly covers large areas of the ground in cave passages of Hirlatzhöhle, as in this outcrop (Fig. 20). By Schauberger (1983) this sediment was called floury sand. The thickness of the sediment is variable, but can be up to 8 cm next to the walls, where it is predominantly undisturbed. The material is fine grained and seems to comprise mainly of silt and fine sand particles. Sample HIH 10 was taken from this sediment.

O-20 150 m after Wetterscheide

Sample HIH 20 was taken at Ostzubringer at 1,131 m a.s.l., 150 m after Wetterscheide. The sediment is an orange-brownish clay with sometimes blackish areas and had a thickness of about 30 cm. At a second outcrop at 1,250 m a.s.l. the clay was up to 50 cm thick (L. Plan, personal communication).

5.1.4 Günter-Stummer-Höhle

Günter-Stummer-Höhle is the highest situated cave and three outcrops were studied there.

O-17 Mammutlabyrinth, SS 164

The bottom of outcrop 17 (Fig. 24) consists of dark brown-reddish cave loam that has an unconsolidated, crumbly-like texture (Fig. 25). There are compact clay components within the sediment with an average size of 2 – 4 cm. As a result, the sorting of the sediment is very poor. This is the general appearance of the dark cave loam in Günter-Stummer-Höhle. At this outcrop the thickness is about 1.1 m (Fig. 22) and the compact clay components are especially found on top. These components (GSH 03) are in the interior orange-brownish and have black spots. The appearance is strongly reminiscent of samples MH T03 and MH T04 from Mammuthöhle.

In addition, in the lower part of the outcrop clay components occur with a size up to 10 cm that are either dark reddish (GSH 01) or greenish (GHS 02). The latter has sometimes a dark reddish coating with a thickness up to 1 cm.

O-18 Mammutlabyrinth, SS 125

In outcrop 18 (Fig. 24) there is on top of Dachsteinkalk a layer of cemented cave sediment that partially forms rounded lumps with a height up to 5 cm (see appendix). The hand sample (GSH 04) is fine grained and has a brownish colour with black spots. Its appearance reminds of sample GSH 03 in a solidified state.

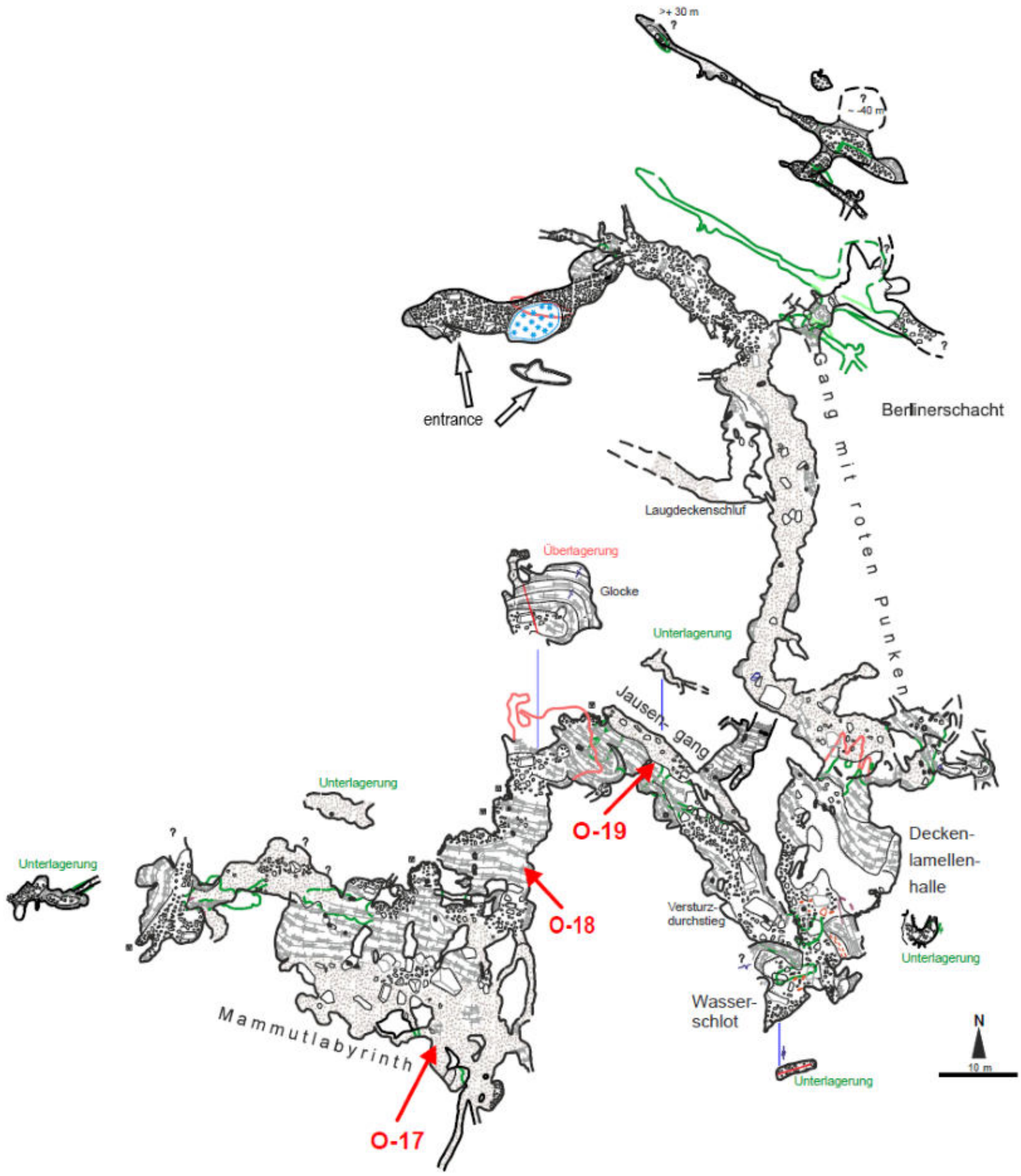

Figure 24: The plan view of Günter-Stummer-Höhle with the marked outcrops (modified from Funk and Plan, 2021).

Figure 25: Outcrop 17: Unconsolidated dark cave loam in a passage of Mammut-labyrinth in Günter-Stummer-Höhle (photo by L. Plan).

O-19 Jausengang, SS 118

There is once again a 3 cm thick layer of cemented cave sediment on top of Dachsteinkalk in outcrop 19 (Fig. 24). This outcrop also shows a thin black layer with a thickness of up to 1 cm in between (see appendix). The cemented sediment looks orange-brownish and has black spots with an extent of several mm. The layer also occurs on the wall, where it forms lumps of 5 cm height. From there sample GSH 05 was taken.

5.1.5 Caves outside Dachstein Massif

Two comparative caves were selected – Eisriesenwelt and Schönberg-Höhlensystem – and a sample was taken from each of them.

O-7 Eisriesenwelt - Kirchendach

At Kirchendach was an already existing outcrop. There, a light brown-greyish silty-sandy sediment was the base layer of a sequence. At the bottom it was coarser grained and Augensteine with a size up to 1 cm could be found. At the top was a 50 cm thick, dark brown-reddish clay (Plan et al, 2021) and from there the reference sample ERW KD was taken.

O-15 Schönberg-Höhlensystem - E of Gigantendom

Another reference sample (SHS 02) was brought from E of Gigantendom and N of Blockabstieg in Raucherkarhöhle within the Schönberg-Höhlensystem. The unconsolidated sediment is dark brown and very poorly sorted. The colourful (whitish, reddish, bright and dark brown), predominantly rounded siliciclastic components have a size up to 3 cm. The components also include semi-solidified conglomerates, which are encrusted with a black layer.

5.2 Bulk mineralogy

The XRD analysis of the bulk samples shows that all of them consist of quartz, muscovite, and chlorite (except sample HIH 10). In addition, K-feldspar is almost always present in traces, missing only in the samples MH T11, MH T13, and HIH 09 which are samples of the bright cave loam.

Going more into detail and looking separately at all the cave sediments, it can be seen that in the greenish sediments (MH T02, MH T07, MH T08) – as the lowermost examined layer – quartz, muscovite, and chlorite are dominant. The XRD patterns display also traces of K-feldspar and goethite. Only the sample MH T07 comprises traces of calcite as well.

Next, the dark cave loam from Mammuthöhle (MH T01, MH T03, MH T04, MH T09, MH T10, MH T12) and the sample of Hirlatzhöhle (HIH 20) consist of quartz, K-feldspar, muscovite, and chlorite (Fig. 26). All the minerals do not show a high intensity. Goethite is present except in sample MH T10, and in sample MH T03 hematite instead of goethite is detected as a Fe-oxide in the bulk composition. Kaolinite is detectable in MH T01, MH T03, and MH T09, but the XRD patterns of the clay fractions shows more clearly that this mineral is always present. MH T10 shows differences in the intensity of the minerals compared to the other dark cave loam samples. This can be seen in the highly dominant quartz, followed by a dominant muscovite whereas the other two identified minerals K-feldspar and chlorite are only present in traces.

The samples coming from Günter-Stummer-Höhle on the other hand, show a slightly different composition because they contain the minerals boehmite and anatase. In addition, chlorite and muscovite are once again present as well as the Fe-oxides hematite (GSH 01) or goethite (GSH 02, GSH 03). Quartz appears only in traces, which can be better seen in the XRD patterns of the clay mineralogy.

Bright cave loam was found in Mammuthöhle as well as Hirlatzhöhle. From Mammuthöhle two samples could be derived. MH T11 comes from a darker area with a massive appearance. The XRD analysis presents a high intensity of calcite and there are traces of quartz, muscovite, and chlorite. Sample MH T13 is from a

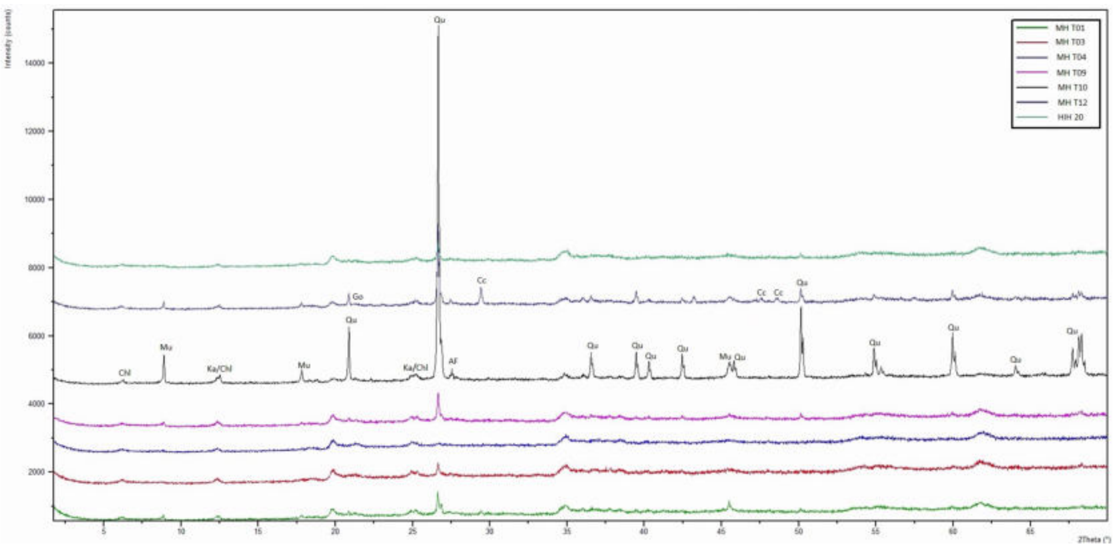

Figure 26: X-ray diffraction patterns of the bulk mineralogy of all samples (MH T01, MH T03, MH T04, MH T09, MH T10, MH T12) of dark cave loam from Mammuthöhle and Hirlatzhöhle. AF = alkali feldspar, Cc = calcite, Chl = chlorite, Go = goethite, Ka = kaolinite, Mu = muscovite, Qu = quartz.

brighter, but very thinly laminated lamina. Here, calcite, quartz, muscovite, plagioclase as well as chlorite could be detected. Again, calcite is by far the mineral with the highest intensity.

The samples from Hirlatzhöhle can be classified into three samples (HIH 03, HIH 07, HIH 09) of the darker laminae of bright cave loam and two (HIH 04, HIH 08) of the brighter laminae. The results show that the bulk mineralogy of the darker laminae consists mainly of calcite and secondary of quartz, dolomite, ankerite, muscovite, and chlorite (Fig. 27). HIH 03 and HIH 07 contain K-feldspar as well, and the latter also goethite. In contrast, the brighter laminae are assembled by the same minerals, however, the intensities of calcite and quartz are each slightly higher (Fig. 28). In sample HIH 08 there is no kind of feldspar.

The bright cave loam was also analysed semiquantitatively (see appendix) and the previously described results can be shown more detailed and confirmed by percentages. The bright laminae of Hirlatzhöhle have slightly higher values of calcite (83 %) and also of quartz (7 %). The bulk clay mineralogy is with a fraction of 6 % not so strongly represented as in the samples of dark laminated bright cave loam. There, samples HIH 03 and HIH 09 show consistent values of decreased calcite (75 %), quartz (5 %), and enriched bulk clay mineralogy (15 %). Sample HIH 07 follows the same pattern, however, the percentage of clay minerals is with 60 %

drastically higher and the percentage of calcite lower (31 %). These trends can also be seen at the samples of brighter and darker laminae from Mammuthöhle, but the relative values are slightly different. The composition of MH T11 as a brighter lamina consists of 78 % calcite, 2 % quartz, and 20 % clay minerals. In comparison, the darker lamina (MH T13) has 83 % calcite, 3 % quartz, and 15 % clay minerals.

XRD was conducted for the remaining samples as well except SHS 02 and DRH 01. The sample from Mammuthöhle MH T05 comes from a reddish clay layer which is alternating with Augenstein laminae. In this sample the minerals quartz, calcite, K-feldspar, muscovite, chlorite, kaolinite, and goethite were detected. ERW KD consists dominantly of quartz as well as minor of K-feldspar, muscovite, chlorite, and goethite. The remaining samples of Hirlatzhöhle – HIH 05 and HIH 10 – are different. HIH 05 is the sandy layer on top of the profile from Lehmklamm and shows a very high amount of calcite, followed with a distance by quartz and in traces by dolomite, K-feldspar, muscovite, as well as chlorite. HIH 10 is a sample of the widespread ground cover and is mainly build up of dolomite, which has by far the highest intensity, calcite, and quartz. The minerals K-feldspar and muscovite are only found in traces in the sample.

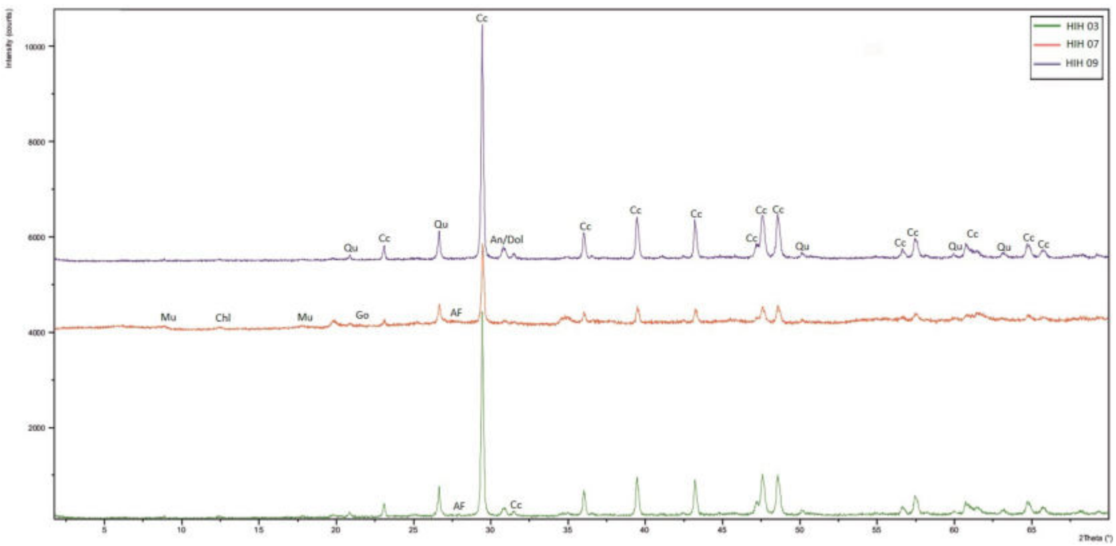

Figure 27: X-ray diffraction patterns of the bulk mineralogy of the dark laminae of bright cave loam from samples of Hirlatzhöhle. AF = alkali feldspar, An = ankerite, Cc = calcite, Chl = chlorite, Dol = dolomite, Mu = muscovite, Qu = quartz.

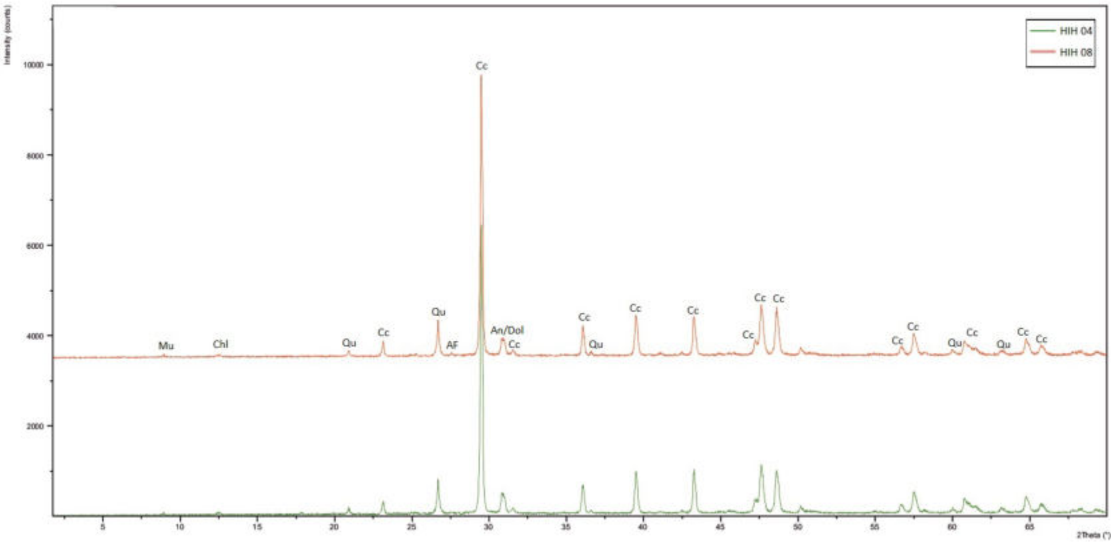

Figure 28: X-ray diffraction patterns of the bulk mineralogy of the brighter laminae of bright cave loam from samples of Hirlatzhöhle. AF = alkali feldspar, An = ankerite, Cc = calcite, Chl = chlorite, Dol = dolomite, Mu = muscovite, Qu = quartz.

5.3 Clay mineralogy

The results show that the clay minerals chlorite (peaks at 14.2 Å, 7.1 Å, 4.75 Å, 3.55 Å), illite (peaks at 10.1 Å, 5 Å), and kaolinite (peaks at about 7.16 Å, 3.58 Å, they overlap with chlorite) are always present. No matter if the samples are from the greenish sediment, the dark cave loam (Fig. 29), the bright cave loam, or of a reference sample.

Smectite could only be detected in the samples from Hirlatzhöhle (Fig. 30), MH T13 from Mammuthöhle, and the reference sample SHS 02. For the former, it is part of the composition of both kind of laminae – the darker and the brighter ones – of the bright cave loam. Smectite is recognisable due to a basal reflection at 14.5 Å which shifts to about 18 Å in case the sample is treated with magnesium and glycerol.

Regarding the bright cave loam, the semiquantitative analyses of the bulk clay mineralogy show repeating patterns for all clay minerals except smectite. This includes both the samples from Hirlatzhöhle and Mammuthöhle. Illite, kaolinite, and chlorite (not recognisable in samples of Mammuthöhle) are slightly enriched in the darker laminae compared to the bright ones. In general, illite is the most abundant clay mineral and contributes more than half of the bulk clay mineralogy in every sample. Smectite follows as the second common clay mineral in the samples of Hirlatzhöhle. Kaolinite and chlorite have an equally high percentage

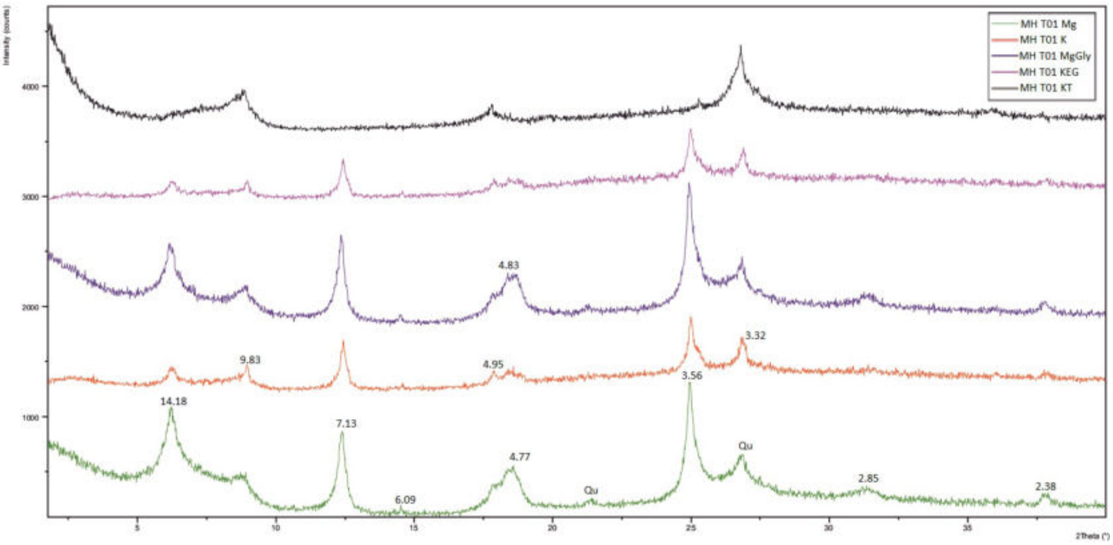

Figure 29: X-ray diffraction patterns of the clay mineralogy of a sample of dark cave loam from Mammuthöhle (MH T01). Saturated with Mg (green), K (red), Mg and glycerol (blue), K and ethylene glycol (pink), and heated to 550 °C (black); d-values in Å; Qu = quartz.

share with about 10 %.

In the samples of the dark cave loam, greenish sediment and the reference samples mixed-layered minerals are present. They can also be seen in the bright cave loam samples from Mammuthöhle, but from Hirlatzhöhle mixed-layered minerals are contained in traces, if at all. Due to the recognisable reflections at around 12 Å, 6 Å, and 4.8 Å, the minerals could be composed of regular interstratifications of illite and chlorite. The remaining peaks resulting from this illite/chlorite-mineral could be hidden because of overlapping with peaks of other minerals.

In the clay mineralogical XRD patterns, the peaks of quartz and calcite are also clearly visible if these minerals are a part of the composition. In the samples from Günter-Stummer-Höhle boehmite shows a strong peak and secondary also hematite in sample GSH 01 and anatase in sample GSH 02.

5.4 Grain size analysis

The grain size analysis was not carried out for every sample, however, there are results for each sediment type within the sediment profile.

The greenish sediment (MH T02, MH T07, MH T08) covers a grain size distribution from fine clay to medium sand and therefore, it is rather poorly sorted. However, a dominant grain size fraction is silt where the curve shows a steeper rise

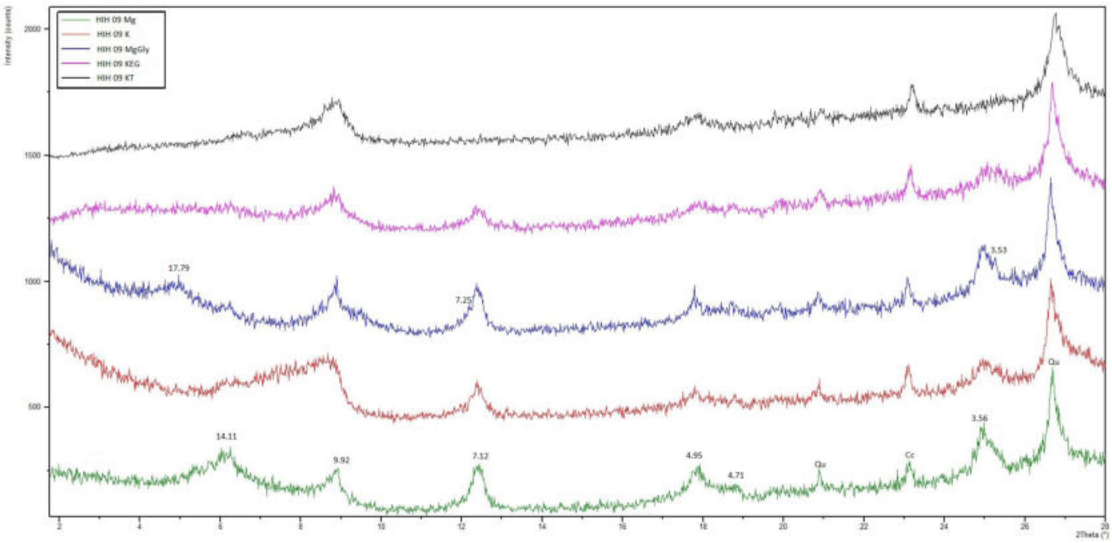

Figure 30: X-ray diffraction patterns of the clay mineralogy of a dark lamina of bright cave loam from Hirlatzhöhle. Saturated with Mg (green), K (red), Mg and glycerol (blue), K and ethylene glycol (pink), and heated to 550 °C (black); d-values in Å; Cc = calcite, Qu = quartz.

than in other sections. Whereas sample MH T02 and MH T08 have a very similar trend of the grain size curve, sample MH T07 has a slightly lower percentage of fine fraction up to medium silt. It is starting already with 18 % of fine clay in contrast to 25 % and the percentage of sediment finer than medium silt is about 70 % of the bulk sample compared to 80 %. In addition, in the sediment of MH T07 also clasts of Augensteine occur occasionally with a particle size up to 5 mm.

The grain size distribution of the dark cave loam from Mammuthöhle (Fig. 31) shows for three samples (MH T01, MH T03, MH T09) a consistent pattern. The samples consist of a relatively high percentage of fine clay (around 50 %), the remaining content includes grain sizes up to fine sand. The relatively flat increase of the grading curve shows that the samples are not very well sorted.

On the contrary, sample MH T04 comprises still of the same particle size range like the other samples of dark cave loam, but displays a relatively steep ascent of its grain size curve in the section of clay. The curve starts at a percentage of fine clay of 66 % and at a cumulative finer mass of about 93 % it flattens rapidly. This means, the sample consists mainly of clay and the contribution of silt as well as fine sand is minor.

Sample MH T10 of the dark cave loam has a rather different grain size distribution curve. The content of clay amounts only to 15 %. Starting from there, the slope of the curve is flat, but getting slightly steeper with an increasing particle size. At last, it flattens again. The size range of the material is from fine clay to coarse sand, which means the sorting of the sample is poor.

The grain size of the sediment from Rieseneishöhle (DRH 01) ranges from clay to coarse gravel. The analysis shows a relatively continuous increase of the grain size distribution, which only flattens out towards medium gravel size. The clay content is the lowest of all the samples analysed and is only 9 %.

The samples of dark cave loam coming from Günter-Stummer-Höhle (GSH 01, GSH 02, GHS 03) show a very similar pattern like the curve of MH T04 (Fig. 31). Only the initial value of the fine clay content is slightly lower (about 60 % for GSH 01 and GSH 03, 46 % for GSH 02) which in turn shifts the curve imperceptibly downwards. The grain sizes range from clay to fine sand, however, the main part lies in the clay fraction.

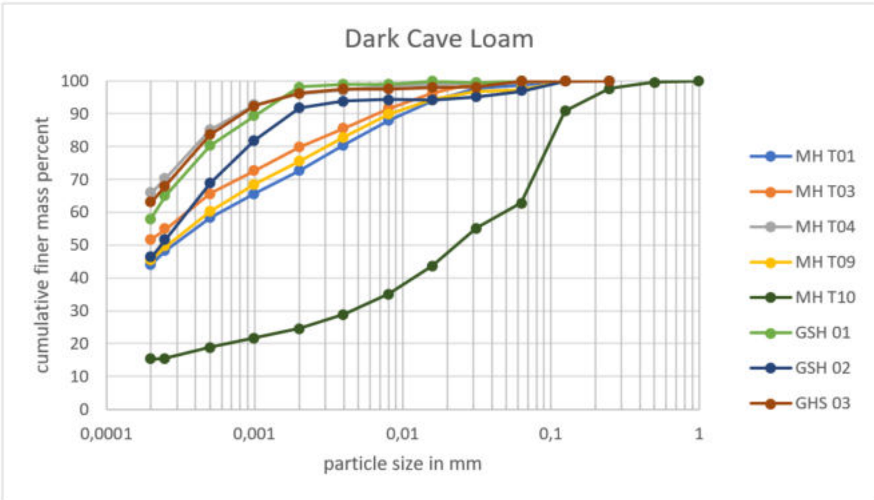

Figure 31: Grain size distribution of all samples of dark cave loam coming from Mammuthöhle, Hirlatzhöhle, and Günter-Stummer-Höhle.

The results of the grain size analysis of the two samples of the bright cave loam from Mammuthöhle (MH T11, MH T13) are similar and the sieve curves therefore superposed. The increase of the curve is rather steeply within the range of fine clay to fine silt and afterwards up to content of coarse silt the slope is decreasing rapidly. The samples have only a grain size range of fine clay to coarse silt, and the material is predominantly well-graded.

The bright cave loam samples of Hirlatzhöhle show a similar s-shaped grain size curve pattern like the samples from Mammuthöhle. The size range from fine clay to coarse silt is the same and the minor contribution of these two mentioned grain sizes as well. However, the grain size content of clay is various. MH T11 and MH T13 have a clay content of about 65 % whereas the samples from Hirlatzhöhle only show percentages up to 44 %. The clay content is also a feature to distinguish the dark and the bright lamina of the bright cave loam. While the dark laminae have an average percentage of clay of 37 %, the bright laminae only show results of 12 %. The silt content up to medium silt is very well graded which can be seen at the steep ascent that flattens rapidly afterwards.

The sample from Eisriesenwelt (ERW KD) shows an almost linear, but relatively flat trend of the sieve curve (see appendix). The slope slightly decreases with an increase of the particle size. The grain size ranges from fine clay to fine sand. The clay content amounts to 62 % and the silt content to 36 %. In contrast, the reference sample from Schönberg-Höhlensystem (SHS 02) shows a broader grain size spectrum, ranging from clay to coarse gravel (see appendix). SHS 02 contains only 26 % clay and from there the curve is increasing flatly until the trend changes to a steeper gradient at coarse sand at about 55 % of the bulk sample.

A grain size analysis was undertaken for sample MH T05 as well (see appendix). The curve has a linear, not very steep increase that flattens dramatically in the section of medium silt. The grain sizes coarser than medium silt up to fine sand only have a minor significance, whereas clay is represented of cumulative mass percent of 70 % of the material.

5.5 Total organic carbon

The TOC as well as the TIC contents were conducted for every sample. The TOC contents range from 0.0 % to 0.2 % for all the sediments (Tab. 2). A distinctive difference between the sediments regarding the TOC content can not be recognised because the range of the decimal place is within its error.

The TIC contents are from 0.0 % to 13.8 %. The greenish sediments and the dark cave loam have clearly lower TIC percentage (0.0 to 1.1 %) than the bright cave loam. The latter can be distinguished predominately into a darker and brighter lamina from TIC as well when looking at the samples from Hirlatzhöhle. Darker laminae (HIH 03, HIH 07, HIH 09) have a lower TIC percentage (2.6 % to 8.6 %), whereas the samples HIH 04 and HIH 08 of the brighter laminae vary from 9.4 % to 9.5 %. The two samples from Mammuthöhle (MH T11, MH T13) do not show such significant values.

The reference samples show a low TIC percentage for the samples MH T05 (0.5 %) and ERW KD (0.1 %) and a higher one for HIH 05 (11.5 %), ERW KD (0.1 %), and HIH 10 (13.6 %).

Table 2: Results of TOC analyses of all samples. DRH = Rieseneishöhle, ERW = Eisriesenwelt, GSH = Günter-Stummer-Höhle, HIH = Hirlatzhöhle, MH T = Mammuthöhle, SHS = Schönberg-Höhlensystem. Green = greenish sediment, brown = dark cave loam, dark yellow = dark lamina of bright cave loam, light yellow = bright lamina of bright cave loam, white = reference sample.

sample	TOC in %	TIC in %	sediment characterisation
MH T01	0.1	0.1	dark cave loam
MH T01	0.1	0.1	dark cave loam
MH T02	0.1	0.1	greenish sediment
MH T02	0.1	0.1	greenish sediment
MH T03	0.1	0.0	dark cave loam
MH T03	0.1	0.0	dark cave loam
MH T04	0.1	0.0	dark cave loam
MH T04	0.1	0.0	dark cave loam
MH T05	0.1	0.5	reddish clay
MH T05	0.1	0.5	reddish clay
MH T07	0.1	1.1	greenish sediment
MH T07	0.0	1.1	greenish sediment
MH T08	0.1	0.1	greenish sediment
MH T08	0.1	0.1	greenish sediment
MH T09	0.0	0.0	dark cave loam
MH T09	0.1	0.0	dark cave loam
MH T10	0.0	0.0	dark cave loam
MH T10	0.0	0.0	dark cave loam
MH T11	0.1	8.0	bright cave loam
MH T11	0.1	9.4	bright cave loam
MH T12	0.1	0.8	dark cave loam
MH T12	0.1	0.8	dark cave loam
MH T13	0.1	8.0	bright cave loam
MH T13	0.1	8.0	bright cave loam
ERW KD	0.1	0.1	brown-reddish clay
ERW KD	0.1	0.1	brown-reddish clay
HIH 03	0.1	7.5	bright cave loam
HIH 03	0.1	7.5	bright cave loam
HIH 04	0.1	9.5	bright cave loam
HIH 04	0.1	9.5	bright cave loam
HIH 05	0.1	11.4	sand lamina
HIH 05	0.1	11.5	sand lamina
HIH 07	0.2	2.6	bright cave loam
HIH 07	0.2	2.6	bright cave loam
HIH 08	0.1	9.4	bright cave loam
HIH 08	0.1	9.4	bright cave loam
HIH 09	0.1	8.6	bright cave loam
HIH 09	0.1	8.6	bright cave loam
HIH 10	0.2	13.6	ground cover
HIH 10	0.2	13.6	ground cover
SHS 02	0.1	0.0	coarse brownish sediment
SHS 02	0.1	0.0	coarse brownish sediment
DRH 01	0.0	1.3	coarse brownish sediment
DRH 01	0.0	1.3	coarse brownish sediment
GSH 01	0.0	0.0	dark cave loam
GHS 01	0.0	0.0	dark cave loam
GSH 02	0.0	0.0	dark cave loam
GHS 02	0.0	0.0	dark cave loam
GHS 03	0.2	0.0	dark cave loam
GSH 03	0.2	0.0	dark cave loam

5.6 Microscopy

The thin section of a concretion (MH T06; Fig. 32; detailed pictures, see appendix) shows in the upper two-thirds layering of darker, brown-greenish layers and brighter beige ones. However, the layers are not always throughout the whole thin section. The layers have a variable thickness, ranging from few µm up to about 5 mm, with the darker layers being mostly thinner than the brighter ones. In addition, the brighter layers are often coarser. Within the layers, there is a trend of grading from coarser to finer particle sizes recognisable.

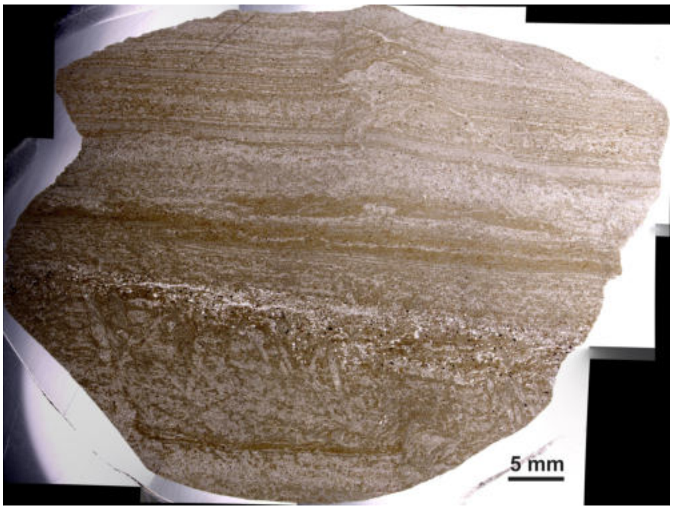

Figure 32: Thin section of a concretion (MH T06). Layering can be seen, as well as water escape structures in the upper and bioturbation in the lower third.

Regarding the mineralogical composition, there is a majority of quartz, followed by reddish as well as black minerals, and mica. Mica is more common in the darker, finer-grained layers and seems to be mostly light mica. The quartz grains are mainly angular to subangular and are predominant monocrystalline, but sometimes also polycrystalline. The reddish and black Fe-bearing minerals have a subangular to rounded form. The phyllosilicates and some of the reddish minerals are rod-shaped. These minerals show a certain orientation in the areas of the layering. The coarser minerals have in general tangential contacts.

In the lower part of the thin section layering is almost non-existent, instead the sediment seems disturbed, and some veins are recognisable. In between of the disturbed material there is a lamina of coarser grain sizes up to 1 mm, however, the average size is about 0.25 mm.

Another noticeable texture is a dome-like form with a height of about 1 cm in the upper third of the thin section that seems to evolve from the layers.

Sample HIH 01 (see appendix) of Hirlatzhöhle is a conglomerate. It has grain sizes up to 1 cm and is in general poorly sorted. The polymictic components are mostly rounded to subangular. The conglomerate is grain supported with tangential contacts. A red-brownish clay coating is regularly around the components, and there are areas of calcite cement as well. Cement is especially seen around pores and calcite minerals seem to be bladed.

The lithic, polymictic fragments consist mainly of bright grey carbonates that consist of fossil fragments like foraminifera (A. Lukeneder, personal communication). Next, there are reddish-brownish and bright grey components which are smaller in their particle size. The former often show layering and with crossed polarisers, the bright grey areas turn out to be micritic. The micritic components often have calcite veins. In addition, there are very few lithic clasts of oriented calcite minerals and bright brown ones with a black rim. Last, a white component stands out that consists of quartz with a preferred orientation. Sporadically, rounded, monocrystalline quartz grains can be found. There are also fossils as components in the form of fragments of crinoids and algae in between the lithic components recognisable (A. Lukeneder, personal communication).

The sample HIH 02 (Fig. 33) shows a very poorly sorted conglomerate with a maximum grain size of 0.6 mm. The components that are subangular to rounded are grain supported and have tangential contact. There is no matrix, but the components are regularly coated with a red-brownish clay. Instead, between the components there is rather calcitic cement.

The conglomerate is polymictic and is mainly composed of lithic fragments with variable sizes. White components are polycrystalline quartz, sporadically there can be seen light mica and biotite. The quartz components sometimes show a preferred orientation. More are rarely also monocrystalline quartz and breccia with a grain-size supported texture and quartz as well as mica grains. Furthermore, there are grey, micritic components that are smaller and brown-greyish ones. They consist – visible through crossed polarisers – of coarser grained calcite minerals. Brown-yellowish fragments have often a black rim.

In sample HIH 02 there are also algae (A. Lukeneder, personal communication) and two of them have a size up to 8 mm. One alga is partly surrounded by bladed calcite.

The samples GHS 04 and GSH 05 (see appendix) are both clay-silty sediments. GSH 04 has a light brownish-orange matrix interspersed with dark brownish-reddish areas, which turn out to be very fine-grained Fe-oxides when viewed with higher magnification. Only very few minerals are recognisable in the sediment. They have a particle size < 0.1 mm and identifiable are angular to subangular quartz grains and sporadically also light mica. In addition to the fine-grained Fe-oxides, there are also coarser minerals. These minerals, especially the quartzes, often appear clustered in the form of lenses with relatively clear boundaries. In an area at the edge of the rock, the composition is getting calcitic and coarse calcite minerals are shown. Both samples react with HCl.

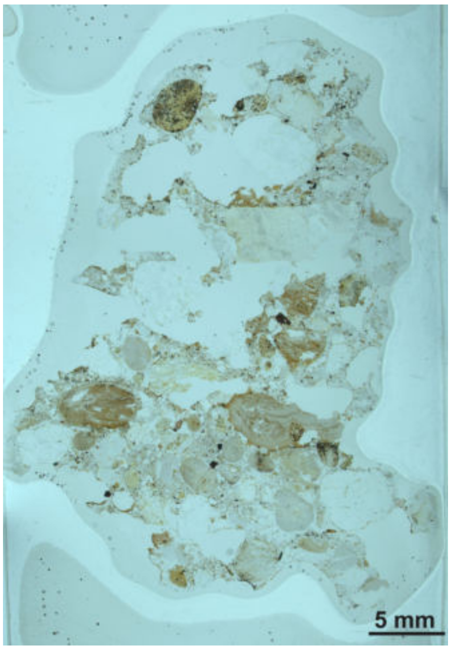

Figure 33: Thin section of a very poorly sorted conglomerate (HIH 02) from Hirlatzhöhle with carbonate and quartz components. In the lower third, algae can be seen.

The sediment GSH 05 has also bright brownish-orange matrix, but there are in addition large darker brownish areas (Fig. 34). These show a coarser composition, however, the minerals that are matrix supported are still hardly recognisable. Frequently occurring are well-rounded quartzes, Fe-oxides, and few micas. In the brighter matrix areas there are sporadically quartz minerals often clustered as mostly well-defined lenses and, in comparison to the darker areas, much rarer Fe-oxides. The Fe-oxides occur as coarse-grained as well as very fine-grained minerals. The latter creates small dark reddish blurs like it is also the case in sample GSH 04.

Within the brighter matrix, there is a part of a few mm diameters that seems to be broken up. In between the matrix segments are coarser-grained, angular to subangular quartzes and Fe-oxides as well as calcitic cement. Throughout the thin section are veins filled with cement.

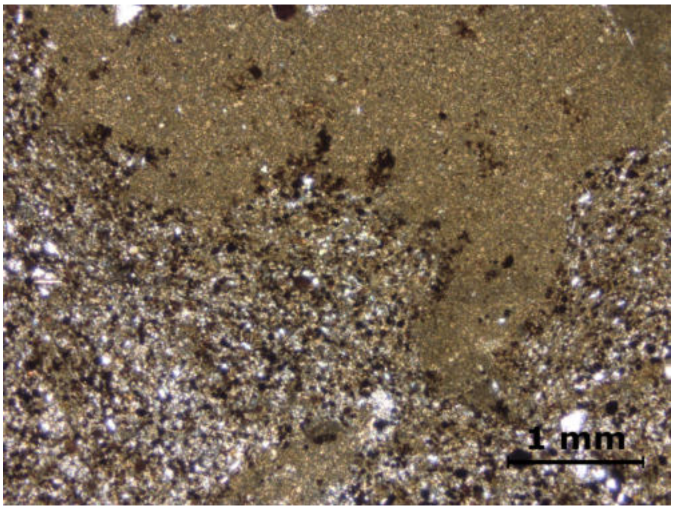

Figure 34: Detailed thin picture with crossed polarisers of the fine-grained brighter and coarser-grained darker areas of thin section GSH 05 from Günter-Stummer-Höhle.

6 Discussion

In the previous chapter the results of the sediment samples were presented, now these data are to be discussed with regard to the already known work. The focus is on the individual layers of the idealised profile and their change over height, but in particular on the sedimentological differences between the bright and the dark laminae of the bright cave loam. Also of interest is the comparison of the sediments from the caves from Dachstein Massif with those from Totes Gebirge and Tennengebirge.

6.1 Idealised profiles of the Dachstein cave sediments

Bethke (2020) developed an idealised profile (Fig. 9) of the cave sediments at the northern rim of the Dachstein Massif from data from the Mammuthöhle and Rieseneishöhle around 1,400 m a.s.l. Comparing the profile with the results obtained from this work, differences appear, especially regarding the thicknesses of the individual layers. Furthermore, the profile could be complemented with additional samples and the already used examination methods XRD and grain size analyses were extended by XRD of clay mineralogy and TOC analyses.

The observations in the caves and the results led to new idealised, but altitude-depending profiles (Fig. 35). Hirlatzhöhle is proposed to be – at least at the outcrops visited – of Berger Cave Level due to its hight (L. Plan, personal communication) whereas Mammuthöhle and Rieseneishöhle are a part of the Giant Cave Level, and Günter-Stummer-Höhle is considered to be in the Ruin Cave Level.

The **greenish Augenstein sediment** is the basis of the profile in the caves of the Giant Cave Level (Fig. 35). The name change was made from greenish sediment to greenish Augenstein sediment due to the abundance of Augensteine.

The analyses that were carried out are in concordance with Bethke (2020): the sediment has various grades of sorting and this could be due to several fillings in the depositional period. The sorting as well as the stratification of the material suggest that facies conditions were thalweg or channel facies (Bosch & White, 2004; Bethke, 2020).

The mineralogical bulk sample composition comprises quartz, K-feldspar, muscovite, chlorite, goethite, and rarely calcite. The absence of carbonate-providing minerals is also shown in the low TIC content. Also, there is no evidence for

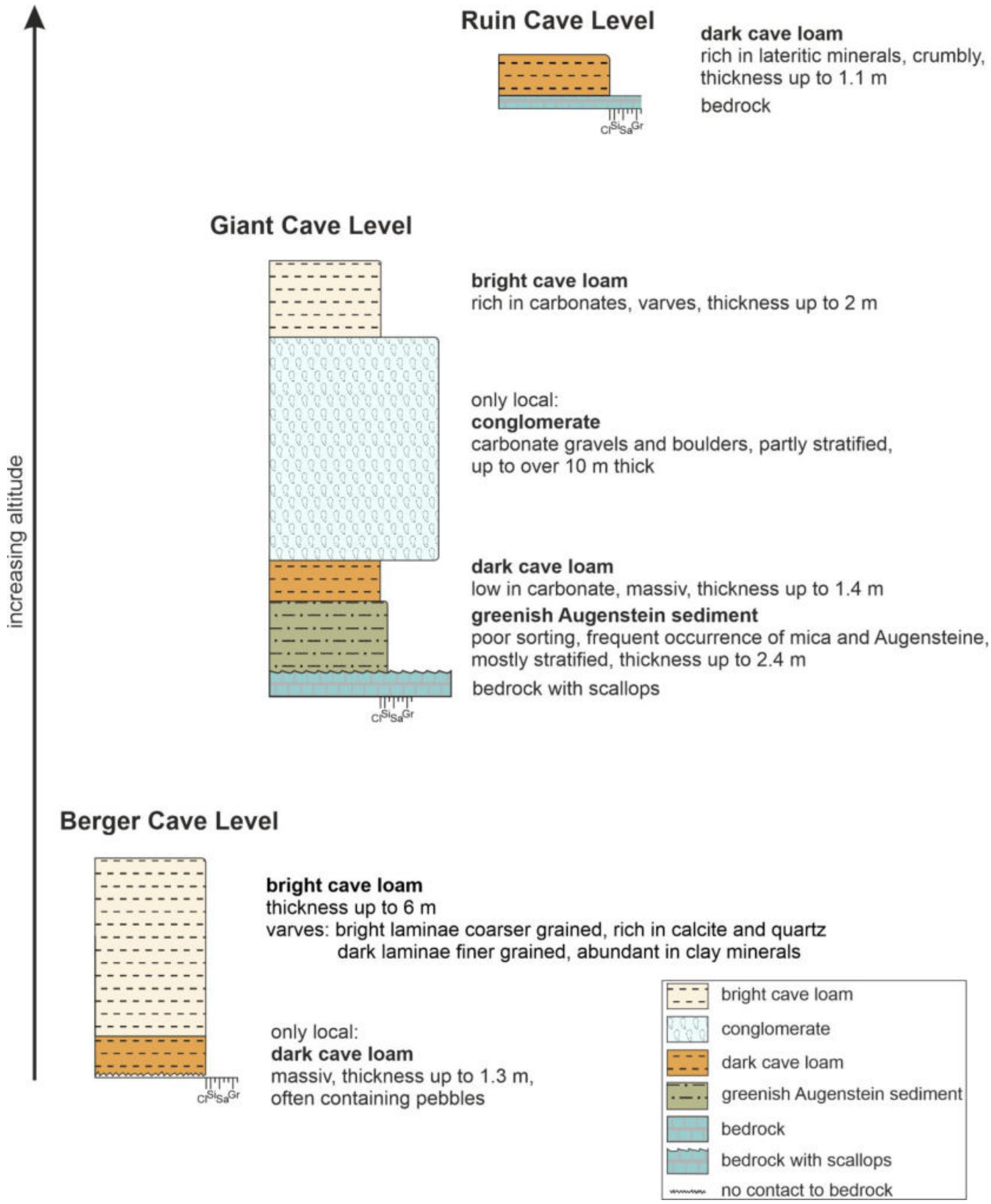

Figure 35: Altitude-depending, idealised profiles of cave sediments in Berger Cave Level, Giant Cave Level, and Ruin Cave Level of Dachstein Massif.

organic matter, which is indicated by the results of the TOC analysis. This was expected due to its assumed origin as an erosional product of the Augenstein Formation. The thickness of the greenish Augenstein sediment is up to 2.4 m, which could be observed in Rieseneishöhle. In Mammuthöhle it had only a maximum thickness of 65 cm in the outcrops visited.

The concretions with MH T06 as an example are assumed to be developed within the greenish Augenstein sediment. Concretions are defined as selective consolidations within sandy sediments that form under the action of local waters. Therefore, they compose of sand and as a binding material act mainly clay and calcite (Seemann, 1973). The concretions are also known from Rieseneishöhle where the material is coarser, but consists as well of depositions of laminated Augenstein Formation that are cemented with clay and calcite (Seemann et al, 1999). According to Audra et al (2002) the concretions of Eisriesenwelt contain the weathered residue of the local bedrock and sediments.

The thin section of MH T06 (Fig. 32) shows a laminated concretion and the layers partially have a trend of gradation. Taking into consideration that the greenish Augenstein sediment deposited in the caves due to several fillings of eroded material (Bethke, 2020), the gradation may also indicate the flooding events, just on a smaller scale. The fining-upwards layers show the decreasing energy level within an event.

The dome-like structures that were seen in the upper third of the thin section can be interpreted as water-escape structures. Water-escape structures are distinctive soft-sediment features, and they are a product of consolidation of saturated sediments (Lowe, 1975; Dasgupta & Chatterjee, 2019). Within a consolidated sediment, basic mechanisms like fluidization or liquefaction occur due to an interaction of fluid and solid simultaneously or immediately after deposition (Lowe, 1975). The dome-like structure is created when trapped pore fluids escape in an upwelling motion, while forming a pillar at the same time in the sediment. This sediment dewatering is triggered by processes such as seismic events (Dasgupta & Chatterjee, 2019).

The water-escape structures are predominately recognisable in sediments with sand or silt grain sizes (Lowe, 1975), however, layers with different grain sizes respond in general differently to the vibrations (Dasgupta & Chatterjee, 2019). The examined concretion composes of grain sizes in the sand and silt range, and also the greenish Augenstein sediment consists mainly of these sizes.

Salomon et al (2018) observed soft-sediment deformation structures in saturated sediments in Hirlatzhöhle as well. The structures were classified as seismically triggered episodic events during the last glaciation and are found within the bright cave loam. In Mammuthöhle comparable structures can be found in outcrop 6 (Fig. 17b), also in the bright cave loam. They have not been studied in detail, but the structures are probably of similar origin.

The disturbed sediment in the lower third of the thin section of MH T06 could show bioturbation and in this case the corridors would be burrows of organisms. The same consideration applies to the traces found in sample MH T04 of dark cave loam. However, why the burrows occur only locally – at outcrop 3 within cm range – and which troglobiont organisms could be responsible for the structures is a matter of discussion.

The **dark cave loam** shows a brown, sometimes reddish, colour and has a massive appearance. The maximum observed thickness is 1.4 m, which is a distinctive difference to Bethke (2020). On average, it was 60 to 80 cm. The sediment occurred in every cave studied in Dachstein Massif, regardless of the altitude (Fig. 35). The analysed sediment from Rieseneishöhle was not classified as a dark cave loam by Bethke (2020), however, the colour is a similar dark brown and the composition of the bulk mineralogy as well as the clay mineralogy are corresponding with the data of the dark cave loam of the other caves.

The grain size of the dark cave loam ranges from clay to fine sand, is not very well sorted, and has a high percentage of fine clay. However, it is mentionable that although the samples MH T03 and MH T04 are from the same location at Krippensteingang in Mammuthöhle, the grain size distribution curves show different patterns. The latter was taken from the area where burrows could be observed and comprises mainly of clay, whereas for sample MH T03 – like the other samples of dark cave loam – the silt fraction is of importance as well.

The sample MH T10 of dark cave loam has also a coarser appearance in Mammuthöhle which could be confirmed in the grain size distribution analysis. Due to the coarseness of the sample, quartz and muscovite are much more frequent than in the other samples of the dark cave loam. In addition, the sample from Rieseneishöhle (DRH 01) is much coarser as well, and coarse clasts of Augenstein Formation can be found. Therefore, the deposition of these samples took place under higher energy conditions.

The grain size range of the sediment indicates a deposition at backswamp or slackwater facies conditions (Bosch & White, 2004), as Bethke (2020) already assumed. However, sediments of slackwater facies are often characterised to be well laminated (Bosch & White, 2004), which is not the case for the massive dark cave loam.

The dark cave loam contains in general of quartz, muscovite, chlorite, illite, kaolinite, goethite or hematite, K-feldspar, and rarely also of calcite. Therefore, the TIC results are concordantly low as well. Bethke (2020) proposed that the dark cave loam originates from palaeosol due to the presence of illite and goethite (Schachtschabel et al, 1984). This palaeosol may originate from Augenstein Formation (Bethke, 2020).

However, the composition refers only to the dark cave loam in Mammuthöhle, Rieseneishöhle, and Hirlatzhöhle. In Günter-Stummer-Höhle on the Ruin Cave Level on the other hand boehmite, anatase, chlorite, muscovite, and hematite or goethite compose the sediment. Boehmite as an Al-oxide-hydroxide is a typical mineral that occurs in laterite (Borger & Widdowson, 2001). Laterite is an in-situ subaerial weathering product of a protolith bedrock, developing under tropical or subtropical climatic conditions (Widdowson, 2009).

The characteristics of a laterite is an enrichment of less mobile elements like Fe and Al (Borger & Widdowson, 2001; Widdowson, 2009). Also, anatase forms as the most common titanium dioxide weathering product in this kind of environment (Milnes & Fitzpatrick, 1989). At the same time – like it can also be observed in the XRD patterns – silica, alkaline earth metals, and alkali metals, which show a greater mobility, are depleted due to the conditions of aggressive weathering (Borger & Widdowson, 2001; Widdowson, 2009).

In XRD analyses of samples from Mammuthöhle the minerals gibbsite and boehmite were detected (Seemann, 1973). However, in the examined samples from Mammuthöhle of this study as well as from Bethke (2020) none of these minerals could be found. Furthermore, the small grain size of the material of Günter-Stummer-Höhle may also indicate that the analysed sediment is a laterite because due to the high degree of weathering, the grain sizes are reduced.

The presence of laterite is an indication for a humid tropical or equivalent climate and is therefore a record for paleoenvironmental conditions for this region (Widdowson, 2009). A warming trend was predominant in Paleocene and during the Early Eocene (Fig. 36), which accumulated into a climatic optimum with tropical conditions at the Paleocene to Eocene border. From the Middle Eocene onwards, the circumstances changed to a cooler climate (Zachos et al, 1993). This Cenozoic cooling trend was only interrupted by a short-term subtropical event in Middle Miocene times (Holbourn et al, 2015).

These climatic data could be an indicator that the laterite was not formed later than the Mid-Miocene Climatic Optimum because the conditions prevailing afterwards would not have been favourable for lateritization (Widdowson, 2009).

The intensive weathering takes especially place during the periods of stagnant uplifting (Kuhlemann et al, 2008). However, the lateritization process terminates as soon as climatic or also tectonic changes occur and then erosion of the laterite proles follows (Borger & Widdowson, 2001). According to Kuhlemann et al (2008), the humid to semihumid weathering conditions are favourable for the formation of kaolinite as well as laterite minerals, whereas temperate and humid climates enhance the formation of illite. These clay minerals are together with chlorite and mixed-layered minerals present in the composition of the dark cave loam in the Giant Cave Level.

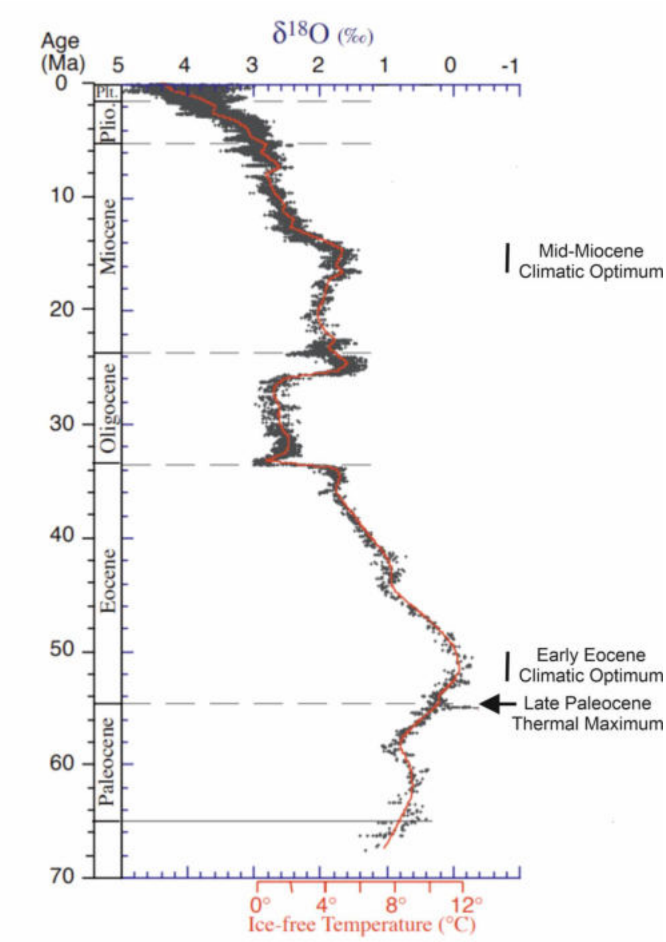

Figure 36: Temperature curve during Cenozoic, generated from pelagic sediments. Climatic optima can be seen during Late Paleocene, Early Eocene, and Middle Miocene. The $\delta^{18}O$ scale gives an indication of the ice sheet development, high values imply permanent ice sheets (modified from Zachos et al, 2001, and references therein).

In addition, according to Thiedig (1970) there are also clayey palaeosols in the Eastern Alps with mostly a reddish or yellowish colour that are known to be formed under subtropical pre-Pleistocene climatic conditions. Kuhlemann et al (2008) suggested that the formation of the palaeosols was between 10 Ma and 2.7 Ma. Therefore, the soils are interpreted to be an indicator of a climatic change in the Pliocene before the onset of glaciations (Audra et al, 2007). The exact time of formation can differ depending on the local climatic environments (Kuhlemann et al, 2008).

Audra et al (2007) proposed that the cave sediments originating from these soils were eroded during a period of cooling and were washed into the caves, supposedly during the Pleistocene (Kuffner, 1998). Samples of these palaeosols from all over the NCA were analysed by Kuhlemann et al (2008). The results show in the area of Dachstein Massif regarding the clay mineralogy the presence of illite, chlorite, and in a minor quantity also of kaolinite and smectite, which appear as mixed-layer minerals. The same minerals except smectite occur in the dark cave loam. However, according to Kuhlemann et al (2008) also vermiculite is a frequent mineral that could not be detected at all. Although the dark cave loam might originally have been partially soil, the TOC value is low. Hence, the palaeosol had to be organic-poor respectively organic-free.

All in all, the dark cave loam could be originally of both, either palaeosol or laterite. The original material might be developed at different times during Cenozoic (Zachos et al, 1993; Kuhlemann et al, 2008; Holbourn et al, 2015), and it could also be elevation dependent. Laterite formed rather in humid tropical conditions (Widdowson, 2009), which was mainly the case prior to Middle Miocene (Fig. 36; Zachos et al, 1993; Holbourn et al, 2015).

The Ruin Cave Level, as Frisch et al (2002) suggested, was developed from Eocene to Oligocene. During the uplifting process of the NCA in Miocene times (Frisch et al, 2000), this level could be acting as a trap for the eroding lateritic sediments. Therefore, the laterites in Günter-Stummer-Höhle could be interpreted as an indication that the Ruin Cave Level indeed formed before the Middle Miocene.

Later, when the Giant Cave Level also existed in the Upper Miocene (Frisch et al, 2001), the laterite was already eroded at the surface and only pre-Pleistocene types of soil with a lower degree of weathering were washed into the caves situated in lower altitudes (Audra et al, 2007; Kuhlemann et al, 2008). Altitude specific sediments that were transported into caves were also observed by Kuffner (1998).

Within the dark cave loam, compact clay components with either a dark reddish (GSH 01) or greenish colour (GSH 02) could be found. The colour is due to the respective prevailing oxygen conditions during the process of weathering (Köster & Schwertmann, 1993). Both samples contain Fe-oxides, which is confirmed by the XRD analyses. The green colour of the sediment occurs in anoxic conditions (Köster & Schwertmann, 1993) whereas the red colour in oxidizing ones. That is also the reason for the thin reddish coat of the green component because the surface of the mud-clasts was exposed to the air.

The clayey-silty solidified layer on top of Dachsteinkalk in some parts of Günter-Stummer-Höhle is cemented sediment. Eventually also cemented dark cave loam because the composition according to the observations of the thin sections correspond to the XRD bulk mineralogy results of the samples from Mammuthöhle. Nevertheless, it seems to contain a higher content of calcite, which is shown by the reaction with HCl. The cementation could have been taken place along paths where calcareous water flows, causing also the observed lumping of the sediment. Therefore, the areas described as matrix could as well be micrite with a high content of clay minerals. The clustered quartz minerals could represent former burrows of organisms that were filled in. The burrows were either actively filled by the organisms or after being abandoned, passively sealed with material from the surface (Wetzel, 2015).

In Mammuthöhle **conglomerates** are deposited locally on top of the dark cave loam. They can have a thickness up to 10 m (Bethke, 2020). The components reach a diameter of up to 0.2 m (Bethke, 2020) and consist mainly of carbonates, but also Augensteine and pseudo-pisolitic iron ore can be present. The carbonates are probably transported into the cave from the immediate surroundings and are therefore of Dachsteinkalk Formation origin (Mandl, 2000). Bethke (2020) associated the deposition of the conglomerates to the diamicton facies due to the unsorted and unbedded appearance (Bosch & White, 2004).

In Hirlatzhöhle conglomerates occur as well (HIH 01, HIH 02). The majority of the components of HIH 01 and some of HIH 02 have a bright grey colour and show an abundance of fossils like foraminifera (Fig. 37). In addition, algae and crinoids are further recognisable components. All these fossils are indicators that the main clasts are of Dachsteinkalk Formation, which formed in shallow marine facies (Mandl, 2000). Also, the other carbonates – often reddish or micritic – could be attributed to the Dachsteinkalk Formation because the platform in general shows a cyclic layering ("Lofer facies") due to sea-level changes. In the course of the different intertidal to subtidal settings, reddish respectively colourful argillaceous carbonates interpreted as reworked soil, dolomitic limestone, and a massive limestone as the main as well as last member of the cyclothems developed (Fischer, 1964).

In contrast, HIH 02 consists besides the components of Dachsteinkalk Formation predominately of quartz, mainly of polycrystalline one. Therefore, these components that are sometimes also slightly metamorphically overprinted are originally from the Augenstein Formation (Frisch et al, 2001). The blackish rim around some clasts might be a weathering phenomenon where the surface begins to transform.

The subangular to rounded components in general indicate a certain transport route from the provenance to the sedimentation as conglomerates. The depositional conditions of the conglomerates in Hirlatzhöhle, especially at outcrop 9, are in situ. The primary matrix seemed washed out and replaced instead by secondary calcitic cement.

The pebbles from outcrop 11 in Hirlatzhöhle seem to be remnants of the Werfen Formation (G. Mandl, personal communication). The Werfen Formation is characterised by three sections: Quartzite at the base, followed by thick schists and limestone at the top (Tollmann, 1985). The samples are most likely to be assigned to the Werfen schist, which is described by Tollmann (1985) as being a red, violet, grey, green, or brown sandstone with a foliated structure.

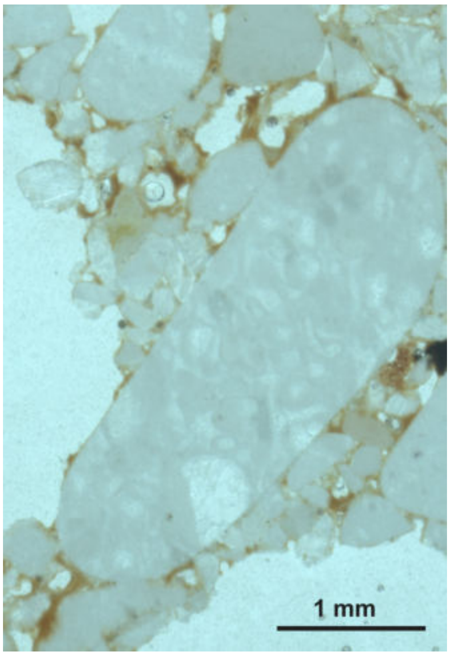

(a)

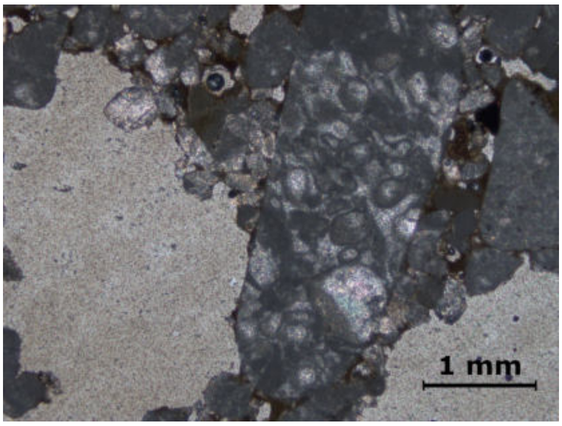

(b)

Figure 37: Detailed thin section pictures of a fossil-rich, clay-coated Dachsteinkalk clast surrounded by other carbonate grains. (a) Fossils indicate a shallow marine milieu during deposition. (b) The various fossils are better visible due to the crossed polarisers.

However, it is unclear whether the consolidated and unconsolidated conglomerates can be associated to the deposition of the conglomerates of Mammuthöhle or how they could be incorporated into the idealised profile because no direct contact to the bright cave loam could be observed.

The **bright cave loam** as the topmost possible section of the idealised profile shows a decreasing thickness with increasing sea level of the investigated caves, ranging from 6 m in Hirlatzhöhle to non-existence in Günter-Stummer-Höhle (Fig. 35). The dark and bright laminae were analysed separately if possible, which was not the case with the samples from Mammuthöhle. There, the samples are not pure laminae of bright cave loam and this is also clearly shown in the results. The mainly clayey material as well as the good sorting indicate sedimentation in stagnant water conditions and therefore a slackwater facies (Bosch & White, 2004; Bethke, 2020).

6.2 Bright and dark laminae of the bright cave loam

The bright and dark laminae of the bright cave loam are interpreted as being annual, fluvio-lacustrine varve-like deposits (Spöcker, 1925; Audra et al, 2002) due to the glacial blocking of karst springs (Franke & Illing, 1963; Schauberger, 1983). During the depositions in summer there is snowmelt runoff and the varves are pale as well as coarser grained whereas the clay particles remain in the water column and therefore, the winter varves are characterised as being darker and fine-grained (Fig. 38; Zolitschka et al, 2015).

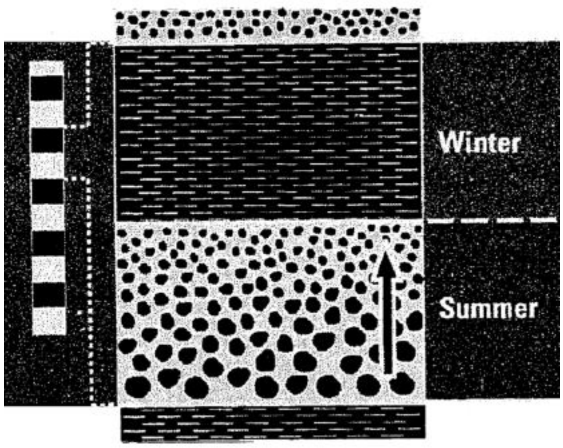

Figure 38: Schematic model of formations of varves during summer (sand/coarse silt) and winter (fine silt/clay; modified from Sturm and Lotter, 1995).

The results of this work as well as the data carried out by Salomon et al (2018) show indeed differences in colour and grain sizes of the laminae of dark cave loam (Fig. 39). The analysed dark laminae have a finer grain size fraction and the clay minerals are more abundant, which is well recognised in the semiquantitative analysis (Fig. 40). The occurring clay minerals in the bright cave loam are illite,

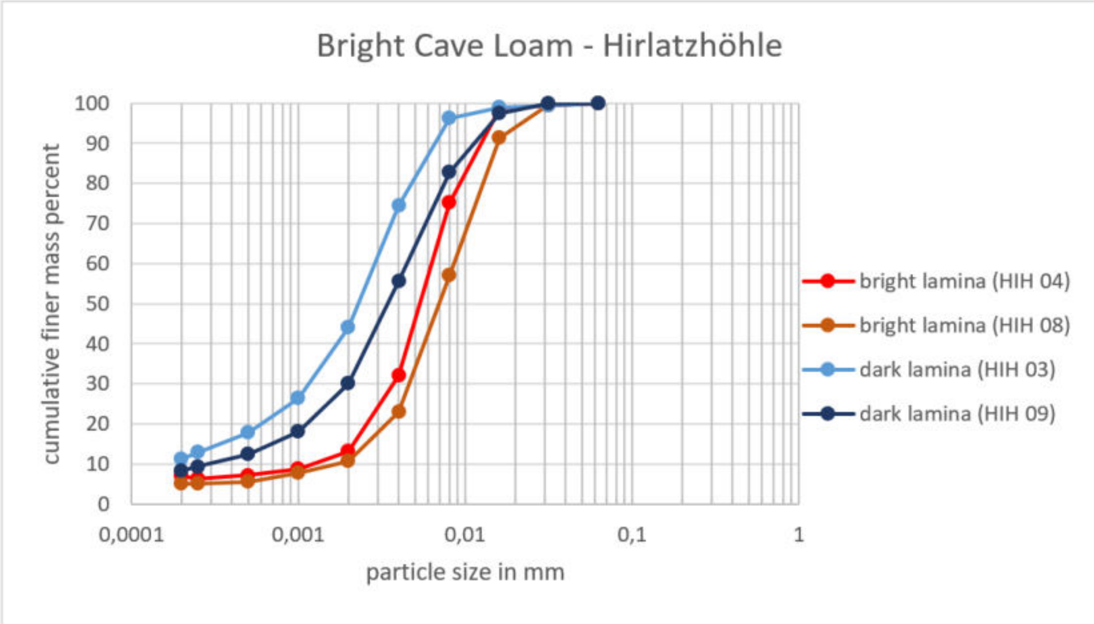

Figure 39: Distribution of the grain sizes of bright (blueish) and dark laminae (reddish) of bright cave loam of Hirlatzhöhle.

smectite, chlorite, and kaolinite (Fig. 41). For these minerals except smectite a layer-depending abundance pattern is also observable: In the darker laminae illite, chlorite, and kaolinite are slightly enriched in comparison to the bright laminae of the bright cave loam.

Calcite and quartz are more abundant in bright laminae. The different values in carbonate-bearing minerals can also be clearly seen in the TIC results. In addition, the bright laminae are more silt dominated and on average also clearly thicker. This could be due to the fact that during spring and summer, the meltwater supplies a larger sediment load under higher energy conditions. Gradation could not be observed like it is often the case in lacustrine varves (Zolitschka et al, 2015). The results of Salomon et al (2018) are very well in accordance, but they were also detecting biotite which could not be confirmed.

If the varves developed due to annual, rhythmic processes, they can be used for dating the time span of deposition. Salomon et al (2018) have applied this and according to the thicknesses of the laminae of the sediment a deposition time span of 0.5 - 1.8 ka was calculated. However, the dating should be taken with caution because varve chronologies may show internal inconsistencies and therefore necessitate an independent verification in the form of for example absolute dating methods (Zolitschka et al, 2015).

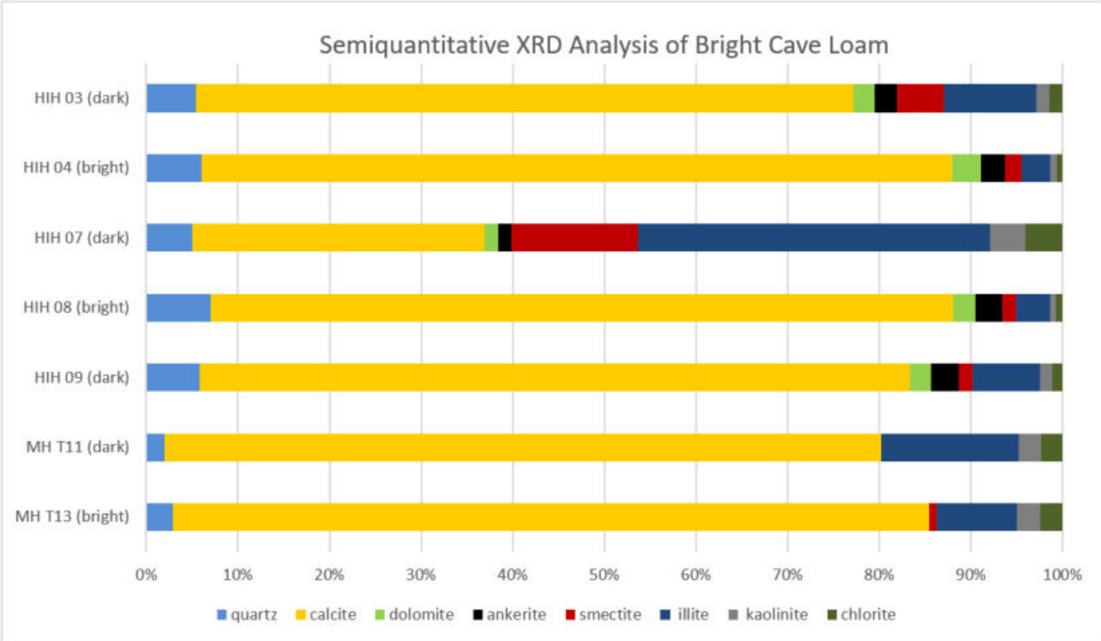

Figure 40: Semiquantitative XRD analysis of bulk composition of all samples of bright cave loam.

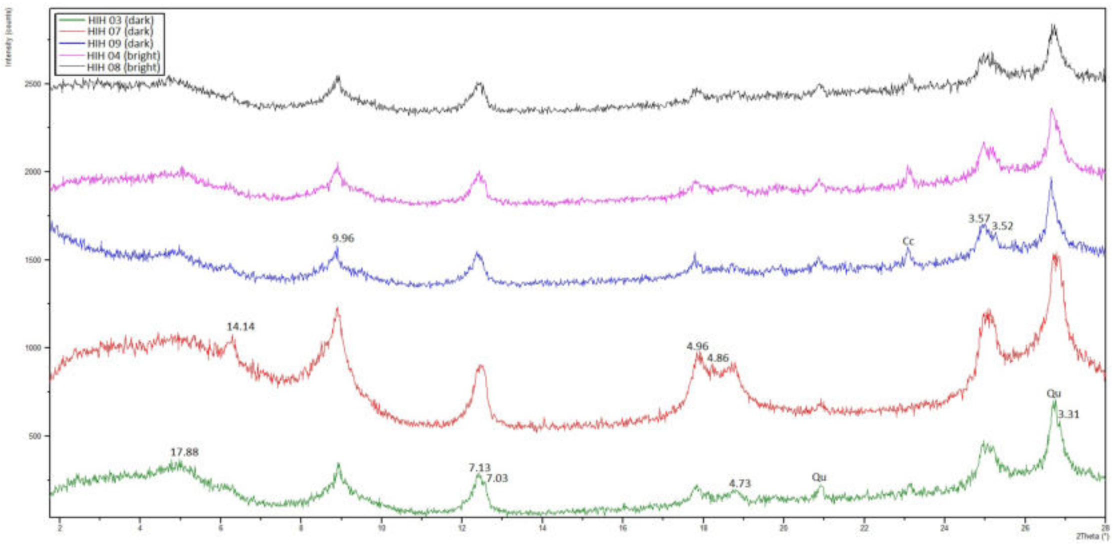

Figure 41: X-ray diffraction patterns of clay mineralogy of dark and bright laminae of bright cave loam from Hirlatzhöhle. Shown are the samples saturated with Mg and glycerol; d-values in Å; Cc = calcite, Qu = quartz.

6.3 Comparison with sediments of caves outside Dachstein Massif

Finally, the results of the samples from the two caves outside of Dachstein Massif should be related to the previous interpretations. The sample from Schönberg-Höhlensystem – SHS 02 – is in its appearance and grain size distribution well comparable with the sample from Rieseneishöhle (DRH 01). Maybe because of this, the deposition process of the sediments in the caves was very similar. Also, Kuffner (1998) described palaeosol outcrops on the surface of Totes Gebirge. Therefore, palaeosol as the original material for the sediment is possible.

XRD measurements were not undertaken, but analyses by Kuffner (1998) showed that the sediments contain especially quartz followed by feldspar, mica, calcite, clay minerals and in a sample from Raucherkarhöhle was also amphibole. In addition, the samples often have a grain size of coarser sand. The Schönberg-Höhlensystem is known to be rich in washed-in cherts and radiolarites (Kuffner, 1998), which can be confirmed by the siliceous clasts of the sample SHS 02.

In Eisriesenwelt in Tennengebirge a repeating profile was described by Plan et al (2021) that had a green-brownish sediment as a base, followed by a dark brown clay. The absence of the bright cave loam as a topmost layer could be explained due to lower backflooding by the local glacier compared to the Dachstein Massif.

Purely by the description, the bottom layer seems to belong to the greenish Augenstein sediment in terms of development and the Augenstein Formation being the source material. The sample ERW KD is from the clayey layer and could be assigned to the dark cave loam because the appearance, the results of XRD bulk mineralogy and clay mineralogy, as well as the grain size distribution are very well comparable with each other. If it can be assumed that there were eroded palesols all over the NCA (Thiedig, 1970; Audra et al, 2007) and subsequently deposited into the caves (Kuffner, 1998), this process may also apply for the sediment analysed.

7 Conclusion

The purpose of this work was to analyse the sediments of four caves – Hirlatzhöhle, Mammuthöhle, Rieseneishöhle, and Günter-Stummer-Höhle –, which are located at different altitudes. From these analyses and the already existing data of Bethke (2020), idealised altitude-dependent sediment profiles were created.

The lowest studied level is the Berger Cave Level and represented by Hirlatzhöhle. Dark cave loam is found in higher parts, but predominately there is bright cave loam. The sediment is the youngest layer, and it shows a strong altitude dependence, from a thickness up to 6 m in Hirlatzhöhle to non-existence in the higher situated Günter-Stummer-Höhle. The beige sediment is laminated within a mm to cm range and deposited under conditions of slackwater facies (Bethke, 2020). There are indications that the deposits are glacio-lacustrine annual varves: (1) The laminating shows brighter and darker laminae. (2) The brighter laminae are on average thicker than the darker ones. (3) The brighter laminae are enriched in quartz as well as calcite and are coarser grained with a grain sizes dominated by silt. In contrast, the darker laminae are abundant in clay minerals and also have a higher percentage of fine fraction. These differences could be due to the fact that the depositions during spring and summer are caused by meltwaters with a higher energy and more sediment supply, whereas in winter the remaining finer particles sediment (Zolitschka et al, 2015). The results are in concordance with Salomon et al (2018).

In the caves of the Giant Cave Level (Mammuthöhle, Rieseneishöhle) the complete profile can be seen. On top of the bedrock, there is the greenish Augenstein sediment. It is interpreted as being of thalweg or channel facies, and it was deposited throughout several fillings (Bethke, 2020). The sediment can have a thickness of more than 2.4 m. The bulk and clay mineralogical analyses reveal that the composition is quartz, muscovite, and chlorite in a high frequency whereas K-feldspar, goethite, illite, and kaolinite are secondary. The sediment shows a poor sorting, and Augensteine are often recognisable. The composition as well as heavy mineral analyses indicate the Augenstein Formation being the origin for the sediment (Kuffner, 1998; Frisch et al, 2001; Bethke, 2020).

The dark cave loam is the overlaying layer with a thickness up to 1.4 m. The brownish to reddish, massive sediment was deposited under slackwater or backswamp facies conditions (Bethke, 2020). The grain size distribution is mainly of clay and silt, and it comprises quartz, muscovite, goethite or hematite, chlorite, illite, and kaolinite.

Carbonate conglomerates and conglomeratic breccias follow the dark cave loam. However, they occur only in Mammuthöhle and there just locally. The very poorly sorted components are carbonates and secondary also Augensteine as well as pseudo-pisolitic iron ore. They have sizes ranging from sand to boulders. The sediment with a thickness up to 10 m might be of diamicton facies (Bethke, 2020). The last layer is the carbonate-rich bright cave loam, and in this cave level it is up to 2 m thick.

The highest situated level is the Ruin Cave Level (Günter-Stummer-Höhle) where only dark cave loam can be found. In comparison, this loam consists mainly of the clay fraction and boehmite as well as anatase are additionally present, whereas it is very depleted in quartz. The composition and the fine grain size of the material indicate a high degree of weathering and therefore a lateritic origin (Borger & Widdowson, 2001; Widdowson, 2009).

The obtained results of the samples of dark cave loam from the Giant and Berger Cave Level lead to the conclusion that the original material are moderately weathered pre-Pleistocene palaeosols (Thiedig, 1970; Kuhlemann et al, 2008). The lateritic remains from Günter-Stummer-Höhle on the other hand, may result from tropical to subtropical climatic conditions prior to Middle Miocene times (Zachos et al, 1993; Holbourn et al, 2015). Nevertheless, both are classified as dark cave loam that was formed during different time periods in the Cenozoic. With regard to their composition, the samples of the reference caves could also be of dark cave loam of palaeosol origin, but partially with a different depositional history.

With the help of this work new knowledge could be gained about the clastic cave sediments at the northern rim of Dachstein Massif. However, it remains unanswered to which altitude the backflooding meltwater was reaching at the study area and where the bright cave loam stopped depositioning. Furthermore, the altitude dependency of the lateritic dark cave loam has to be investigated. Also, it is of great interest to be able to date these laterites, since they could provide an indication of the age of the caves of the Ruin Cave Level. This would be an important contribution to the reconstruction of the history of the cave formation process in the Dachstein Massif.

8 Acknowledgement

This master's thesis could not be possible without the support of several people. Therefore, I have to express my gratitude and acknowledge their help along my way.

First of all, I would like to thank my supervisor Susanne Gier. She has instructed me to the different methods of analysis and was always open to answer questions. Next, the original impulse for this work came from my co-supervisor Lukas Plan. He introduced me to the extraordinary activity of speleology, and without him there would not be any samples to analyse. Both supported me with interesting discussions and valuable ideas, which facilitated my way to this work. In addition, Lukas Plan also enabled a FEMTech Praktikum at Natural History Museum of Vienna.

Furthermore, I would like to acknowledge Sabine Hruby-Nichtenberger who helped me in the laboratory and Beatrix Bethke where I could do the TOC analysis. Likewise, I thank the people from the lab who produced my thin sections and Alexander Lukeneder for having a look at them. Also, Gerhard Mandl was helpful with his input regarding the sediments in the Hirlatzhöhle.

On the caving tours accompanied me once each, Eva Kaminsky, Michael Nagl, and Toni Tanzberger. Barbara Gruber was there every time with me. Zora Kumm did a lot of lab work at the same time for her thesis, so we gave us much needed moral support throughout the process. A huge thank you to all of you.

Last but not least, my study would not have been possible without my family and my boyfriend. For this I will always be thankful.

References

Agnolin, A.M. (2021). Variability in the use of caves and rockshelters among ethnographic hunter-gatherers and its archaeological implications. *Journal of Anthropological Archaeology, 64*, 1-10

Arnberger, E. (1953). Neue Ergebnisse morphotektonischer Untersuchungen in der Dachstein-Mammuthöhle. *Mitteilungen der Höhlenkommission*, 68-79

Arnberger, E. (1954). Erforschungen und Neuentdeckungen im Dachsteingebiet. *Edelweiß-Nachrichten, 8*, 1-7

Assmann, T., Casale, A., Drees, C., Habel, J.C., Matern, A., & Schuldt, A. (2010). Review: The Dark Side of Relict Species Biology: Cave Animals as Ancient Lineages. In J.C., Habel & T., Assmann (Eds.). *Relict Species: Phylogeography and Conservation Biology* (pp. 91-103). Berlin Heidelberg, Germany: Springer-Verlag

Audra, P., Bini, A., Gabrovšek, F., Häuselmann, P., Hobléa, F., Jeannin, P.Y., Kunaver, J., Monbaron, M., Šušteršič, F., Tognini, P., Trimmel, H., & Wildberger, A. (2006). Cave genesis in the Alps between the Miocene and today: a review. *Zeitschrift für Geomorphologie, 50(2)*, 153-176

Audra, P., Bini, A., Gabrovšek, F., Häuselmann, P., Hobléa, F., Jeannin, P.-Y., Kunaver, J., Monbaron, M., Šušteršič, F., Tognini, P., Trimmel, H., & Wildberger, A. (2007). Cave and Karst Evolution in the Alps and Their Relation to Paleoclimate and Paleotopography. *Acta carsologica, 36(1)*, 53-67

Audra, P., Quinf, Y., & Rochette, P. (2002). The Genesis of the Tennengebirge Karst and Caves (Salzburg, Austria). *Journal of Cave and Karst Studies, 64(3)*, 153-164

Bauer, F. (1955): Pseudomorphosen nach Pyrit aus der Dachstein-Mammuthöhle bei Obertraun. *Jahrbuch des Oberösterreichischen Musealvereines, 100*, 351-358

Behm, M., Plan, L., Seebacher, R., & Buchegger, G. (2016). Dachstein. In C., Spötl, L., Plan, & E., Christian (Eds.). *Höhlen und Karst in Österreich* (pp. 569-

588). Linz, Austria: Oberösterreichisches Landesmuseum

Bethke, K. (2020). Sedimente der Höhlen am Dachstein-Nordrand und ihre Aussage für die Höhlen- und Landschaftsentwicklung [Unpublished master's thesis]. Universität Wien

Bock, H. (1913). Alte Höhlenstromläufe im Inneren des Mittagskogels. In H., Bock, G., Lahner, & G., Gaunersdorfer (Eds.). *Höhlen im Dachstein* (pp. 72–88). Graz, Austria: Verein für Höhlenkunde in Österreich

Bock, H. (1926/27). Zur Altersfrage der Dachsteinhöhlen. *Mitteilungen über Höhlen- und Karstforschung*, 1926 *3*, 72-77, *4*, 105-113, 1927 *1*, 1-19

Bock, H. & Lahner, G. (1913a). Die Dachstein-Mammuthöhle. In H., Bock, G., Lahner, & G., Gaunersdorfer (Eds.). *Höhlen im Dachstein* (pp. 60-71). Graz, Austria: Verein für Höhlenkunde in Österreich

Bock, H. & Lahner, G. (1913b). Die Dachstein-Rieseneishöhle. In H., Bock, G., Lahner, & G., Gaunersdorfer (Eds.). *Höhlen im Dachstein* (pp. 15–34). Graz, Austria: Verein für Höhlenkunde in Österreich

Borger, H. & Widdowson, M. (2001). Indian laterites, and lateritious residues of southern Germany: A petrographic, mineralogical, and geochemical comparison. *Zeitschrift für Geomorphologie, 24(2)*, 177-200

Bosch, R. & White, W.B. (2004). Lithofacies and transport of clastic sediments in karstic aquifers. In I.D., Sasowsky & J., Mylroie (Eds.). *Studies of Cave Sediments* (pp. 1–22). Dordrecht, Netherlands: Springer

Bossert, T. & Buchegger, G. (1998). Beilage: Übersichtskarte 1:10 000. In ARGE Hirlatzhöhlenbuch (Eds.). *Die Hirlatzhöhle im Dachstein Hallstatt.* Hallstatt, Austria: ARGE Hirlatzhöhlenbuch

Dasgupta, P. & Chatterjee, A. (2019). Formation of water-escape structure during shock induced fluidization: The role of permeability contrast. *Journal of Structural Geology, 124*, 1-7

Ehrenberg K. (1964). Ein Jungbärenskelett und andere Höhlenbärenreste aus der Bärenhöhle im Hartlesgraben bei Hieflau (Steiermark). *Annalen des Naturhistorischen Museums Wien, 67*, 189–252

Farrant, A. (2003). Paleoenvironments. Clastic Cave Sediments. In J., Gunn (Ed.). *Encyclopedia of Caves and Karst Science* (pp. 553-555). New York, NY: Routledge

Farrant, A.R. & Smart, P.L. (2011). Role of sediment speleogenesis; sedimentation and paragenesis. *Geomorphology, 134*, 79-93

Fischer, A.G. (1964). The Lofer Cyclothems of the Alpine Triassic. *Kansas Geological Survey, Bulletin, 196*, 107-149

Fischer, K. (1990). Höhlenniveaus und Altreliefgenerationen in den Berchtesgadener Alpen. *Mitteilungen der Geographischen Gesellschaft München,75*, 47-59

Franke, H.W. & Ilming H. (1963). Beobachtungen in der Dachstein-Mammuthöhle (Oberösterreich). *Die Höhle, 14*, 36-40

Frisch, W., Kuhlemann, J., Dunkl, I., & Brügel, A. (1998). Palinspastic reconstruction and topographic evolution of the Eastern Alps during late Tertiary extrusion. *Tectonophysics, 297*, 1-15

Frisch, W., Kuhlemann, J., Dunkl, I., & Székely, B. (2001). The Dachstein paleosurface and the Augenstein Formation in the Northern Calcareous Alps – a mosaic stone in the geomorphological evolution of the Eastern Alps. *International Journal of Earth Sciences, 90*, 500-518

Frisch, W., Kuhlemann, J., Dunkl, I., & Székely, B., Vennemann, T., & Rettenbacher, A. (2002). Dachstein-Altfläche, Augenstein-Formation und Höhlenentwicklung - die Geschichte der letzten 35 Millionen Jahre in den zentralen Nördlichen Kalkalpen. *Die Höhle, 53*, 1-37

Frisch, W., Székely, B., Kuhlemann, J., & Dunkl, I. (2000). Geomorphological evolution oft the Eastern Alps in response to Miocene tectonics. *Zeitschrift für Geomorphologie, 44*, 103-138

Geyer, E., Seebacher, R., Tenreiter, C., & Knobloch, G. (2016). Totes Gebirge. In C., Spötl, L., Plan, & E., Christian (Eds.). *Höhlen und Karst in Österreich* (pp. 569-588). Linz, Austria: Oberösterreichisches Landesmuseum

Gillieson, D. (2003). Sediments. Allochthonous Clastic. In J., Gunn (Ed.). *Ency-*

clopedia of Caves and Karst Science (pp. 633-634). New York, NY: Routledge

Haseke-Knapczyk, H. (1989). *Der Untersberg bei Salzburg. Die ober- und unterirdische Karstentwicklung und ihre Zusammenhänge. Ein Beitrag zur Trinkwassererforschung.* Innsbruck, Austria: Universitätsverlag Wagner

Häuselmann, P. (2004). *Die St. Beatus-Höhlen. Entstehung, Geschichte, Erforschung.* Allschwil, Switzerland: Speleo Projects 256

Häuselmann, P., Plan, L., Pointner, P., & Fiebig, M. (2020). Cosmogenic nuclide dating of cave sediments in the Eastern Alps and implications for erosion rates. *International Journal of Speleology, 49*, 107-118

Holbourn, A., Kuhnt, W., Kochhann, K.G.D., Andersen, N., & Meier, K.J.S. (2015). Global perturbation of the carbon cycle at the onset of the Miocene Climatic Optimum. *Geology, 43(2)*, 123-126

Jelínek (1983). The Mladeč finds and their evolutionary importance. *Anthropologie, 21*, 57-64

Köster, E. (1964). *Granulometrische und morphometrische Meßmethoden an Mineralkörnern, Steinen und sonstigen Stoffen.* Stuttgart, Germany: Ferdinand Enke Verlag

Köster, H.M. & Schwertmann, U. (1993): Beschreibung einzelner Tonminerale. In K. Jasmund & G. Lagaly (Eds.). *Tonminerale und Tone. Struktur, Eigeschaften, Anwendungen und Einsatz in Industrie und Umwelt* (pp. 33-88). Darmstadt: Steinkopff

Kuffner, D. (1998). *Höhlenniveaus und Altflächen im Westlichen Toten Gebirge.* Vienna, Austria: Verband Österreichischer Höhlenforscher

Kuhlemann, J., Taubald, H., Vennemann, T., Dunkl, I., & Frisch, W. (2008). Clay Mineral and Geochemical Composition of Cenozoic Paleosols in the Eastern Alps (Austria). *Austrian Journal of Earth Sciences, 101*, 60-69

Lahner, G. (1937). Morphologie des Salzkammergutes. II. Die Karstlandschaft. *Mitteilungen für Erdkunde, 6(11-12)*, 123-153

Lahner, G. (1948). *Die Dachsteinhöhlen im oberösterreichischen Salzkammergut* *und ihre Bedeutung in der Entstehung der Nördlichen Kalkalpen.* Linz, Austria: Oberösterreichische Landesregierung

Lehmann, O. (1922). Die große Eishöhle im Tennengebirge (Salzburg). (Eisriesenwelt). Ausführlicher Bericht über die Ergebnisse der Höhlenexpedition der Akademie der Wissenschaften in Wien, 1921. *Speläologisches Jahrbuch, 2*, 52-121

Leutner, N. (1998). Forschunsgeschichte von 1949 bis 1962. In ARGE Hirlatzhöhlenbuch (Eds.). *Die Hirlatzhöhle im Dachstein Hallstatt* (pp. 58-88). Hallstatt, Austria: ARGE Hirlatzhöhlenbuch

Lowe, D.R. (1975). Water escape structures in coarse-grained sediments. *Sedimentology, 22*, 157-204

Mandl, G. (2000). The Alpine sector of the Tethyan shelf - Examples of Triassic to Jurassic sedimentation and deformation from the Northern Calcareous Alps. *Mitteilungen der Österreichischen Geologischen Gesellschaft, 92*, 61-77

Milnes, A.R. & Fitzpatrick, R.W. (1989). Titanium and Zirconium Minerals. In J.B., Dixon, S.B., Weed (Eds.). *Minerals in Soil Environments* (2nd ed., pp. 1131-1206). Madison, Wisconsin: Soil Science Society of America

Pacher, M. (1996): Bericht über eine paläontologische Probegrabung in der Dachstein-Rieseneishöhle bei Obertraun (Oberösterreich). *Die Höhle, 47*, 74-79

Pavuza, R. (1998). Hinweise zu den Sedimenten der Hirlatzhöhle. In ARGE Hirlatzhöhlenbuch (Eds.). *Die Hirlatzhöhle im Dachstein Hallstatt* (pp. 205-207). Hallstatt, Austria: ARGE Hirlatzhöhlenbuch

Plan, L., Filipponi, M., Behm, M., Seebacher, R., & Jeutter, P. (2009). Constraints on alpine speleogenesis from cave morphology – a case study from the eastern Totes Gebirge (Northern Calcareous Alps, Austria). *Geomorphology, 106(1-2)*, 118-129

Plan, L., Kaminsky, E., Racine, T., & Koltai, G. (2021). Genetische Interpretation der Eisriesenwelt (Tennengebirge). *Die Höhle, 72*, 117-138

Plan, L. & Xaver, A. (2010). Geomorphologische Untersuchung und genetische Interpretation der Dachstein-Mammuthöhle (Österreich). *Die Höhle, 61*, 18-38

Pointner, P. & Klappacher, W. (2016). Tennengebirge. In C., Spötl, L., Plan, &

E., Christian (Eds.). *Höhlen und Karst in Österreich* (pp. 553-568). Linz, Austria: Oberösterreichisches Landesmuseum

Rosendahl, W., Kampe, S., & Döppe, D. (2005). The scientific discovery of „Ursus spelaeus“. *Abhandlungen der Naturhistorischen Gesellschaft Nürnberg, 45*, 199-214

Salomon, M.L. (2015). Seismogenic-triggered soft sediment deformation (Hirlatzhöhle, Austria) [Unpublished master's thesis]. Universität Wien

Salomon, M., Grasemann, B., Plan, L., Gier, S., & Schöpfer, M.P.J. (2018). Seismically-triggered soft-sediment deformation structures close to a major strike-slip fault system in the Eastern Alps (Hirlatz cave, Austria). *Journal of Structural Geology, 110*, 102-115

Sasowsky, I.D. (2003). Sediments. Autochthonous Clastic. In J., Gunn (Ed.). *Encyclopedia of Caves and Karst Science* (pp. 634-635). New York, NY: Routledge

Schachtschabel, P., Blume, H.-P., Hartge, K.-H. & Schwertmann, U. (1984). *Lehrbuch der Bodenkunde*. Stuttgart, Germany: Ferdinand Enke Verlag

Schauberger, O. (1957). Die Hierlatzhöhle bei Hallstadt (Oberösterreich). *Die Höhle, 3*, 65-67

Schauberger, O. (1983). Geologische und morphologische Beobachtungen in der Hierlatzhöhle (Dachstein). *Schriftenreihe des Heimatmuseums „Ausseerland“, 4*, 1-21

Schultz, L.G. (1964). Quantitative Interpretation of Mineralogical Composition from X-ray and Chemical Data for the Pierre Shale. *Geological Survey Professional Paper, 391(C)*, 1-31

Seemann, R. (1973). Die Genese der Pyrite der Karstgebiete der Nördlichen Kalkalpen [Unpublished dissertation]. Universität Wien

Seemann, R., Brandstätter, F., & Hammer, V.M.F. (1999). Sedimente und Mineralneubildungen in der Dachstein-Rieseneishöhle. *Die Höhle, 50(3)*, 101-115

https://www.spelix.at (2021, November 15)

Spöcker, R.G. (1925). Die Mammuthöhle im Dachstein. *Mitteilungen über Höhlen* *und Karstforschung, 3*, 70-79

Spötl, C. & Plan, L. (2016). Karst und Höhlen. In C., Spötl, L., Plan, & E., Christian (Eds.). *Höhlen und Karst in Österreich* (pp. 1-10). Linz, Austria: Oberösterreichisches Landesmuseum

Springer, R.F. (2012). Clastic Sediments in Caves. In W.B., White & D.C., Culver (Eds.). *Encyclopedia of Caves* (2nd ed., pp. 134-140). Waltham, Oxford, Amsterdam, San Diego: Academic Press

Svoboda, J. (2006). The Structure of the Cave, Stratigraphy, and Depositional Context. In M. Teschler-Nicola (Ed.) *Early Modern Humans at the Moravian Gate. The Mladeč Caves and their Remains* (pp. 27-40). Vienna, Austria: Springer

Thiedig, F. (1970). Verbreitung, Ausbildung und stratigraphische Einstufung neogener Rotlehme und Grobschotter in Ostkaernten (Oesterreich). *Mitteilungen aus dem Geologisch-Paläontologischen Institut der Universität Hamburg, 39*, 97-116

Tollmann, A. (1985). *Geologie von Österreich Band 2: Außerzentralalpiner Anteil.* Vienna, Austria: Franz Deuticke

Warburton, N.M. & Prideaux, G.J. (2021). The skeleton of Congruus kitcheneri, a semiarboreal kangaroo from the Pleistocene of southern Australia. *Royal Society Open Science, 8*, 1-54

Ward,I., Winter, S., & Dotte-Sarout, E. (2016). The lost art of stratigraphy? A consideration of excavation strategies in Australian indigenous archaeology. *Australian Archaeology, 82(3)*, 263-274

Wetzel, A. (2015). Burrows storing an otherwise lost sedimentary record. In D., McIlroy (Ed.) *Ichnology: Papers from ICHNIA III* (pp. 211-224). St. Johns, Canada: Geological Association of Canada

Widdowson, M. (2009). Laterite. In V., Gornitz (Ed.) *Encyclopedia of Paleoclimatology and Ancient Environments* (pp. 515-517). Dordrecht, Netherlands: Springer

Winkler-Hermaden, A. (1957). *Geologisches Kräftespiel und Landformung.* Vienna, Austria: Springer-Verlag

Zachos, J.C., Lohmann, K.C., Walker, J.C.G., & Wise, S.W. (1993). Abrupt Climate Change and Transient Climates During the Paleogene: A Marine Perspective. *The Journal of Geology, 101*, 191-213

Zeitlhofer, H. & Knobloch, G. (2008). Die Raucherkarhöhle (1626/55) als Teil des Schönberg-Höhlensystems. *Die Höhle, 59*, 73-82

Zolitschka, B., Francus, P., Ojala, A.E.K., & Schimmelmann, A. (2015). Varves in lake sediments - a review. *Quarternary Sciences Reviews, 117*, 1-41

List of Figures

List of Tables

Appendix

Dachstein-Mammuthöhle

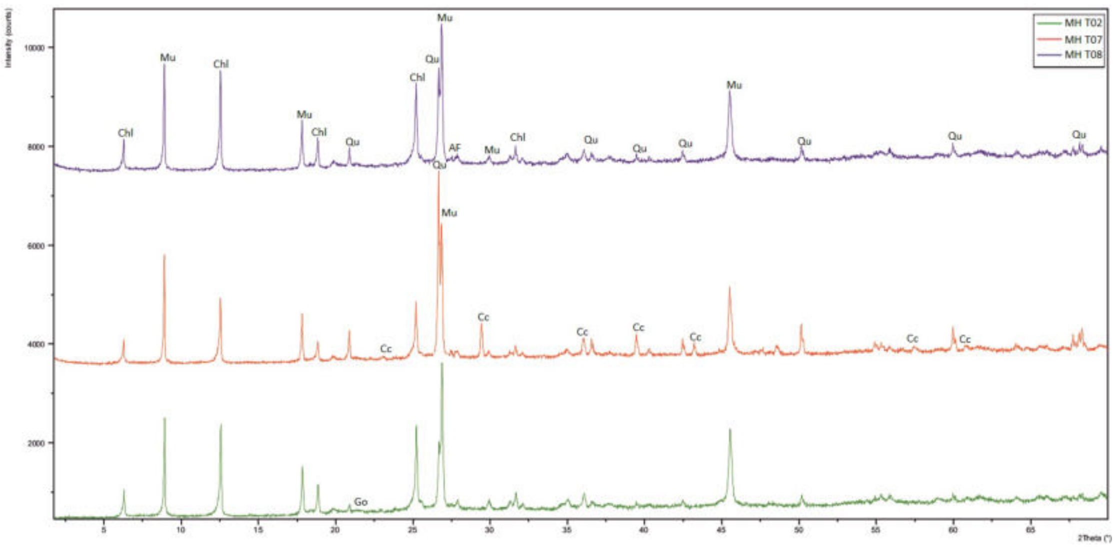

Figure 42: X-ray diffraction patterns of all samples of greenish sediments from Mammuthöhle. AF = alkali feldspar, Cc = calcite, Chl = chlorite, Go = goethite, Mu = muscovite, Qu = quartz.

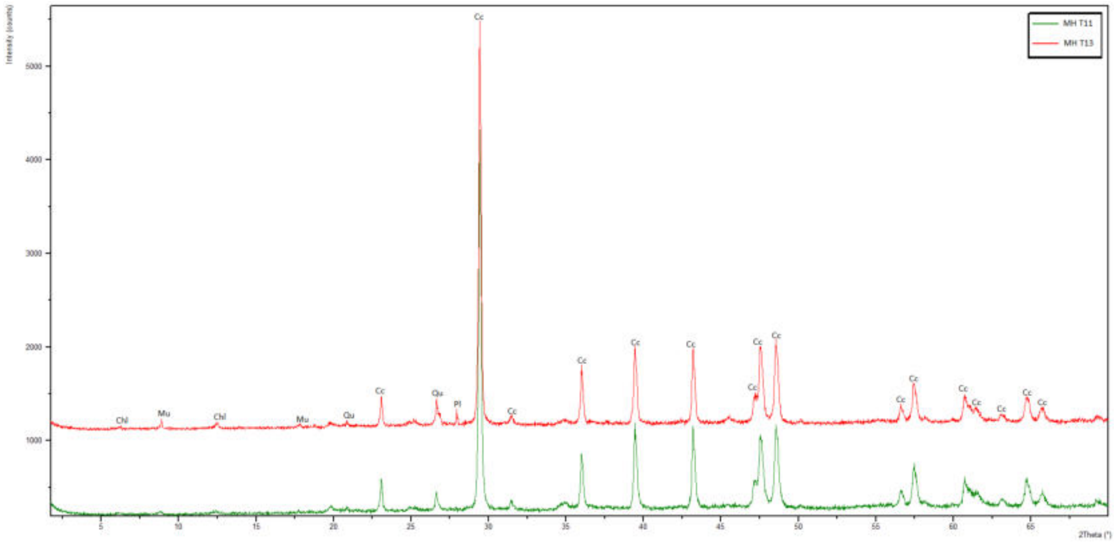

Figure 43: X-ray diffraction patterns of all samples of bright cave loam from Mammuthöhle. Cc = calcite, Chl = chlorite, Mu = muscovite, Pl = plagioclase, Qu = quartz.

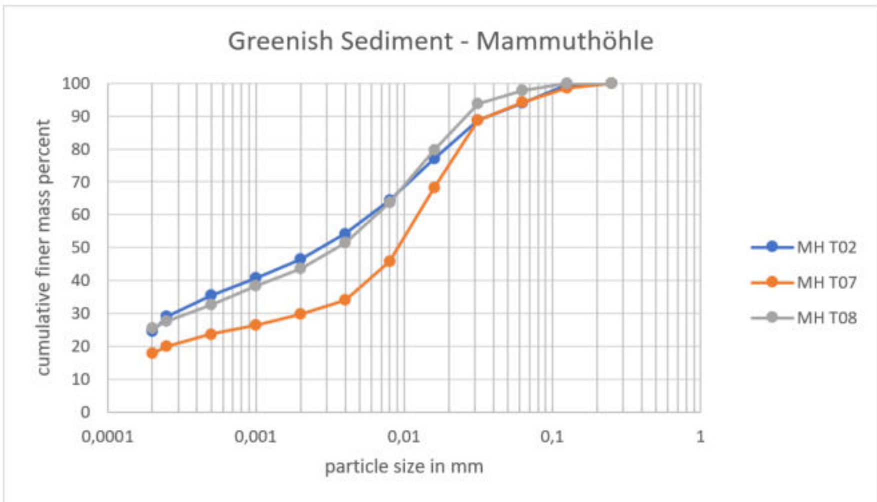

Figure 44: Grain size distribution of all samples of greenish sediments from Mammuthöhle.

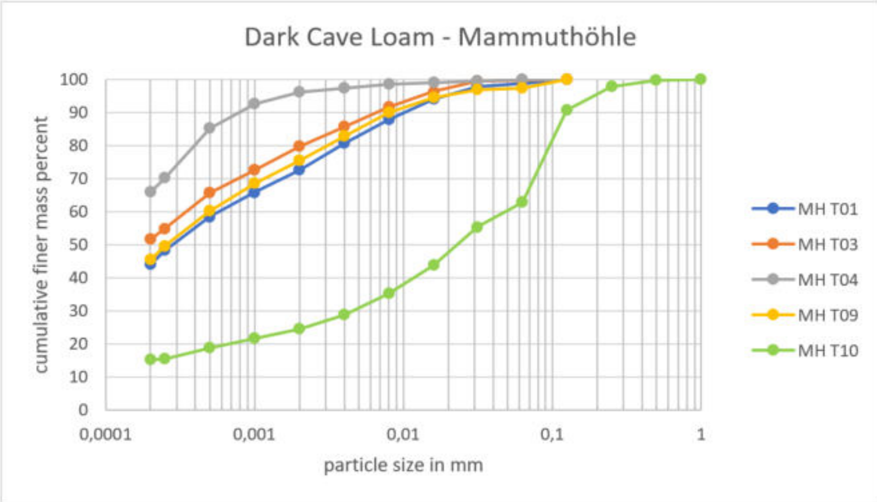

Figure 45: Grain size distribution of all samples of dark cave loam from Mammuthöhle.

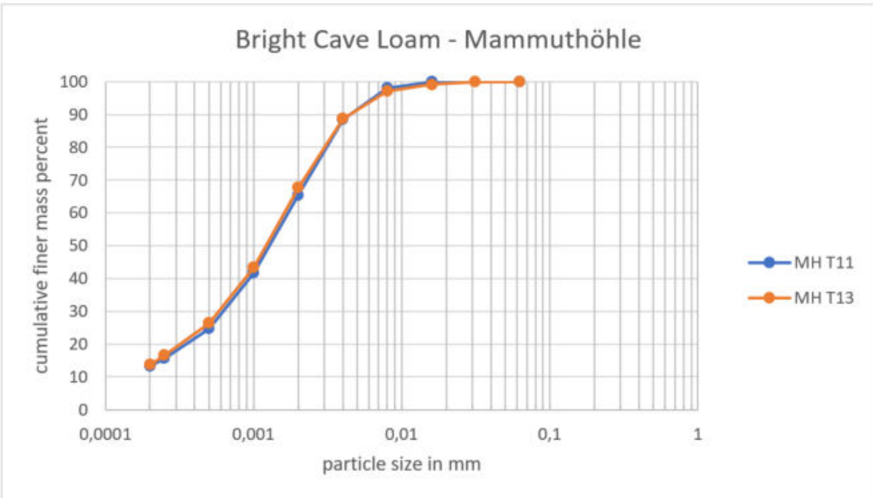

Figure 46: Grain size distribution of all samples of bright cave loam from Mammuthöhle.

O-1 Sklavengang, next to the ladder

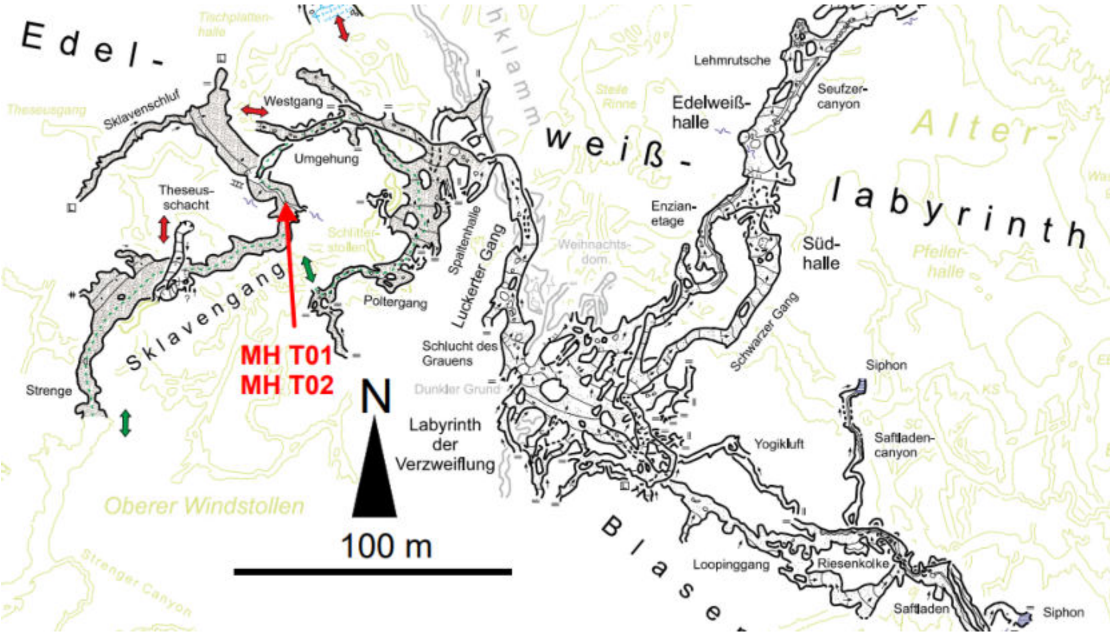

Figure 47: A part of the plan view of Mammuthöhle with the marked sample location of outcrop 1 (modified from Xaver et al, 2010).

(a)

(b)

(c)

(d)

Figure 48: Outcrop 1: (a) – (c) Profile orographically right of the stream. (a) Conglomerates followed by bright cave loam. (b) The conglomerate section with the transition to bright cave loam. (c) The bright cave loam is partially laminated (photos by L. Plan). (d) Profile orographically left of the stream (photo by E. Kaminsky).

O-2 at the end of Atlantis, junction Herkulesschacht and Barbarengang

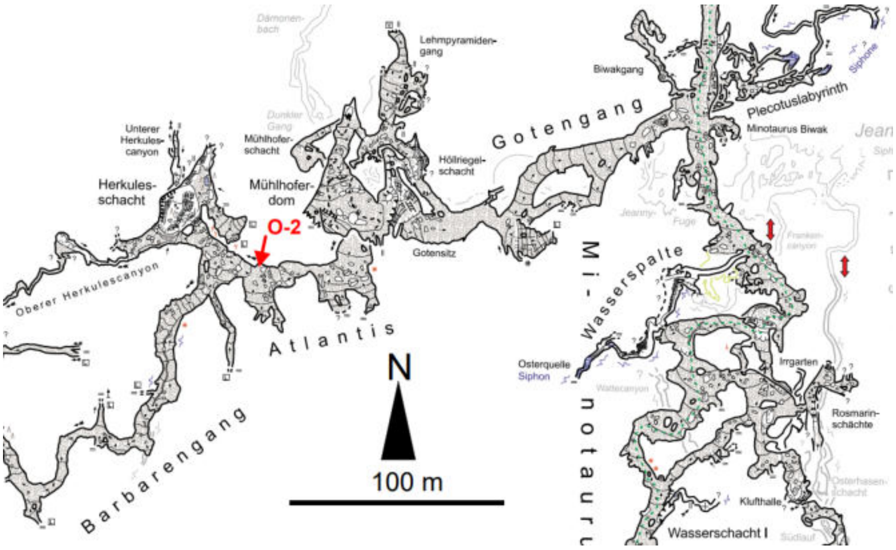

Figure 49: A part of the plan view of Mammuthöhle with the marked location of outcrop 2 (modified from Xaver et al, 2010).

Figure 50: Outcrop 2: The bright cave loam has a depth up to 205 cm and shows desiccation cracks with a depth of 50 to 60 cm (photo by E. Kaminsky).

O-3 Krippensteingang, shortly before Huziwand

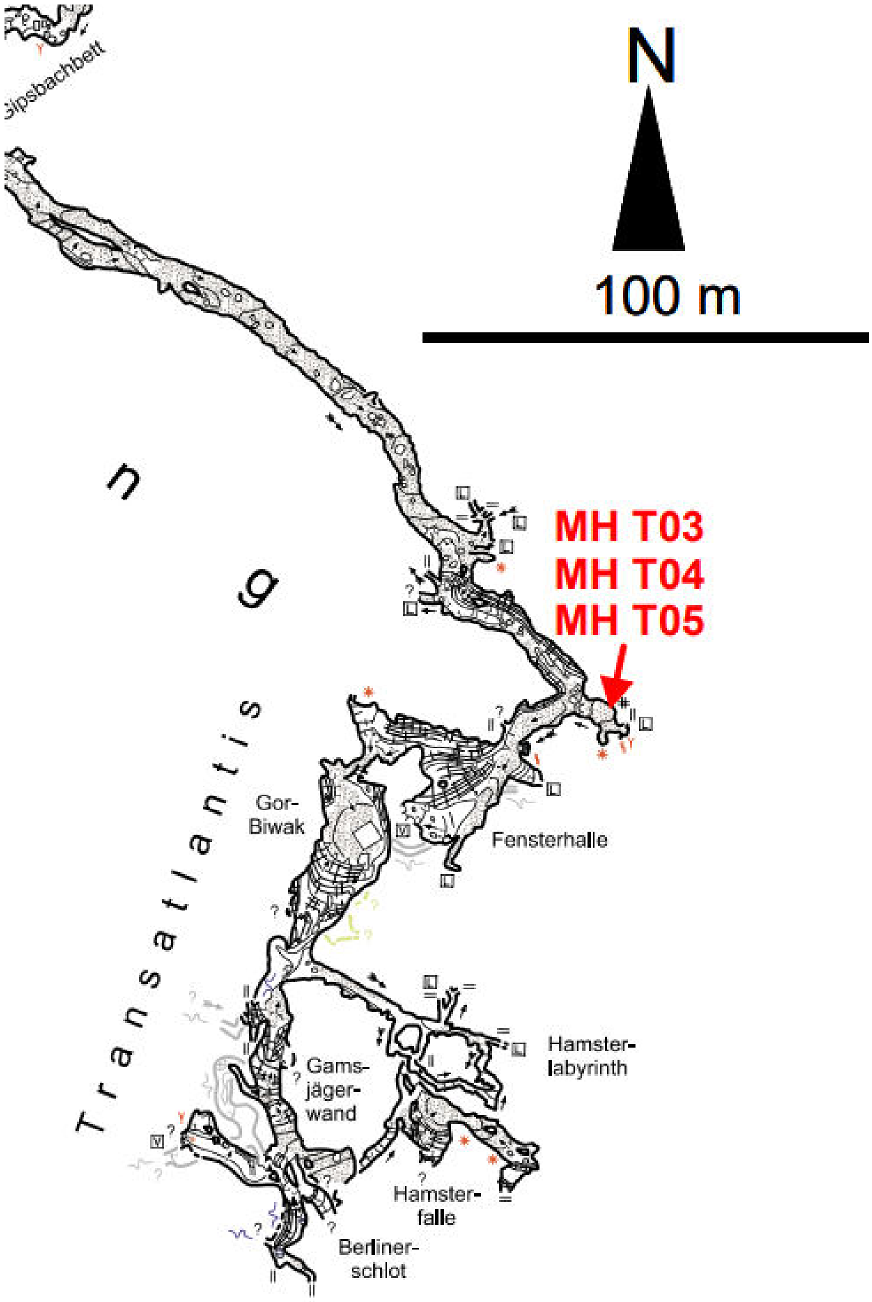

Figure 51: A part of the plan view of Mammuthöhle with the marked sample location of outcrop 3 (modified from Xaver et al, 2010).

Figure 52: Outcrop 3: Krippensteingang and on the right side of the picture the ascent to the niche (photo by E. Kaminsky).

(a)

(b)

(c)

(d)

(e)

(f)

Figure 53: Outcrop 3: Detailed pictures of sediments in the niche at Krippenstein-gang. (a) Overview picture of the niche (photo by L. Plan). (b) Dark cave loam shows a coarser part in the lowest 10 cm. (c), (d) The dark cave loam has parts where bioturbation can be seen (photos by L. Plan). (e) Bright cave loam on top of dark cave loam shows desiccation cracks and (f) has fractures along the laminae.

Figure 54: Outcrop 3: Concretions protrude from Huziwand (photo by L. Plan).

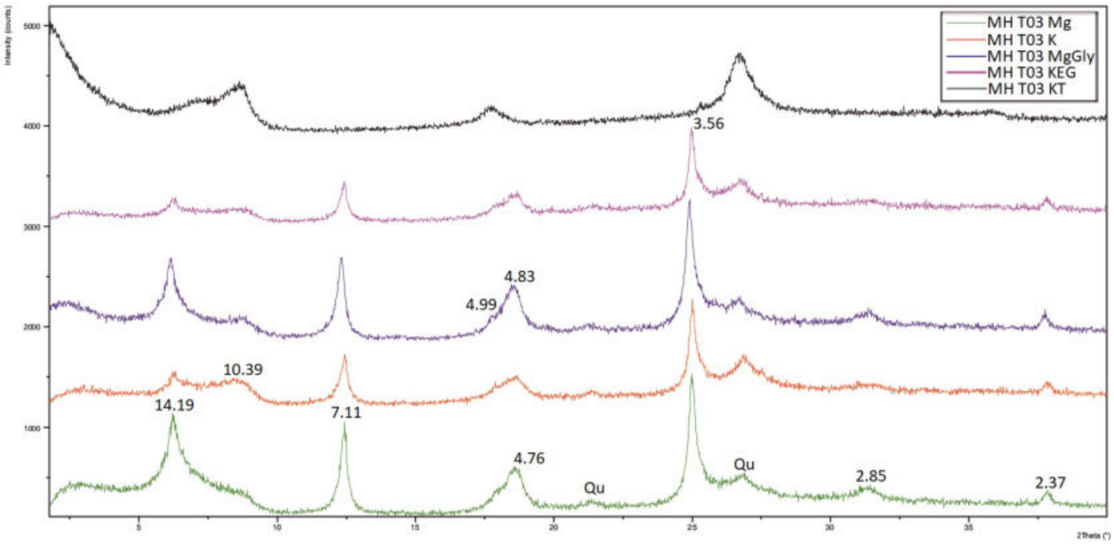

Figure 55: X-ray diffraction patterns of clay mineralogy of dark cave loam sample MH T03. Saturated with Mg (green), K (red), Mg and glycerol (blue), K and ethylene glycol (pink), and heated to 550 °C (black); d-values in Å; Qu = quartz.

O-4 after junction Solaris, SS 100

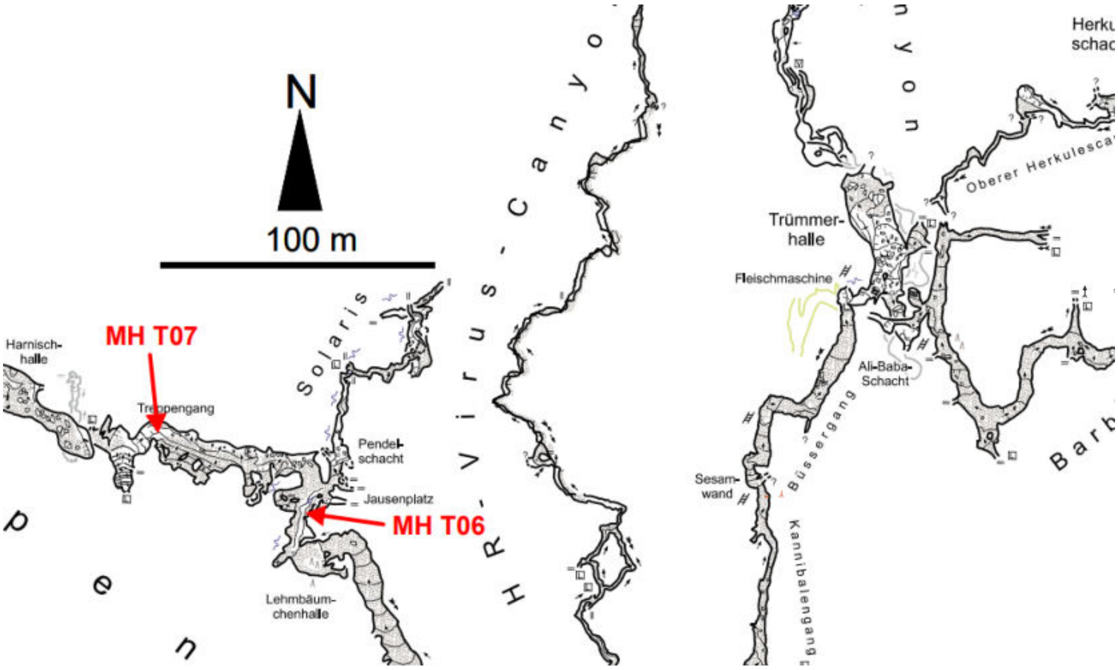

Figure 56: A part of the plan view of Mammuthöhle with the marked sample locations of outcrop 4 (MH T07) and 5 (MH T06; modified from Xaver et al, 2010).

(a)

(b)

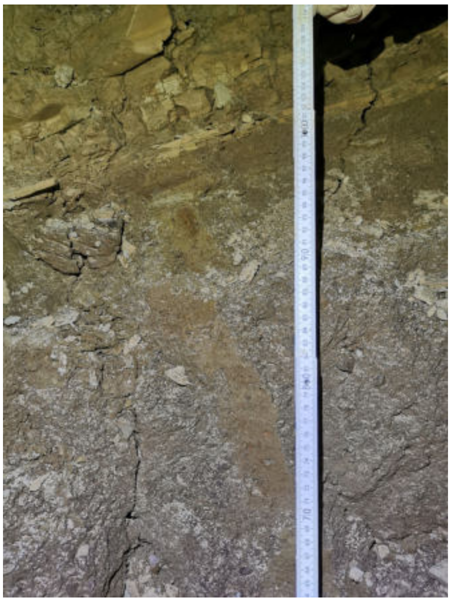

(c)

(d)

Figure 57: Outcrop 4: (a) Profile of the sedimentary succession. Detailed pictures show (b) greenish sediment at the base of the profile with the sample location of MH T07, (c) dark cave loam with the transition to bright cave loam, and (d) varve-like textured bright cave loam with laminae of reworked clasts of bright and dark cave loam (photos by L. Plan).

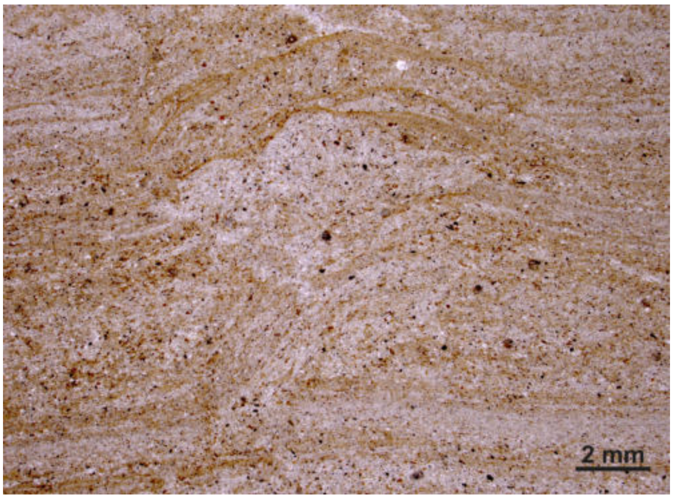

(a)

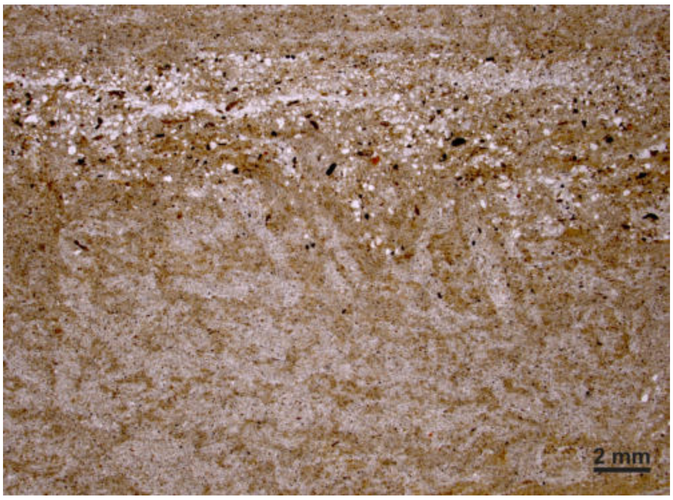

(b)

Figure 58: Detailed thin section pictures of the concretion MH T06. (a) Water-escape structures in the upper third, and (b) bioturbation in the lower third of the concretion.

O-6 Sklavengang, next to Strenge

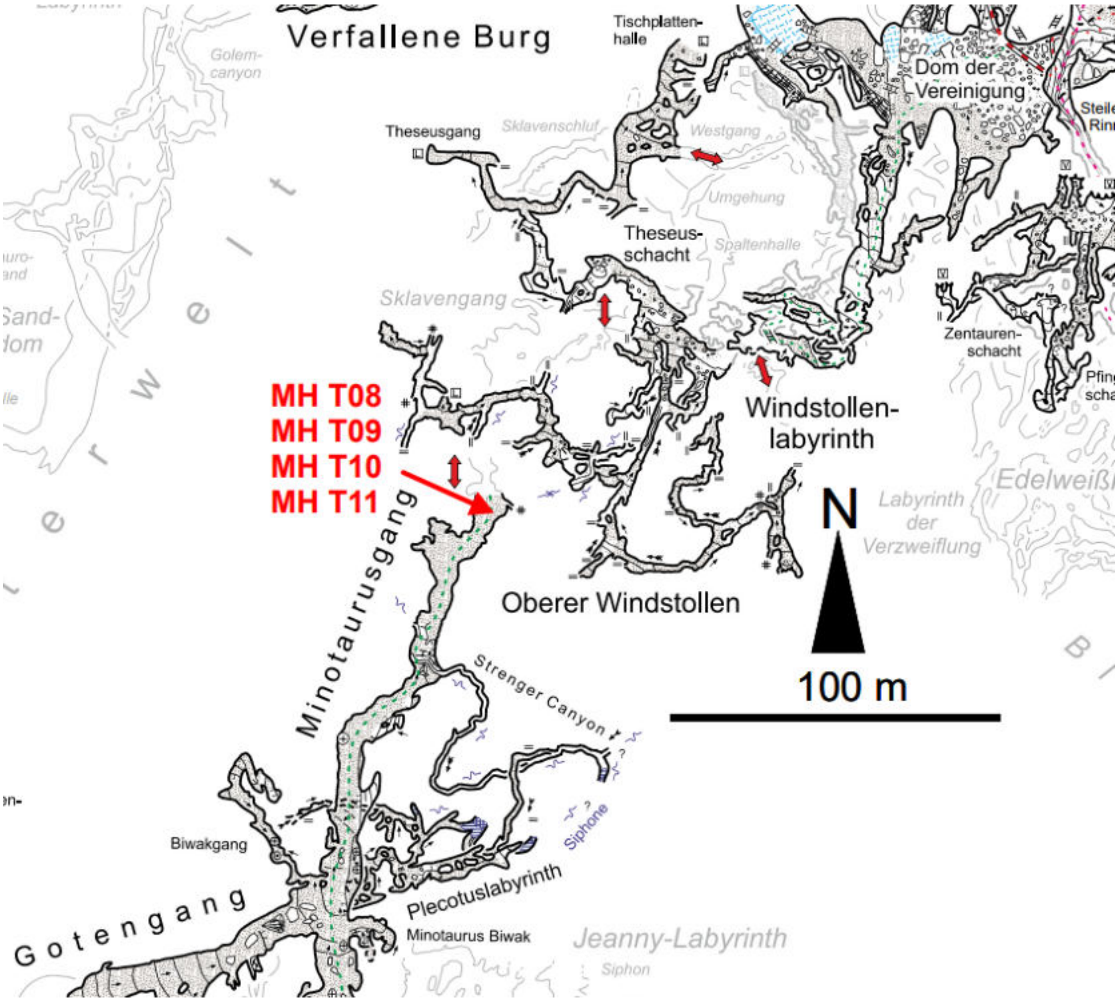

Figure 59: A part of the plan view of Mammuthöhle with the marked sample location of outcrop 6 (modified from Xaver et al, 2010).

(a)

(b)

Figure 60: Outcrop 6: Picture compilation of profile. (a) Upper part of the profile showing conglomerate and bright cave loam at the top. (b) Lower part of the profile with greenish sediment, dark cave loam and the base of the conglomerate.

(a) (b)

(c) (d)

Figure 61: Outcrop 6: Detailed pictures of the profile from base to top. (a) Greenish sediment with sandy, mica-rich layers and lenses of dark cave loam. (b) Upper, coarser grained part of dark cave loam and the transition to fine-grained conglomerate. (c) Grain-supported, poorly sorted carbonate conglomerate. (d) Sharp transition from conglomerate to laminated bright cave loam.

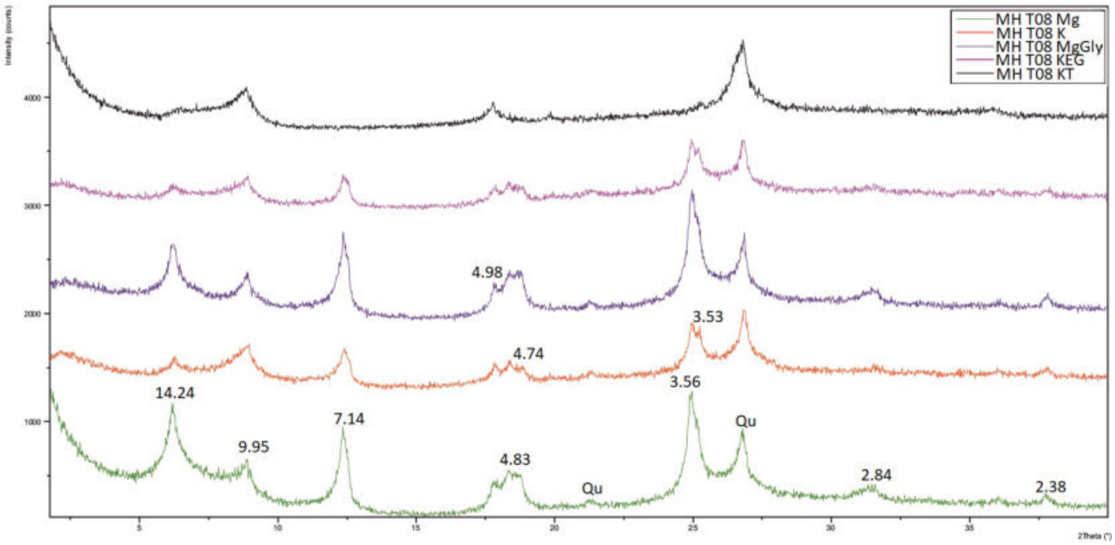

Figure 62: X-ray diffraction patterns of clay mineralogy of sample MH T08. Saturated with Mg (green), K (red), Mg and glycerol (blue), K and ethylene glycol (pink), and heated to 550 °C (black); d-values in Å; Qu = quartz.

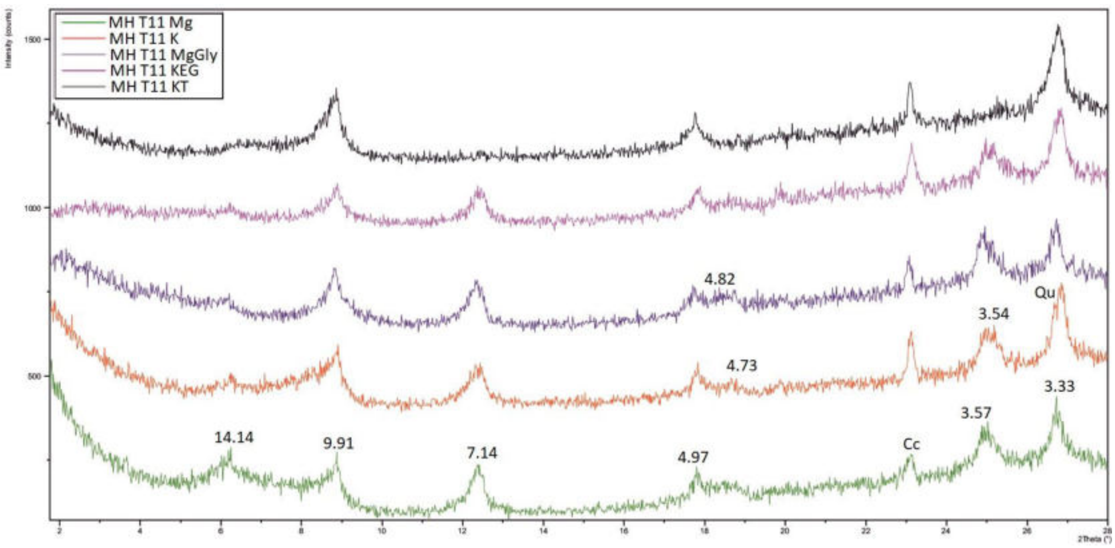

Figure 63: X-ray diffraction patterns of clay mineralogy of sample MH T11. Saturated with Mg (green), K (red), Mg and glycerol (blue), K and ethylene glycol (pink), and heated to 550 °C (black); d-values in Å; Cc = calcite, Qu = quartz.

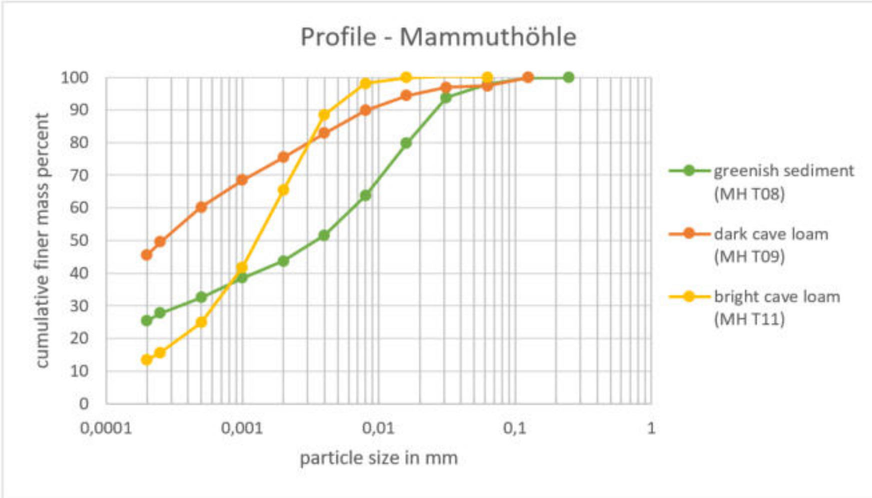

Figure 64: Grain size distribution of greenish sediment, dark cave loam, and bright cave loam of outcrop 6.

O-14 Paläotraun

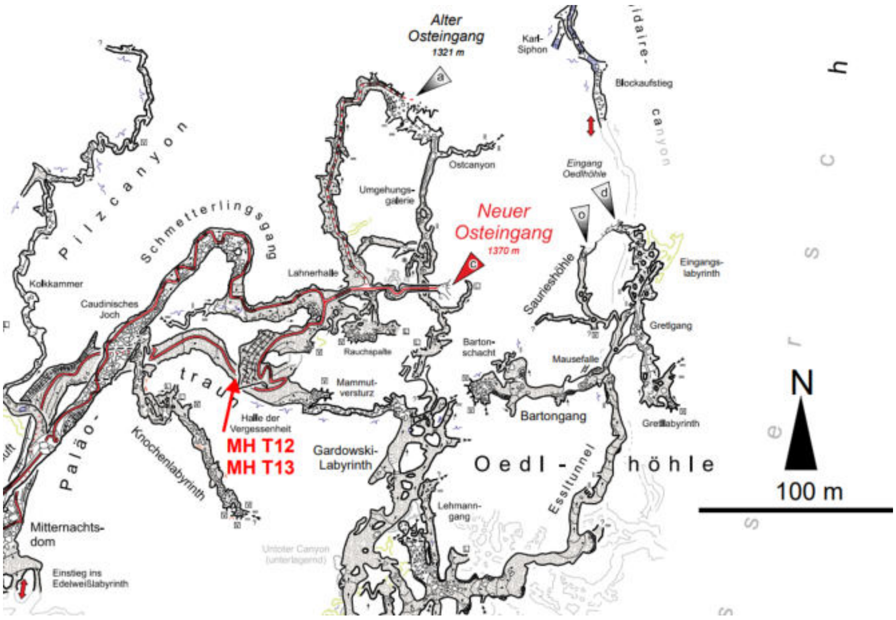

Figure 65: A part of the plan view of Mammuthöhle with the marked sample location of outcrop 14 (modified from Xaver et al, 2010).

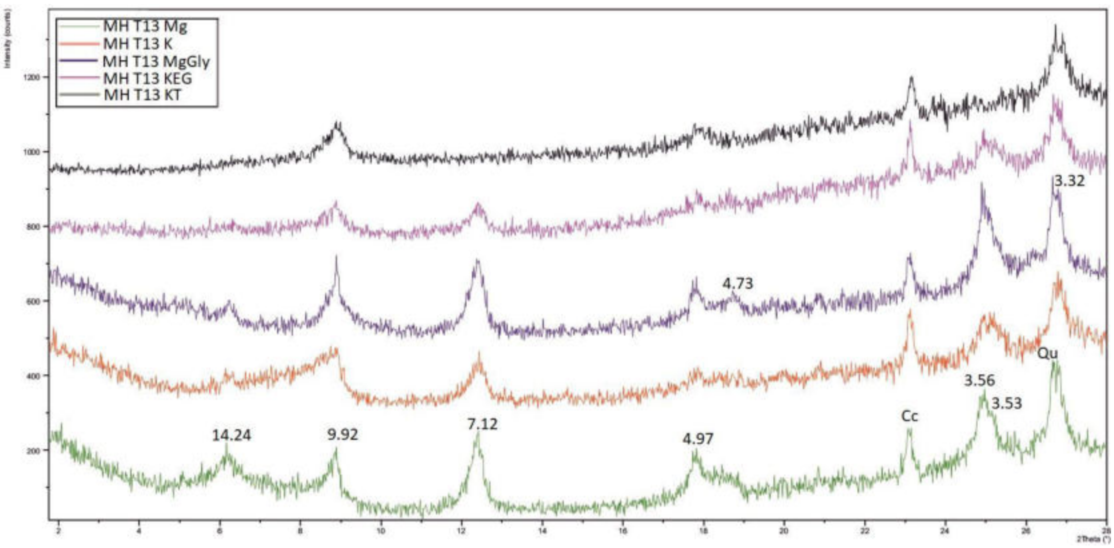

Figure 66: X-ray diffraction patterns of clay mineralogy of sample MH T13. Saturated with Mg (green), K (red), Mg and glycerol (blue), K and ethylene glycol (pink), and heated to 550 °C (black); d-values in Å; Cc = calcite, Qu = quartz.

O-16 Dachstein-Rieseneishöhle - Lehmhalle

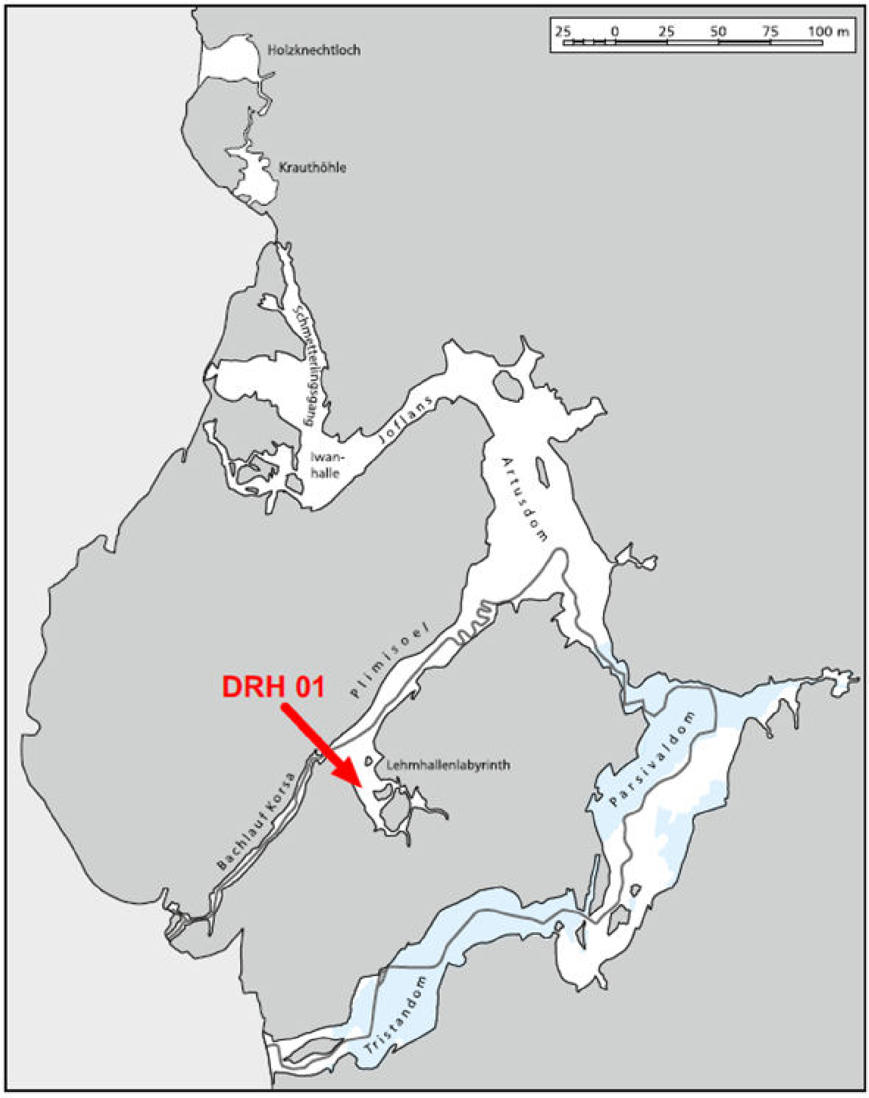

Figure 67: Location of sample DRH 01 (modified from A. Neumann, 1999).

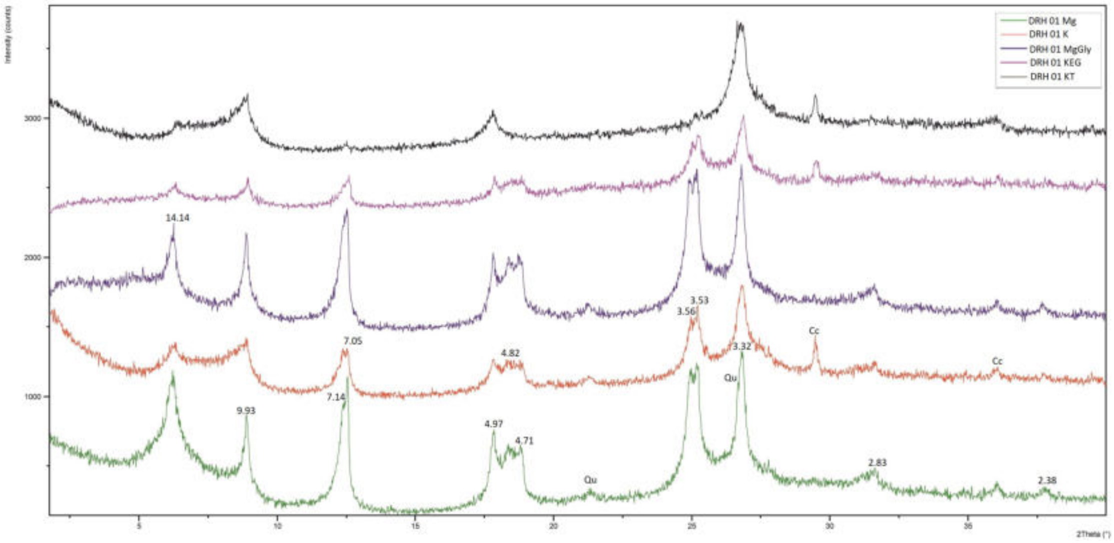

Figure 68: X-ray diffraction patterns of clay mineralogy of sample DRH 01. Saturated with Mg (green), K (red), Mg and glycerol (blue), K and ethylene glycol (pink), and heated to 550 °C (black); d-values in Å; Cc = calcite, Qu = quartz.

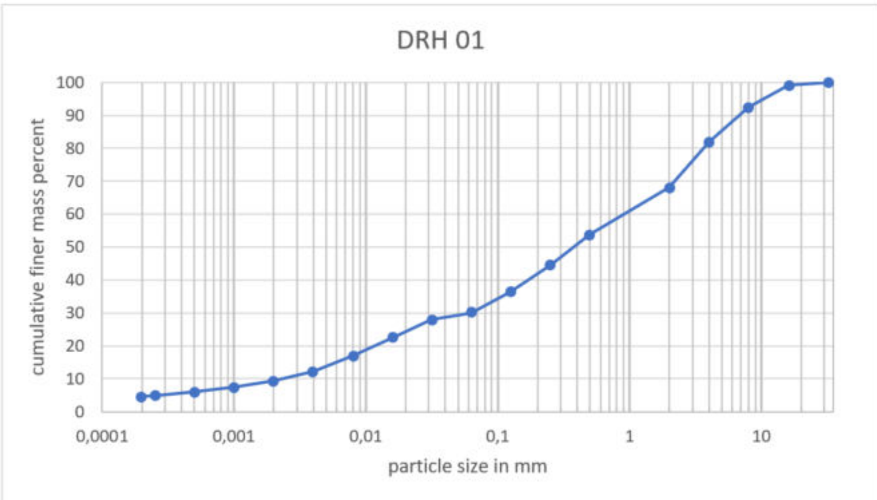

Figure 69: Grain size distribution of sample DRH 01.

Hirlatzhöhle

O-8 Aufsteigender Tunnel, before ramp

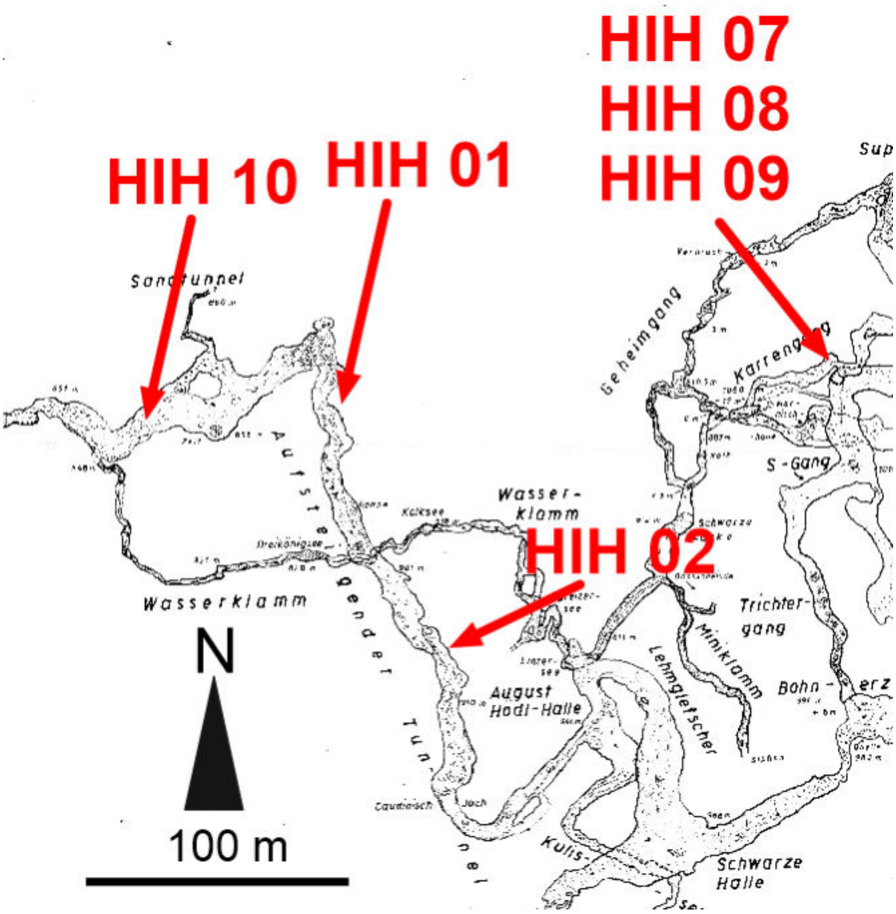

Figure 70: A part of the plan view of Alter Teil of Hirlatzhöhle with the marked sample locations of outcrop 8 (HIH 01), 9 (HIH 02), 12 (HIH 07, HIH 08, HIH 09) and 13 (HIH 10; modified from Fritsch, 1969).

(a)

(b)

Figure 71: Outcrop 8: (a) Loosely lying conglomerate boulders with various diameters. (b) Sample HIH 01 of the conglomerate, which is poorly sorted and has mainly carbonate clasts in a red-brownish matrix (photos by L. Plan).

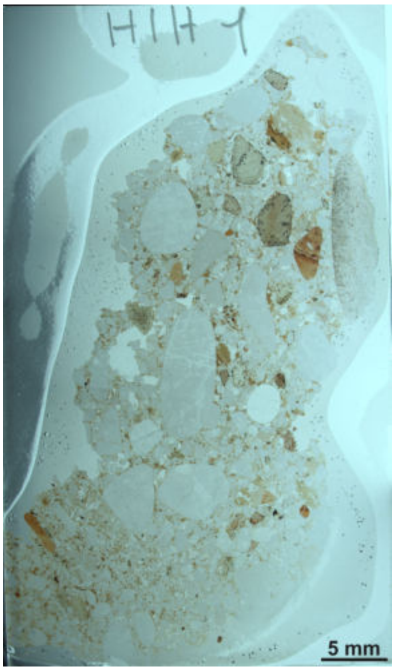

(a)

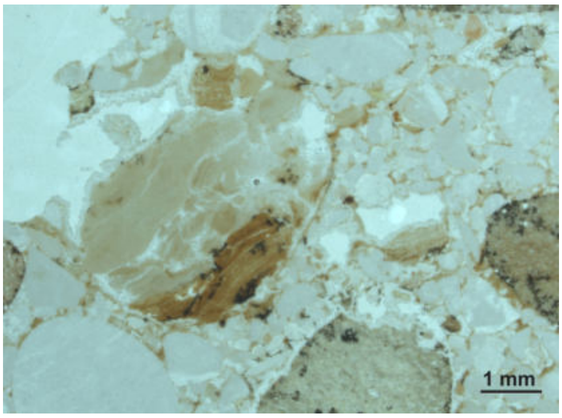

(b)

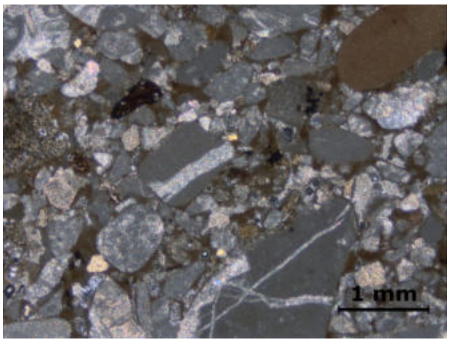

(c)

Figure 72: Thin section of the conglomerate HIH 01. (a) Overview picture of the poorly sorted, polymictic conglomerate. The components are mostly carbonates. (b) Detailed picture of an alga in the conglomerate, which is an indicator for a shallow marine facies. (c) Detailed picture with crossed polarisers of calcite grains and micritic components that are interspersed with calcite veins. The yellowish grains are quartz.

O-9 Aufsteigender Tunnel, upper part

(a)

(b)

Figure 73: Outcrop 9: (a) Conglomerate with a thickness of 2 m. (b) Sample HIH 02 of the conglomerate, showing matrix-supported, very poorly sorted carbonate and quartz clasts (photos by L. Plan).

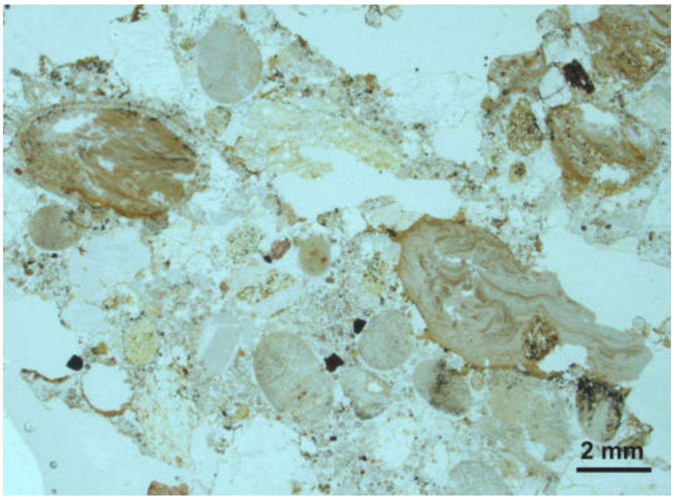

(a)

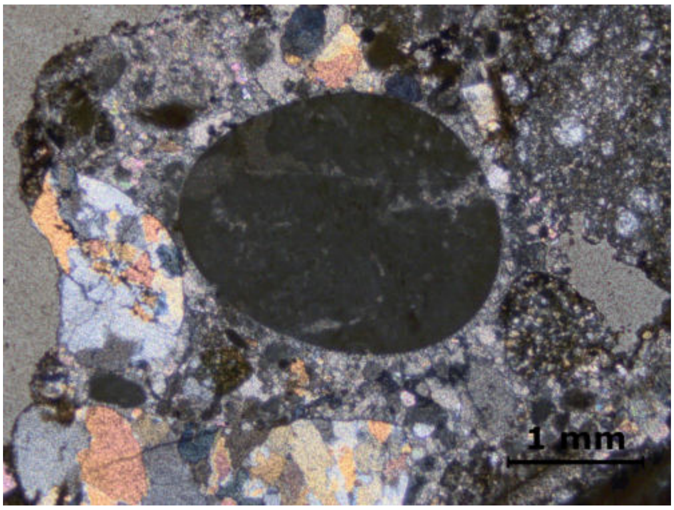

(b)

Figure 74: Detailed thin section pictures of the conglomerate HIH 02. (a) Picture of the algae that indicate shallow marine facies. (b) Picture with crossed polarisers of the lithic components (polycrystalline quartz, micritic, and metamorphic components) and the calcite cement. In very few areas there is also micrite.

O-10 Lehmklamm, orographically right

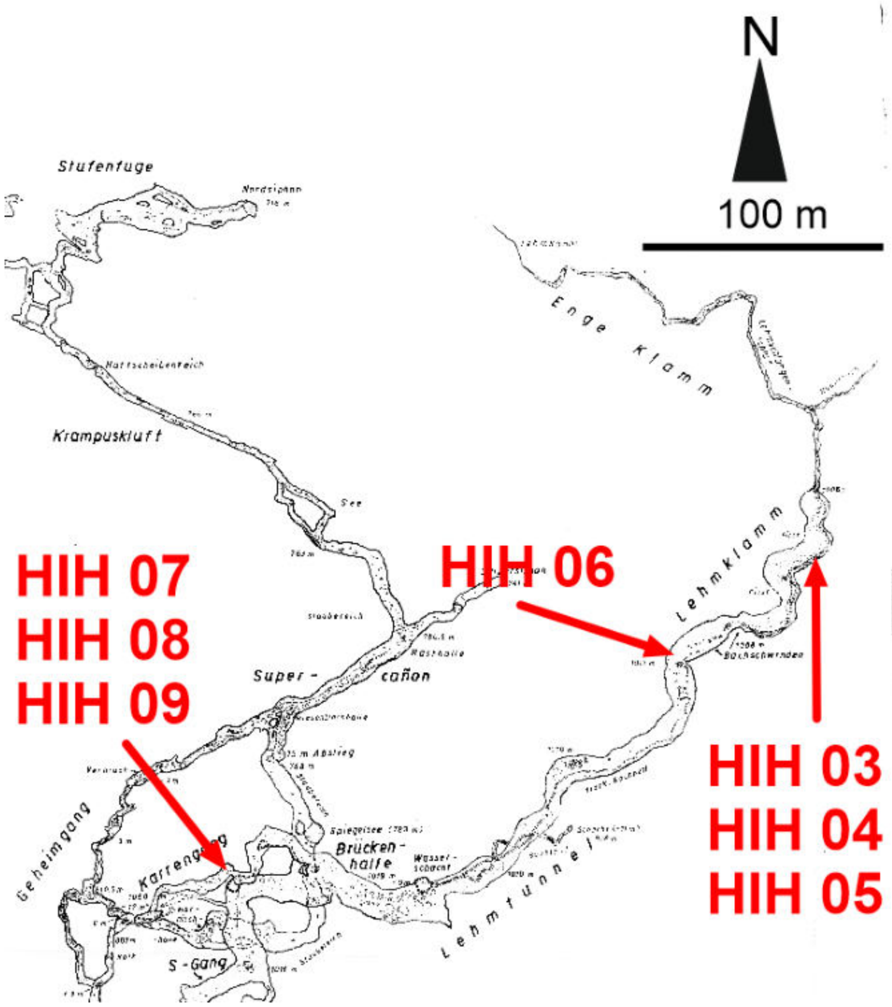

Figure 75: A part of the plan view of Alter Teil of Hirlatzhöhle with the marked sample locations of outcrop 10 (HIH 03, HIH 04, HIH 05), 11 (HIH 06), and 12 (HIH 07, HIH 08, HIH 09; modified from Fritsch, 1969).

(a)

(b)

Figure 76: Outcrop 10: (a) Dark and bright laminae of the bright cave loam. (b) Sandy layer on top of bright cave loam with climbing ripples that indicate a paleo flow towards NE (to the right in the photo; photos by L. Plan).

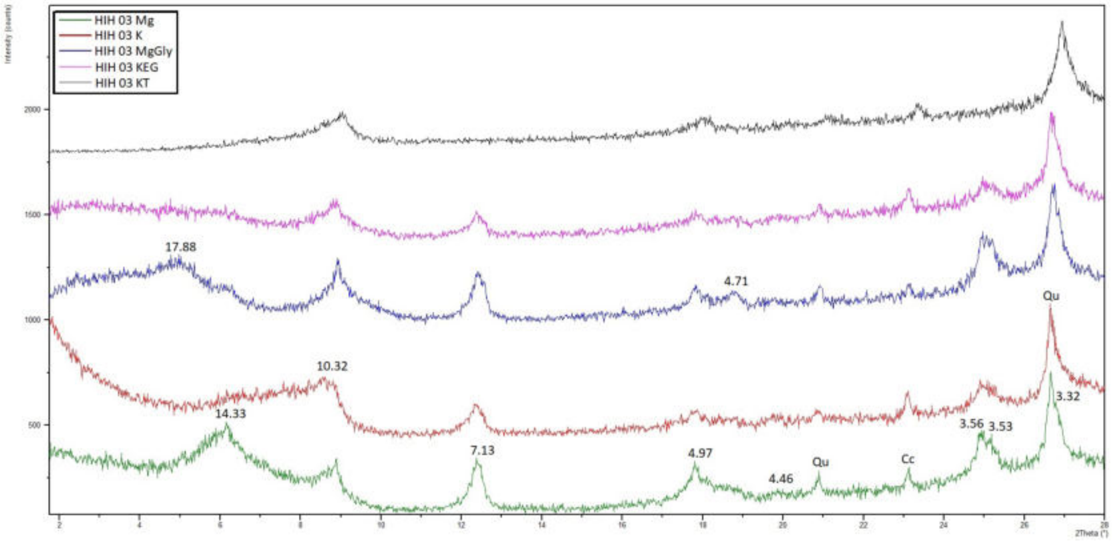

Figure 77: X-ray diffraction patterns of clay mineralogy of sample HIH 03. Saturated with Mg (green), K (red), Mg and glycerol (blue), K and ethylene glycol (pink), and heated to 550 °C (black); d-values in Å; Cc = calcite, Qu = quartz.

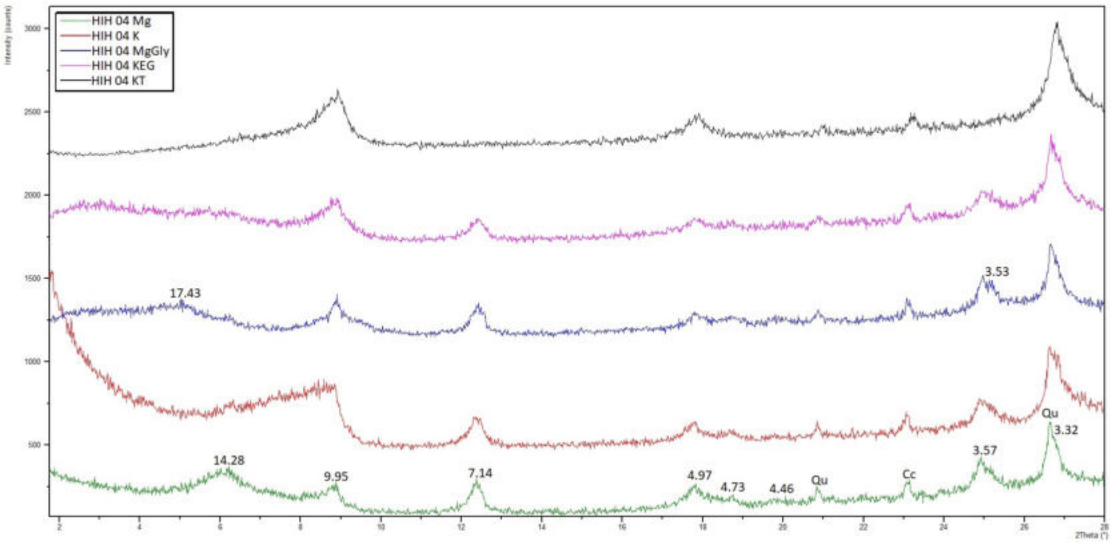

Figure 78: X-ray diffraction patterns of clay mineralogy of sample HIH 04. Saturated with Mg (green), K (red), Mg and glycerol (blue), K and ethylene glycol (pink), and heated to 550 °C (black); d-values in Å; Cc = calcite, Qu = quartz.

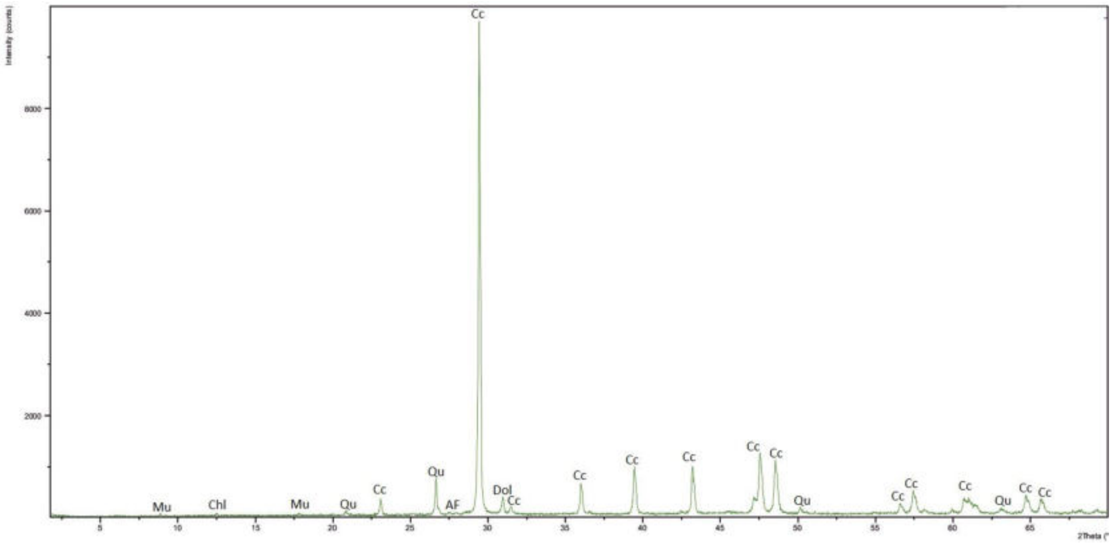

Figure 79: X-ray diffraction pattern sample HIH 05. AF = alkali feldspar, Cc = calcite, Dol = dolomite, Chl = chlorite, Mu = muscovite, Qu = quartz.

O-11 Lehmbachschwinde

Figure 80: Outcrop 11: Unconsolidated conglomerate comprises well-rounded carbonate and blackish components (photo by L. Plan).

O-12 between S-Gang and Brückenhalle

Figure 81: Outcrop 12: Detailed image of the darker and brighter laminae of bright cave loam. The knife indicates the position of the taken samples HIH 08 (bright lamina below) and HIH 09 (dark lamina at the same hight; photo by L. Plan).

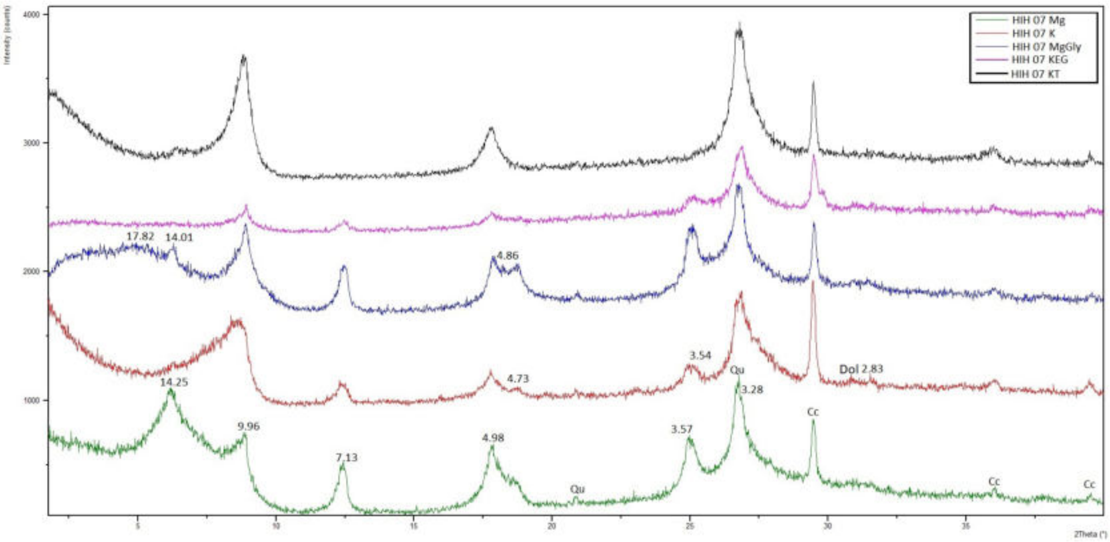

Figure 82: X-ray diffraction patterns of clay mineralogy of sample HIH 07. Saturated with Mg (green), K (red), Mg and glycerol (blue), K and ethylene glycol (pink), and heated to 550 °C (black); d-values in Å; Cc = calcite, Dol = dolomite, Qu = quartz.

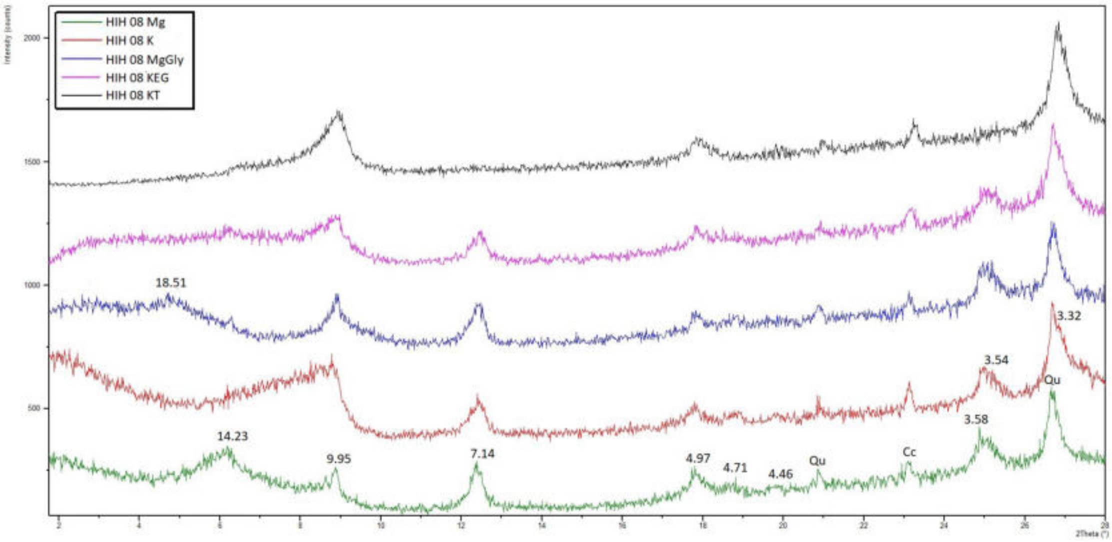

Figure 83: X-ray diffraction patterns of clay mineralogy of sample HIH 08. Saturated with Mg (green), K (red), Mg and glycerol (blue), K and ethylene glycol (pink), and heated to 550 °C (black); d-values in Å; Cc = calcite, Qu = quartz.

O-13 between bivouac and junction Wasserklamm

Figure 84: Outcrop 13: Whitish, sandy-silty cover of cave passages (photo by L. Plan).

O-20 150 m after Wetterscheide

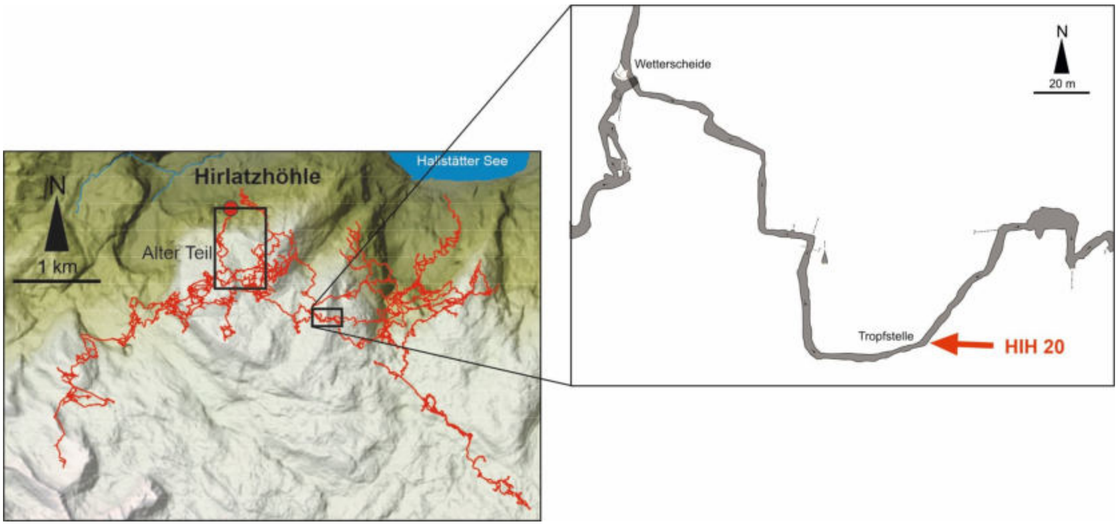

Figure 85: General plan of Hirlatzhöhle (modified from Plan and Bauer, 2016), the rectangles mark Alter Teil and a detailed plan view with the sample location of HIH 20 (modified from Hallinger, 2019).

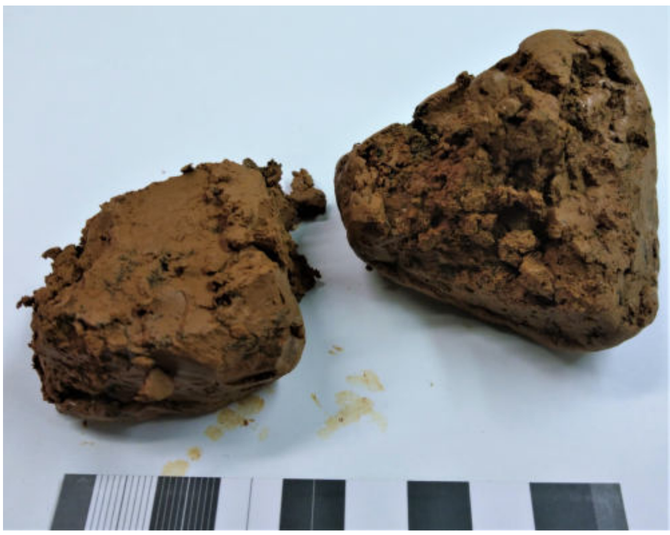

Figure 86: Outcrop 20: Brownish, clayey sample (HIH 20) of dark cave loam.

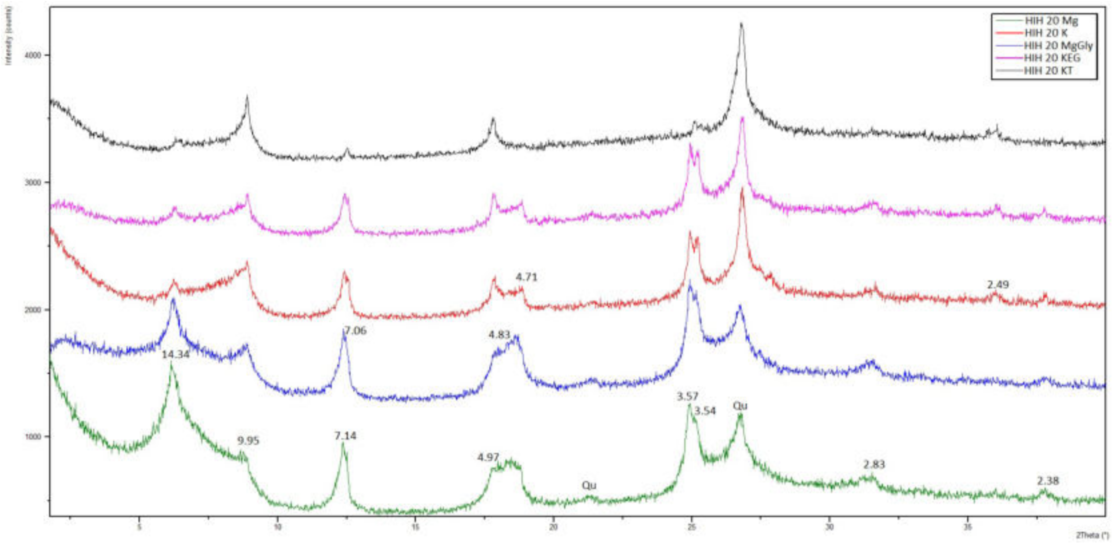

Figure 87: X-ray diffraction patterns of clay mineralogy of sample HIH 20. Saturated with Mg (green), K (red), Mg and glycerol (blue), K and ethylene glycol (pink), and heated to 550 °C (black); d-values in Å; Qu = quartz.

Günter-Stummer-Höhle

O-17 Mammutlabyrinth, SS 164

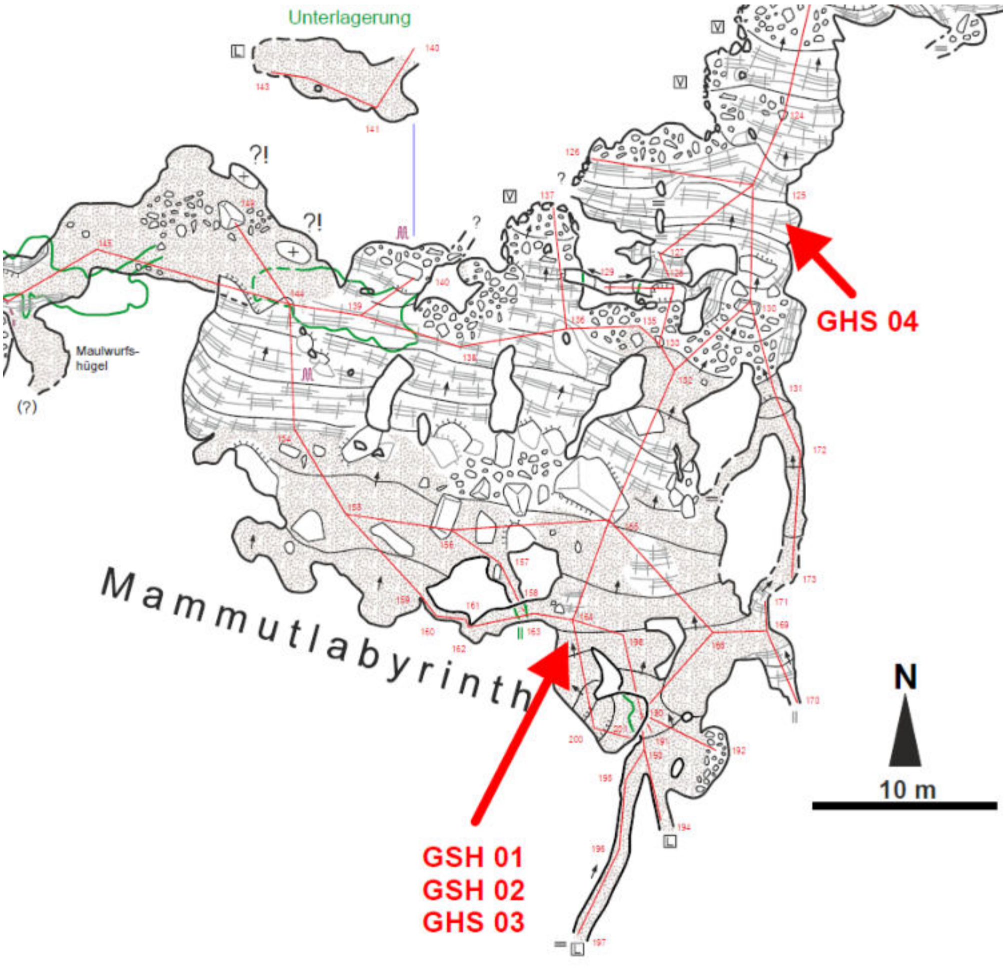

Figure 88: A part of the plan view of Günter-Stummer-Höhle with the marked sample locations of outcrop 17 (GSH 01, GSH 02, GSH 03) and 18 (GSH 04; modified from Funk and Plan, 2021).

(a)

(b)

(c)

Figure 89: Outcrop 17: Detailed pictures of the appearance of dark cave loam in Günter-Stummer-Höhle. (a) Reddish-brown dark cave loam that has a crumbly consistence (photo by L. Plan). (b) Sample GSH 01 is a dark reddish clay component from the base of dark cave loam. (c) Sample GSH 02 is a clay component that shows a greenish core with a dark reddish coating, and it is from the base of the dark cave loam.

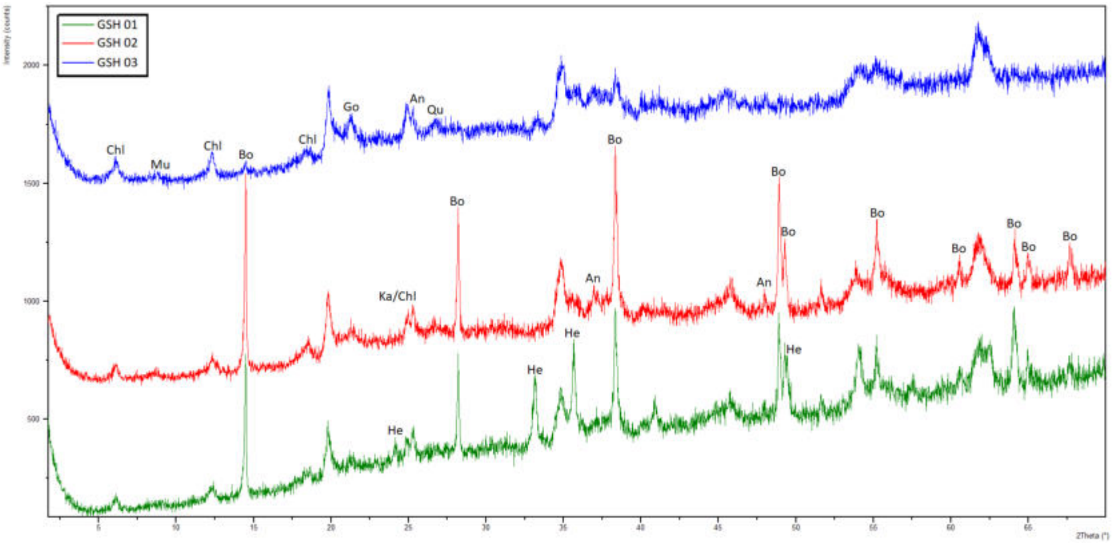

Figure 90: X-ray diffraction patterns of all samples of dark cave loam from Günter-Stummer-Höhle. An = anatase, Bo = boehmite, Cc = calcite, Chl = chlorite, Go = goethite, He = hematite, Ka = kaolinite, Mu = muscovite, Qu = quartz.

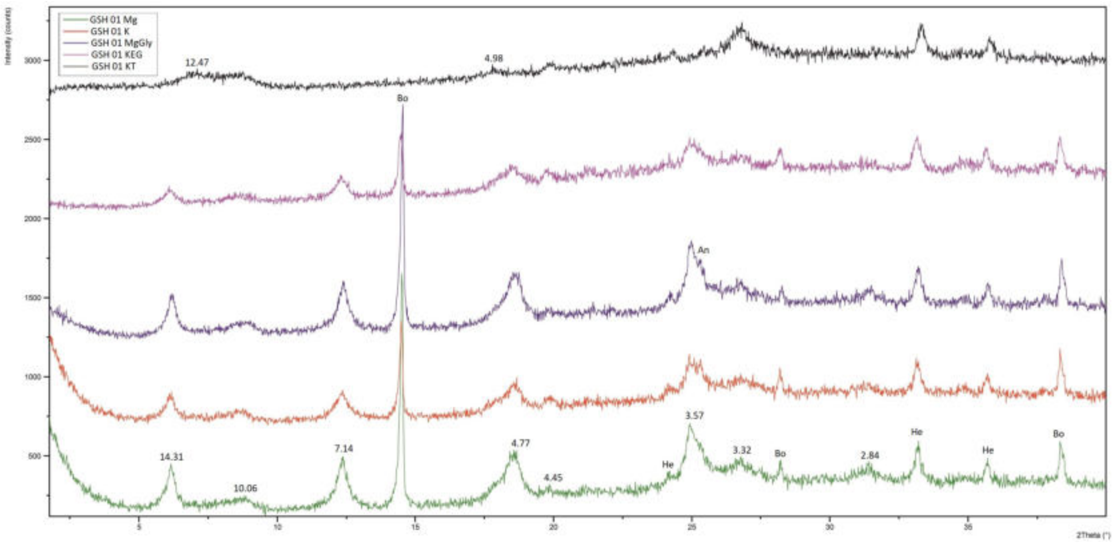

Figure 91: X-ray diffraction patterns of clay mineralogy of sample GSH 01. Saturated with Mg (green), K (red), Mg and glycerol (blue), K and ethylene glycol (pink), and heated to 550 °C (black); d-values in Å; An = anatase, Bo = boehmite, He = hematite.

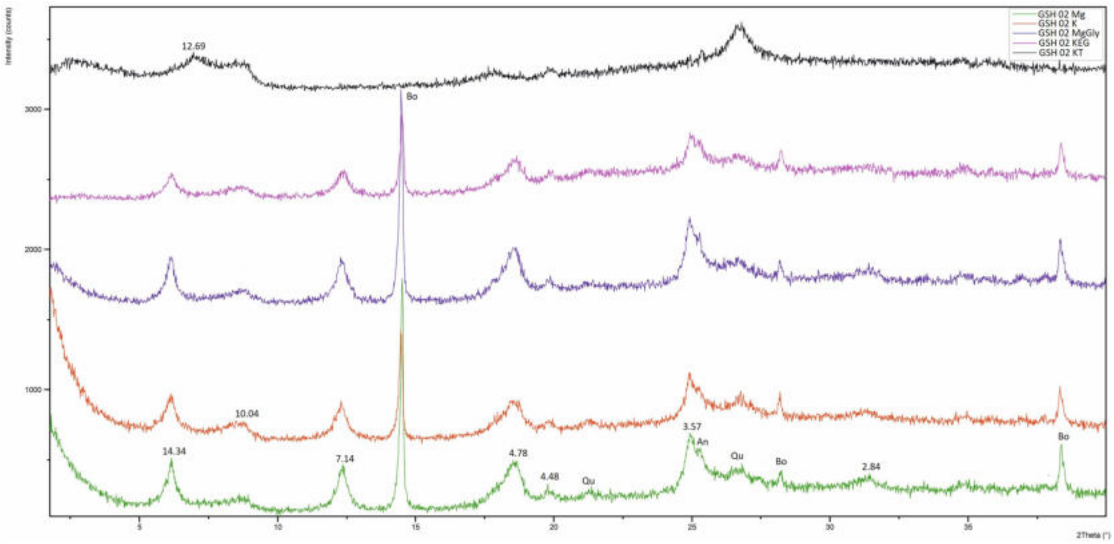

Figure 92: X-ray diffraction patterns of clay mineralogy of sample GSH 02. Saturated with Mg (green), K (red), Mg and glycerol (blue), K and ethylene glycol (pink), and heated to 550 °C (black); d-values in Å; An = anatase, Bo = boehmite, He = hematite, Qu = quartz.

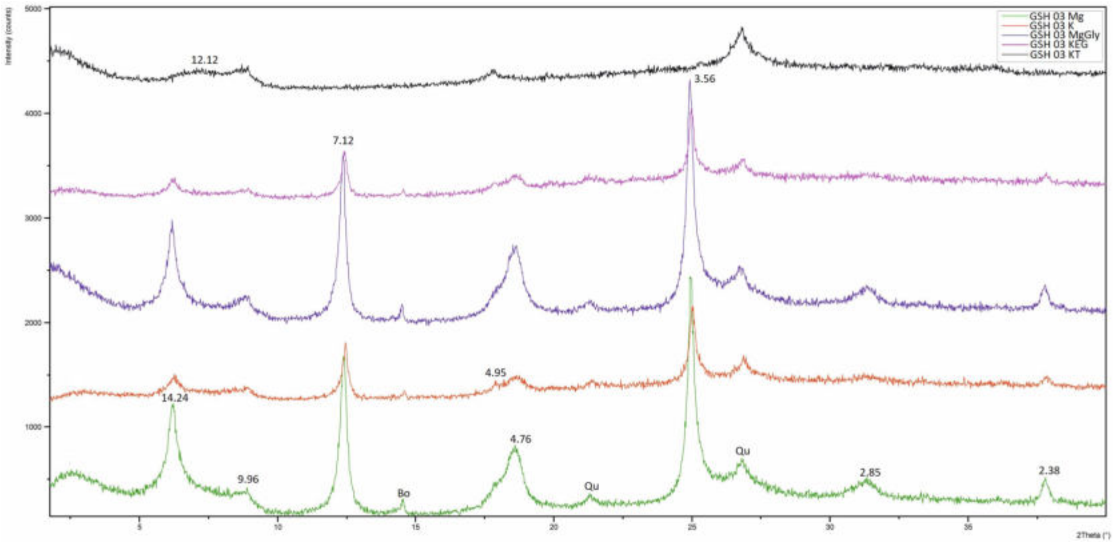

Figure 93: X-ray diffraction patterns of clay mineralogy of sample GHS 03. Saturated with Mg (green), K (red), Mg and glycerol (blue), K and ethylene glycol (pink), and heated to 550 °C (black); d-values in Å; Bo = boehmite, Qu = quartz.

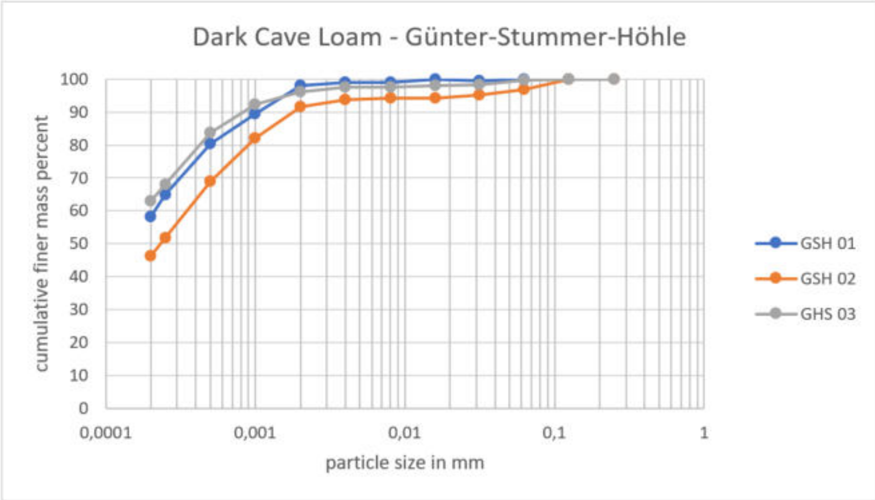

Figure 94: Grain size distribution of all samples of dark cave loam from Günter-Stummer-Höhle.

O-18 Mammutlabyrinth, SS 125

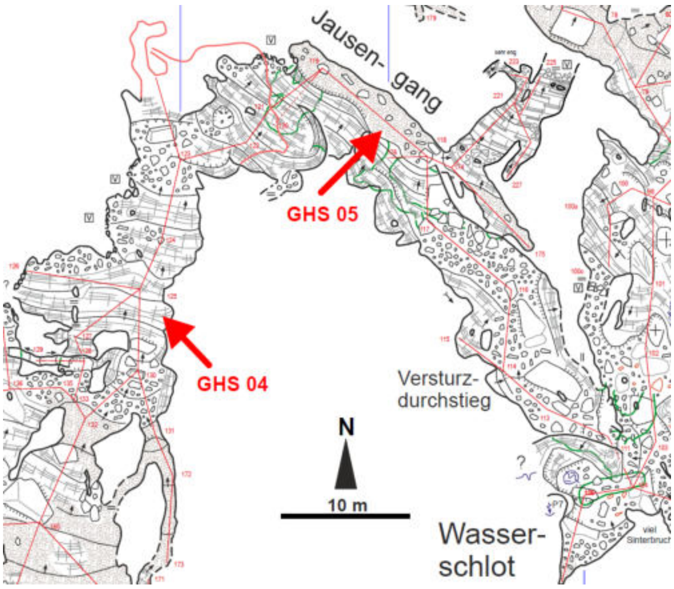

Figure 95: A part of the plan view of Günter-Stummer-Höhle with the marked sample locations of outcrop 18 (GSH 04) and 19 (GHS 05; modified from Funk and Plan, 2021).

Figure 96: Outcrop 18: Fine-grained, brownish layer on top of Dachsteinkalk (photo by L. Plan).

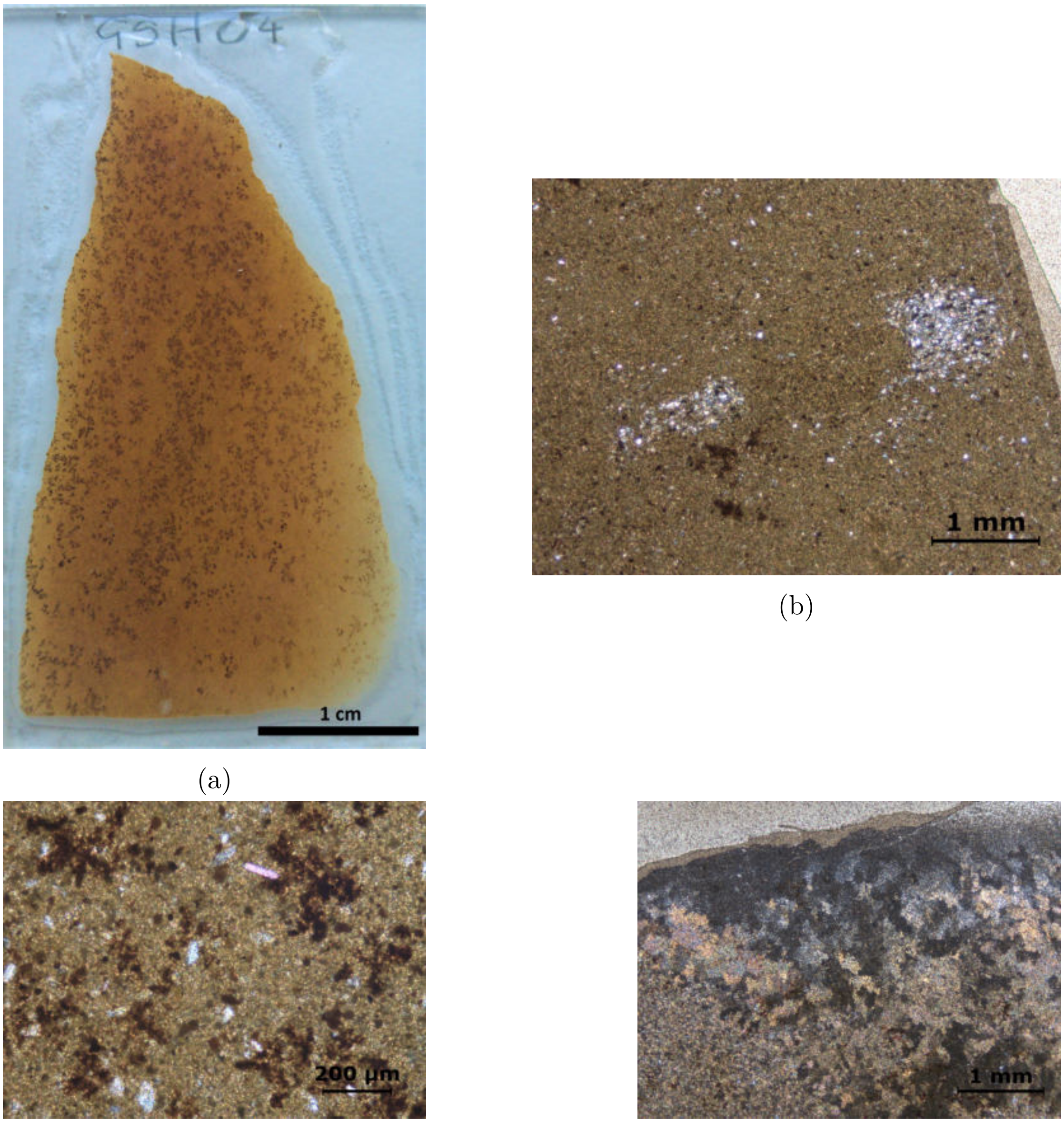

(a) (b) (c) (d)

Figure 97: Thin section of sample GSH 04. (a) Overview picture of the thin section. (b) Detailed picture with crossed polarisers of well-defined lenses of coarser quartz grain in brownish matrix. The lenses could be burrows of organisms. (c) In the detailed picture with crossed polarisers quartz and mica grains can be seen as well as areas of Fe-oxides. (d) Detailed picture with crossed polarisers of an area with coarser-grained calcite minerals.

O-19 Jausengang, SS 118

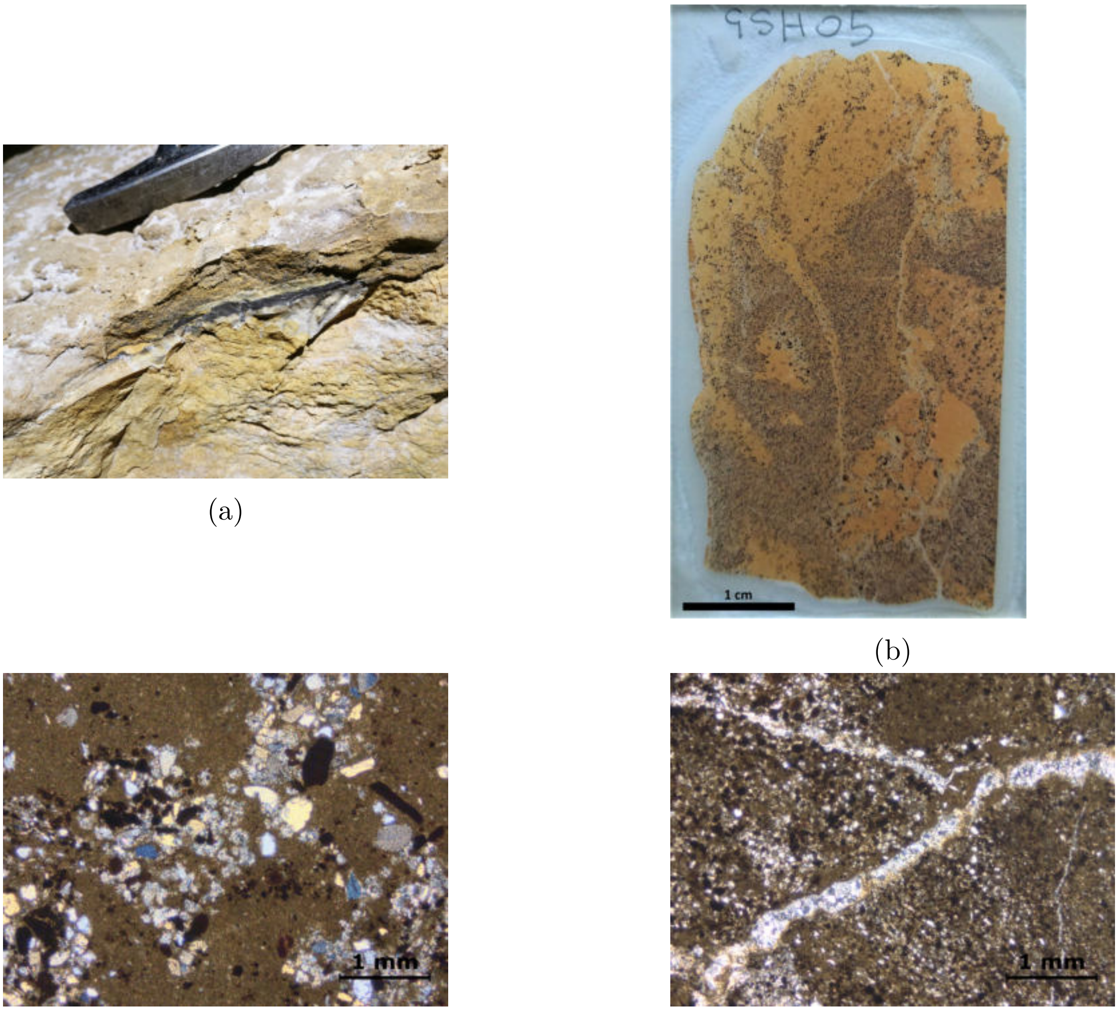

(a) (b) (c) (d)

Figure 98: Outcrop 19: (a) Orange-brownish layer (GSH 05) on top of Dachsteinkalk with a black layer in between (photo by L. Plan). (b) – (d) Thin section of sample GSH 05. (b) Overview picture of the thin section. (c) Detailed picture with crossed polarisers of broken up matrix with coarser-grained quartz and Fe-oxides as well as calcitic cement in between. (d) Detailed picture with crossed polarisers of secondary calcite veins.

Summarized results

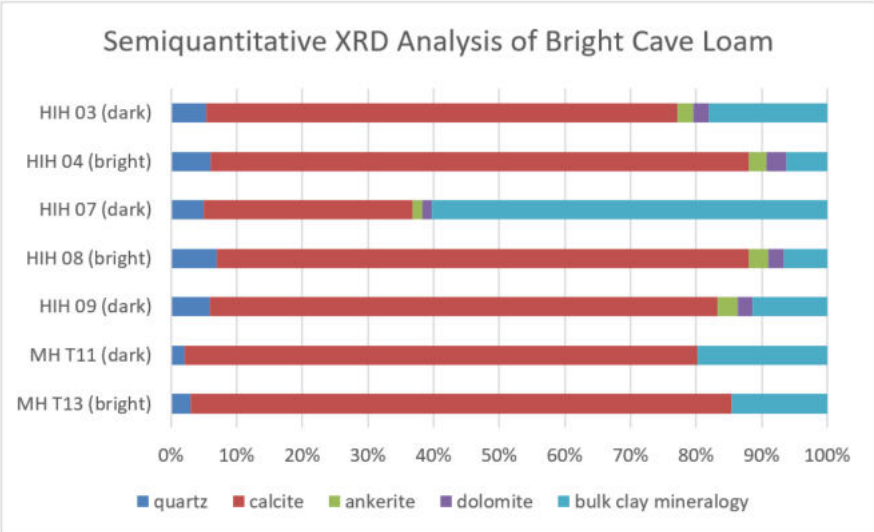

Figure 99: Semiquantitative XRD analysis of bulk composition without a detailed bulk clay mineralogy of all samples of bright cave loam.

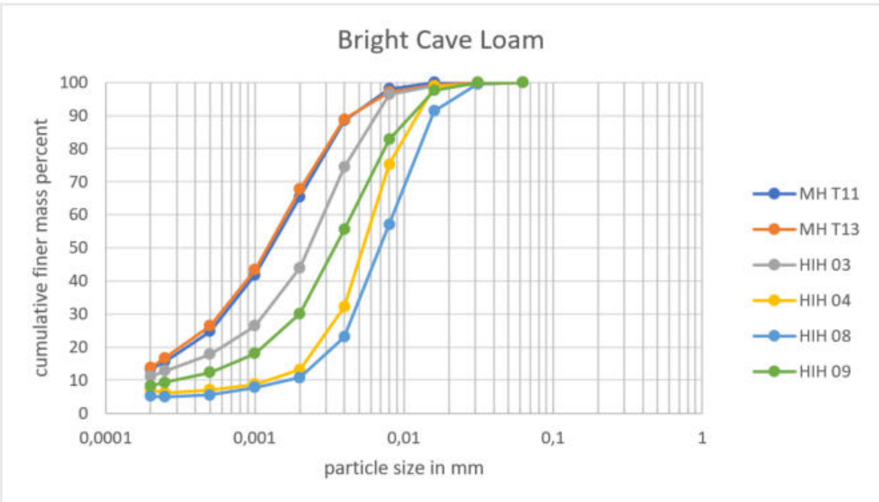

Figure 100: Grain size distribution of all samples of bright cave loam.

Caves outside Dachstein Massif

O-7 Eisriesenwelt

Figure 101: General plan of Eisriesenwelt and a detailed plan view with the marked sample location of ERW KD (modified from Plan et al, 2021).

(a)

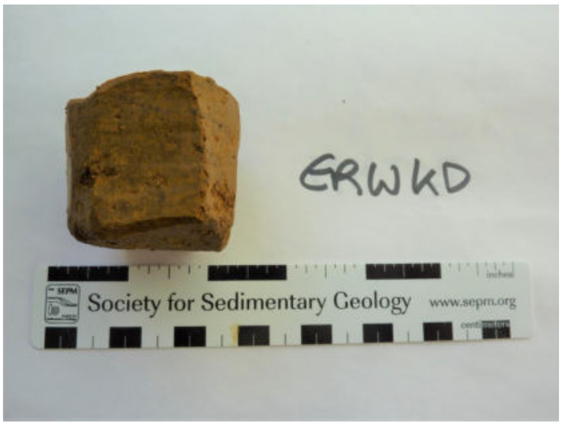

(b)

Figure 102: Outcrop 7: (a) Overview picture of the outcrop situation, pen for scale (photo by L. Plan). (b) Detailed picture of sample ERW KD, which is a dark brown-reddish clay (photo by S. Gier).

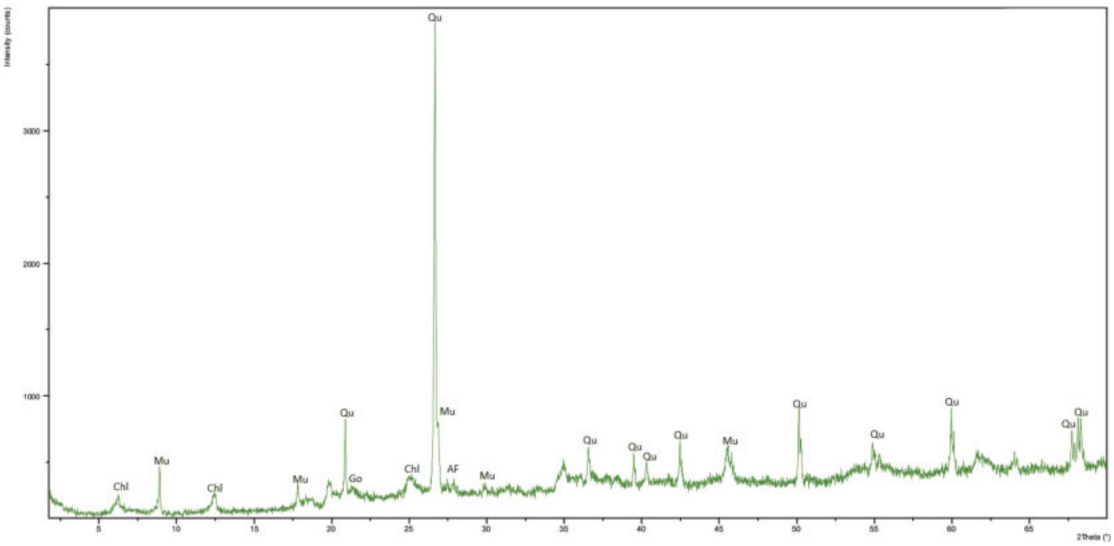

Figure 103: X-ray diffraction patterns of bulk sample of sample ERW KD. AF = alkali feldspar, Chl = chlorite, Go = goethite, Mu = muscovite, Qu = quartz.

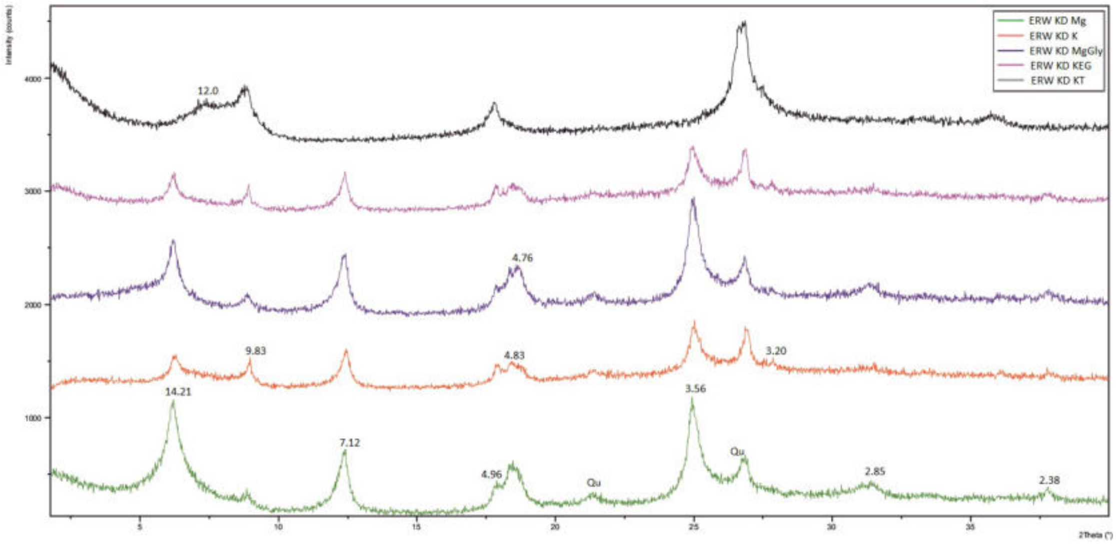

Figure 104: X-ray diffraction patterns of clay mineralogy of sample ERW KD. Saturated with Mg (green), K (red), Mg and glycerol (blue), K and ethylene glycol (pink), and heated to 550 °C (black); d-values in Å; Qu = quartz.

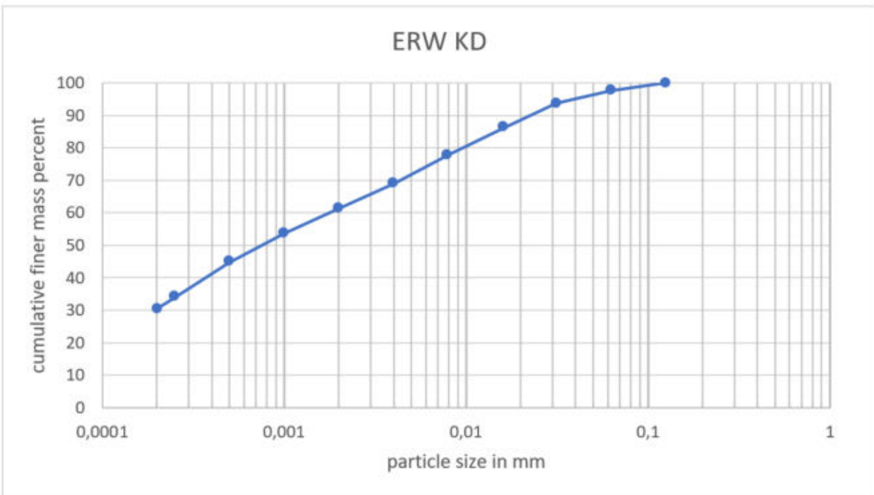

Figure 105: Grain size distribution of sample ERW KD.

O-15 Schönberg-Höhlensystem

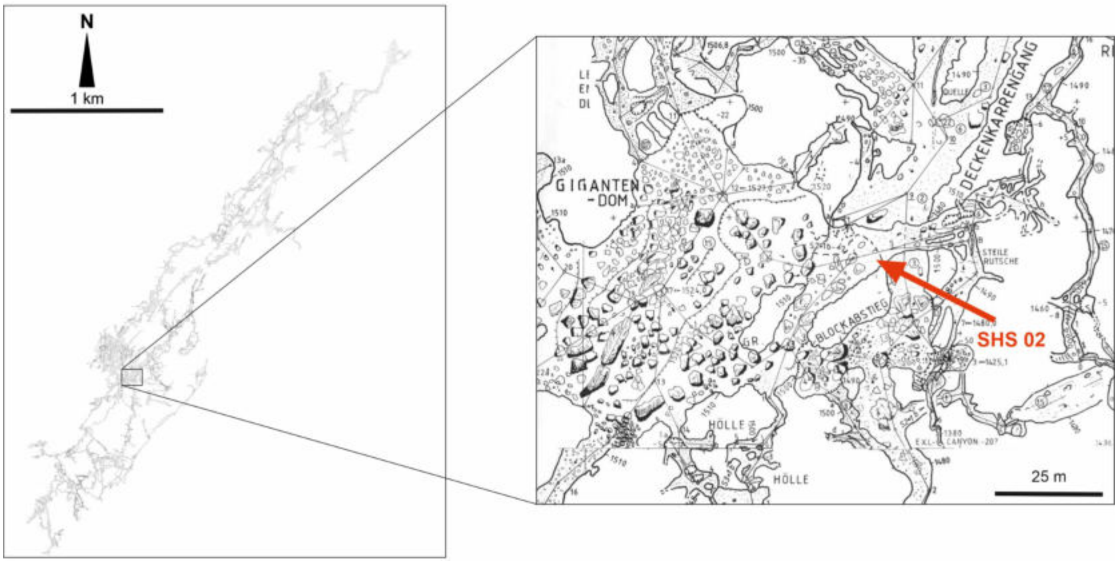

Figure 106: General plan of Schönberg-Höhlensystem and a detailed plan view with the marked sample location of SHS 02 (modified from Landesverein für Höhlenkunde in Oberösterreich).

(a) (b)

Figure 107: Outcrop 15: (a) Overview picture of the outcrop situation. (b) Detailed picture of sample SHS 02, which is a dark brown, poorly sorted sediment (SHS 02; photos by L. Plan).

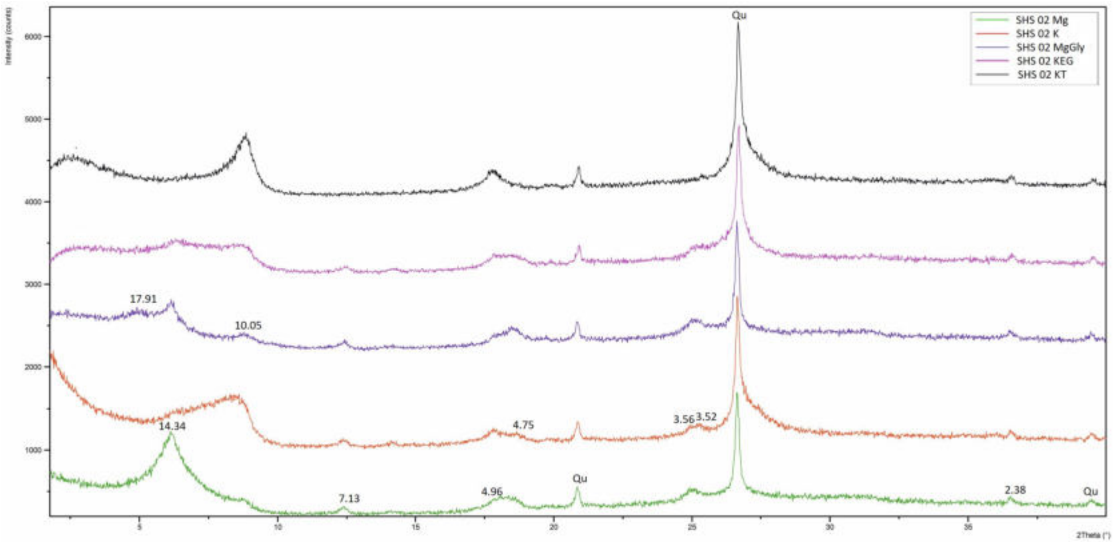

Figure 108: X-ray diffraction patterns of clay mineralogy of sample SHS 02. Saturated with Mg (green), K (red), Mg and glycerol (blue), K and ethylene glycol (pink), and heated to 550 °C (black); d-values in Å; Qu = quartz.

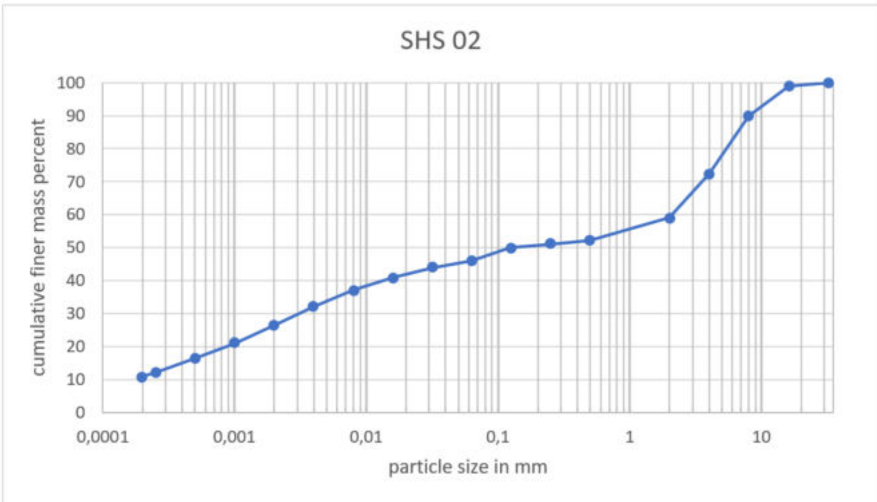

Figure 109: Grain size distribution of sample SHS 02.

Table 3: Overview of all samples, the associated outcrops, and a short sediment description. DRH = Rieseneishöhle, ERW = Eisriesenwelt, GSH = Günter-Stummer-Höhle, HIH = Hirlatzhöhle, MH T = Mammuthöhle, SHS = Schönberg-Höhlensystem.

sample	cave	date	outcrop	position	description
MH T01	Dachstein-Mammuthöhle	12/03/2021	1	Sklavengang, next to ladder	dark cave loam
MH T02	Dachstein-Mammuthöhle	12/03/2021	1	Sklavengang, next to ladder	greenish sediment
	Dachstein-Mammuthöhle	12/03/2021	2	at the end of Atlantis, junction Herkulesschacht and Barbarengang	bright cave loam
MH T03	Dachstein-Mammuthöhle	13/03/2021	3	Krippensteingang, shortly before Huziwand	dark cave loam
MH T04	Dachstein-Mammuthöhle	13/03/2021	3	Krippensteingang, shortly before Huziwand	dark cave loam with bioturbation
MH T05	Dachstein-Mammuthöhle	13/03/2021	3	Krippensteingang, after crossing	reddish clay alternating with Augenstein layer
MH T06	Dachstein-Mammuthöhle	13/03/2021	5	junction Solaris	concretion
MH T07	Dachstein-Mammuthöhle	13/03/2021	4	after junction Solaris, SS 100	greenish sediment
MH T08	Dachstein-Mammuthöhle	14/03/2021	6	Sklavengang, next to Strenge	greenish sediment with lenses of dark cave loam
MH T09	Dachstein-Mammuthöhle	14/03/2021	6	Sklavengang, next to Strenge	dark cave loam
MH T10	Dachstein-Mammuthöhle	14/03/2021	6	Sklavengang, next to Strenge	coarser dark cave loam
MH T11	Dachstein-Mammuthöhle	14/03/2021	6	Sklavengang, next to Strenge	bright cave loam with partially varve-like structure and massive areas, dark layer
MH T12	Dachstein-Mammuthöhle	14/06/2021	14	Paläotraun	dark cave loam
MH T13	Dachstein-Mammuthöhle	14/06/2021	14	Paläotraun	bright layer of bright cave loam
ERW KD	Eisriesenwelt	03/2021	7	Kirchendach	brown-reddish clay
HIH 01	Hirlatzhöhle	13/06/2021	8	Aufsteigender Tunnel, before ramp	poorly sorted, matrix-supported conglomerate with mainly carbonate, rarely quartz clasts, diameters up to 5 cm
HIH 02	Hirlatzhöhle	13/06/2021	9	Aufsteigender Tunnel, upper part	poorly sorted and matrix-supported conglomerate with carbonate and quartz clasts of diameters up to 2 cm
HIH 03	Hirlatzhöhle	13/06/2021	10	Lehmklamm, orographically right	dark layer of bright cave loam
HIH 04	Hirlatzhöhle	13/06/2021	10	Lehmklamm, orographically right	bright layer of bright cave loam
HIH 05	Hirlatzhöhle	13/06/2021	10	Lehmklamm, orographically right	sand layer on top of bright cave loam
HIH 06	Hirlatzhöhle	13/06/2021	11	Lehmbachschwinde	black components of conglomerate
HIH 07	Hirlatzhöhle	13/06/2021	12	between S-Gang and Brückenhalle	dark layer of bright cave loam
HIH 08	Hirlatzhöhle	13/06/2021	12	between S-Gang and Brückenhalle	bright layer of bright cave loam
HIH 09	Hirlatzhöhle	13/06/2021	12	between S-Gang and Brückenhalle	dark layer of bright cave loam
HIH 10	Hirlatzhöhle	13/06/2021	13	between bivouac and junction Wasserklamm	whitish silty-sandy ground cover
HIH 20	Hirlatzhöhle	11/2021	20	150 m after Wetterscheide	dark cave loam
SHS 02	Schönberghöhlensystem	08/2021	15	E of Gigantendom	brownish sediment with very poor sorting and components up to 3 cm
DRH 01	Dachstein-Rieseneishöhle	18/09/2021	16	Lehmhalle	dark brown loam with poor sorting
GSH 01	Günter-Stummer-Höhle	18/09/2021	17	Mammutlabyrinth, SS 164	within crumbly dark cave loam are brown-reddish compact clay components with a diameter up to 10 cm
GSH 02	Günter-Stummer-Höhle	18/09/2021	17	Mammutlabyrinth, SS 164	within crumbly dark cave loam are greenish compact clay components with a reddish coating and a diameter up to 10 cm
GSH 03	Günter-Stummer-Höhle	18/09/2021	17	Mammutlabyrinth, SS 164	brown-reddish dark cave loam with a crumbly consistence
GSH 04	Günter-Stummer-Höhle	18/09/2021	18	Mammutlabyrinth, SS 125	rock of fine-grained, brownish sediment
GSH 05	Günter-Stummer-Höhle	18/09/2021	19	Jausengang, SS 118	rock of fine-grained, orange-brownish sediment